MULTI-PHYSICS MODELING OF GEOMECHANICAL SYSTEMS WITH COUPLED HYDROMECHANICAL BEHAVIORS

by

AHMAD MOHAMED
B.S. University of Garyounis, 2003

A thesis submitted in partial fulfillment of the requirements
for the degree of Master of Science
in the Department of Civil, Environmental, and Construction Engineering
in the College of Engineering and Computer Science
at the University of Central Florida
Orlando, Florida

Spring Term
2013

Major Professor: Hae-Bum Yun

ABSTRACT

Geotechnical structures under realistic field conditions are usually influenced with complex interactions of coupled hydromechanical behavior of porous materials. In many geotechnical applications, however, these important coupled interactions are ignored in their constitutive models. Under coupled hydromechanical behavior, stress in porous materials causes volumetric change in strain, which causes fluid diffusion; consequently, pore pressure dissipates through the pores that results in the consolidation of porous material.

The objective of this research was to demonstrate the advantages of using hydromechanical models to estimate deformation and pore water pressure of porous materials by comparing with mechanical-only models. Firstly, extensive literature survey was conducted about hydro-mechanical models based on Biot's poroelastic concept. Derivations of Biot's poroelastic equations will be presented. To demonstrate the hydromechanical effects, a numerical model of poroelastic rock materials was developed using COMSOL, a commercialized multiphysics finite element software package, and compared with the analytical model developed by Wang (2000). Secondly, a series of sensitivity analyses was conducted to correlate the effect of poroelastic parameters on the behavior of porous material. The results of the sensitivity analysis show that porosity and Biot's coefficient has dominant contribution to porous material behavior. Thirdly, a coupled hydromechanical finite element model was developed for a real-world example of embankment consolidation. The simulation results show excellent agreement to field measurements of embankment settlement data.

ACKNOWLEDGMENTS

I would like to express my special thanks for my advisor, Assistant Professor Dr. Hae-Bum Yun for giving this opportunity to work under his supervision and for sharing his great knowledge and experience with me. He introduced me to an interesting topic and provided important insight throughout. It has been a privilege and honor to be his student.

I am also thankful for Associate Professor Dr. Manoj Chopra for serving on my committee and providing helpful comments, advices and suggestions. Also, I would like to thank Dr. Amr Sallam who has provided me with some embankment data and for his advices.

Appreciation is also extended to all people who gave the author heartfelt corporation and shared their knowledge and for giving some of their valuable time. My friends, for their endless love, emotional support and belief in me.

Finally, my biggest gratitude is to my family for supporting me throughout my graduate studies.

My parents, Saeid and Aziza, your encouragement and love helped me ease through some of hardest times I have faced. Without you I would never come up to this stage.

TABLE OF CONTENTS

LIST OF FIGURES

LIST OF TABLES

1. INTRODUCTION

1.1. Motivation

Many problems in geotechnical engineering require a profound understanding of interaction between soil skeleton and multiphysics. Because of the interaction between soil skeleton and other transport phenomena, a coupled phenomenon is critical to describe the real behavior and response of soil in present of multiphysical processes.

Hydro-mechanical coupling phenomena are considered to be the most important element for soil consolidation calculations. The first theory to take into account the Hydro-Mechanical coupling effect on soil was introduced by Terzaghi (1923). However, his theory was for one-dimensional consolidation. Later, Biot (1941) extended Terzaghi theory to take into account three-dimensional consolidation. Biot's theory presented a set of energy balance equations, which are known as poroelastic equations.

Biot's equations link strain-stress mass changes to stress and fluid pressure change. Basically, any change in fluid pressure in a porous medium will effect stress-strain behavior in the solid bulk. Biot generalized his equation based on Darcy's law and Hook's law. Hook's equations represent stress-strain relationship. Darcy's law describes the time-dependence of fluid flow as result of non-uniform pore pressure distribution across the porous material. However, Biot's theory has some limitations such as, it is only valid for fully saturated soil with small deformation.

Unsaturated soils are encountered in many engineering applications. Recently, significant attention has been paid to investigate the behavior of coupling in unsaturated soil Antonio (2011).Unsaturated soil consists of three phases which are solid skeleton, pore pressure and air.

The presence of the air in the porous media introduces a more complex system than the system found in saturated soil. Understanding the behavior of unsaturated soil requires knowledge about the interaction between three different processes (mechanical, thermal and fluid movement).

Recently many researches has been conducted to understand and analysis the Thermo-Hydro-Mechanical coupled processes in unsaturated media. Thermo-hydro-mechanical (THM) phenomena are very important to consider in petroleum engineering because the variation of temperature during oil production, would produces growth in thermal stresses in the porous material. As a result, the thermal stresses can cause a failure in the reservoir rock and subsequently alter its porosity and permeability Chen (2009). In addition, this will not only produce progressive alteration on the strength of the porous material, but also will cause changes in the flow regime and the rate of production. Booker and Savvidou (1985) performed a study on the effect of heat source on the consolidation of porous media, their results showed that permeability of the soils is effected by stresses generated by a heat source.

Freeman (2008) presented the effects of temperature variations on the behavior of fluid flow through the porous material. His results demonstrate that temperature directly change the viscosity of the hydrocarbon. Freeman (2008) stated that the stresses in the rock will be effected due change on viscosity of the fluid. The effect will be more noticeable if the thermal loads causes higher effective stresses that cause abnormal porosities

It can be concluded that the different interaction processes occurs in unsaturated media introduce a complex system which required further assumptions to establish a complete a set of governing differential equations that represent the physics of the problem. To reduce the complexity of the Thermo-Hydro-Mechanical model, assumptions are made to reduce the number of model

parameters and formulations. The following assumptions are typically introduce to develop a simple model for unsaturated soil. Soil density is constant, but the porous is compressible. Small deformation is allowed. Water vapor is ignored and the velocity of solid skeleton is ignored Mctigue (1986).

In closing, it may be concluded that a number of studies have been made to show the importance of multiphysics coupling on geomechanics porous. In this research, several numerical models are presented to illustrate the applicability and capability of coupling strategy based on Biot's theory.

1.2. Approach

This chapter has provided a brief history of the role of multiphysics coupling on geomechanics problems. Chapter 2 presented the physical and mathematical background of hydromechanical coupling based on Biot's poroelastic theory. In chapter 3, a complete detailed of reservoir model based on the Biot's poroelastic theory is presented with emphasis on comparing the numerical model results with pervious published data. In Chapter 4, the focus shifts to demonstrate the role of poroelastic parameters on the Hydro-mechanical coupling behavior. Sensitivities studies to illustrate the respond of 2-D rock material are presented. Chapter 5 presence the results of hydromechanical coupling for a real-world example of embankment consolidation. Chapter 6 presents the main conclusions and future recommendations of the study.

2. BACKGROUND

2.1 Biot's Theory Formation

In this section, Biot's poroelastic equations are developed. The poroelastic equations developed in this section follows Wang (2000) approach. The poroelastic equation are developed based on two constitutive relations for applied stress (σ) and pore pressure (p). In addition, governing equations that describe fluid flow in poroelastic medium are also used. The governing equations links the force equilibrium equations and pore pressure. In other words, they show the stress-strain relation between fluid flow and soil skeleton. The movement of fluid in poroelastic media is covered by Darcy's law.

2.1.1Constitutive relations

Generally, poroelastic equations are expressed in terms ε and ζ, where $\varepsilon = \frac{\delta v}{v}$the volumetric change, and ζ is the increment of the fluid content. Wang (2000) assumed that $\varepsilon = \frac{\delta v}{v}$ volumetric strain changes to be positive in tension and negative in case of contraction, stress to be positive in tension. The increment of water ζ is negative if the fluid removed from the storage and positive if the water is added to skeleton volume. The first equation shows that any change in applied stress and pore pressure will cause volumetric strain:

$$\varepsilon = a_{11}\,\sigma + a_{12}\,p \tag{2.1}$$

The second equation shows the increment of water volume due to change in pore pressure

$$\zeta = a_{21}\,\sigma + a_{22}\,p \tag{2.2}$$

The equations above have generic poroelastic coefficients (a_{ij}), which represents the ratio of the change in the dependent variables to change in the independent variables.

The poroelastic coefficients are expressed as the following:

$$a_{11}=\left.\frac{\delta\varepsilon}{\delta\sigma}\right|_{p=0} \equiv \frac{1}{K} \tag{2.3}$$

$$a_{12}=\left.\frac{\delta\varepsilon}{\delta\sigma}\right|_{p=0} \equiv \frac{1}{H} \tag{2.4}$$

$$a_{21}=\left.\frac{\delta\xi}{\delta\sigma}\right|_{p=0} \equiv \frac{1}{H} \tag{2.5}$$

$$a_{22}=\left.\frac{\delta\xi}{\delta\sigma}\right|_{p=0} \equiv \frac{1}{R} \tag{2.6}$$

In the above K is drained bulk modules, and 1/K represent the compressibility of the material. The coefficient 1/H describe the change in the bulk volume due to a pore pressure change, under the application of a constant stress. The coefficient 1/R represent the relation between the change of water volume added or removed from the bulk volume due the change in the pore pressure.

By imposing the four poroelastic coefficients, we can rewrite Equation 2.1 and 2.2 as following:

$$\varepsilon=\frac{1}{\mathrm{K}}\sigma+\frac{1}{\mathrm{H}}\,\mathrm{p} \tag{2.7}$$

$$\zeta = \frac{1}{H}\sigma + \frac{1}{R}\,p \tag{2.8}$$

Biot (1941) showed that (1/R) coefficient specific storage also can be expressed as unconstrained coefficient storage at constrained stress.

$$\delta_\sigma = \frac{1}{R} = \frac{\alpha}{KB} \tag{2.9}$$

Biot's (1941) introduced another coefficient which represent the constrained specific storage at constant strain.

$$\delta_\sigma = \frac{1}{M} = \frac{\alpha}{K_u B} \tag{2.10}$$

Two additional coefficient are introduced by Biot. First, Skempton's coefficient B is introduced to show the ratio of the induced pore pressure to change applied stress for undrained condition.

$$B \equiv -\frac{\delta P}{\delta \sigma}\Big|_{\zeta=0} = \frac{R}{H} \tag{2.11}$$

Generally. Skempton's coefficient range from 0 to 1, Skempton's coefficient shows the distribution of the applied stress between the fluid and soil skeleton.

The second coefficient is known as the Biot-Willis coefficient α:

$$\alpha \equiv \frac{K}{H} \tag{2.12}$$

Now by replacing the coefficient (1/H) in equation (2.7) by (α/K):

$$\varepsilon = \frac{1}{K}\sigma + \frac{\alpha}{K}\, p \qquad (2.13)$$

Now by replacing the coefficient (1/R) in equation (2.8) by coefficient specific storage ($\frac{\alpha}{KB}$) (see equation 2.9).

$$\zeta = \frac{\alpha}{K}\sigma + \frac{\alpha}{KB}\, p \qquad (2.14)$$

By solving Equation 2. 13 for stress, we get:

$$\sigma = K\varepsilon - \alpha\, p \qquad (2.14)$$

Now, substituting Equation 2.14 into Equation 2.13 we get the following:

$$\zeta = \alpha\varepsilon + \frac{\alpha}{K_u B}\, p \qquad (2.16)$$

$$\text{where } K_u = \frac{K}{1-\propto B}, \text{ the undrained specific storage} \qquad (2.17)$$

Now, one should extend poroelastic analysis to cover 3-D formulation. It requires seven linear constitutive equations to describe the general anisotropic state of stress. Three equation to show the relation between normal stress components and pore pressure. The other three equations show the relation between shear strain and the corresponding shear stress components. The seventh equation relates the increment of fluid to mean stress, and pore pressure.

However, by using the principle coordinates, the seven equations are reduced to four equations, because the shear stress and shear strain are zero in the principle coordinates.

$$\varepsilon_1 = \frac{1}{E}\,\sigma_1 - \frac{v}{E}\,\sigma_2 - \frac{v}{E}\,\sigma_3 + \frac{\alpha}{3K}\,P \tag{2.18}$$

$$\varepsilon_2 = -\frac{1}{E}\,\sigma_1 + \frac{v}{E}\,\sigma_2 - \frac{v}{E}\,\sigma_3 + \frac{\alpha}{3K}\,P \tag{2.19}$$

$$\varepsilon_3 = -\frac{1}{E}\,\sigma_1 - \frac{v}{E}\,\sigma_2 - \frac{v}{E}\,\sigma_3 + \frac{\alpha}{3K}\,P \tag{2.20}$$

$$\zeta = \frac{1}{3H}\,(\sigma_1 + \sigma_1 + \sigma_1) + \frac{p}{R} \tag{2.21}$$

The equations can be written in term of shear modulus G, rather than Young's modulus, E, since it is easier to measure.

$$K = \frac{E}{3(1-2v)} \tag{2.22}$$

And

$$G = 2G(1+V) \tag{2.23}$$

where E is the drained Young's modules and ν, Poisson's ratio, are measured under drained conditions (that is, when pressure pore is zero).

$$\varepsilon_{xx} = \frac{1}{2G}\left[\sigma_{xx} - \frac{v}{(1+v)(\sigma_{11}+\sigma_{22}+\sigma_{33})}\right] + \frac{\alpha}{3K}P \tag{2.24}$$

$$\varepsilon_{yy} = \frac{1}{2G}\left[\sigma_{yy} - \frac{v}{1+v}(\sigma_{11}+\sigma_{22}+\sigma_{33})\right] + \frac{\alpha}{3K}\,P \tag{2.25}$$

$$\varepsilon_{zz}= \frac{1}{2G}\left[\sigma_{zz}- \frac{v}{1+v}(\sigma_{11+}\sigma_{22}+\sigma_{33)}\right]+\frac{\alpha}{3K}\ P \tag{2.26}$$

$$\varepsilon_{xy} = \frac{1}{2G}\ \sigma_{xy} \tag{2.27}$$

$$\varepsilon_{xy} = \frac{1}{2G}\ \sigma_{yz} \tag{2.28}$$

$$\varepsilon_{xy} = \frac{1}{2G}\ \sigma_{xz} \tag{2.29}$$

The equations can be cast in general coordinates and resolved for normal and shear stresses, and the shear modulus. Here we assume that changes in pore pressure will not induce shear strains. The full form of the pure compliance formulation thus becomes:

$$\sigma_{xx} = 2G\varepsilon_{xx} + 2G\frac{v}{1-2v}\ \left(\varepsilon_{xx} + \varepsilon_{yy} + \varepsilon_{zz}\right) - \alpha\ P \tag{2.30}$$

$$\sigma_{yy} = 2G\varepsilon_{yy} + 2G\frac{v}{1-2v}\ \left(\varepsilon_{xx} + \varepsilon_{yy} + \varepsilon_{zz}\right) - \alpha\ P \tag{2.31}$$

$$\sigma_{zz} = 2G\varepsilon_{zz} + 2G\frac{v}{1-2v}\ \left(\varepsilon_{xx} + \varepsilon_{yy} + \varepsilon_{zz}\right) - \alpha\ P \tag{2.32}$$

$$\sigma_{xy} = \ 2G\ \varepsilon_{xy} \tag{2.33}$$

$$\sigma_{xy} = \ 2G\ \varepsilon_{xy} \tag{2.34}$$

$$\sigma_{xz} = \ 2G\ \varepsilon_{xz} \tag{2.35}$$

The seven constitutive equation can also be recast in terms of volumetric strain, where ε is expressed as the sum of the three normal strains,

$$\zeta = \alpha \left(\varepsilon_{xx} + \varepsilon_{yy} + \varepsilon_{zz}\right) + \frac{\alpha}{K_u B} P \qquad (2.36)$$

2.1.2 Governing Equations

The poroelastic governing equations coupled the force equilibrium equation with fluid-flow equation. The effect of coupling can be seen because the pore pressure term appears in the force equilibrium equations and the volumetric strain appears in the fluid flow equation.

Force Equilibrium relation

Biot (1941) assumed that mechanical problem is elastostatic. This means that the mechanical problem obtained statically each instant of time. The time required for dynamic wave propagation to transfer stresses across the problem domain is ignored. In other words, in the case of applied sudden forces to the poroelastic body, displacement and fluid pressure with each representative elementary volume (REV) adjusted instantaneously to maintain a state of internal force equilibrium. The normal (σ) and shear (τ) components of the stress tensor are illustrated on an REV as shown in the figure below:

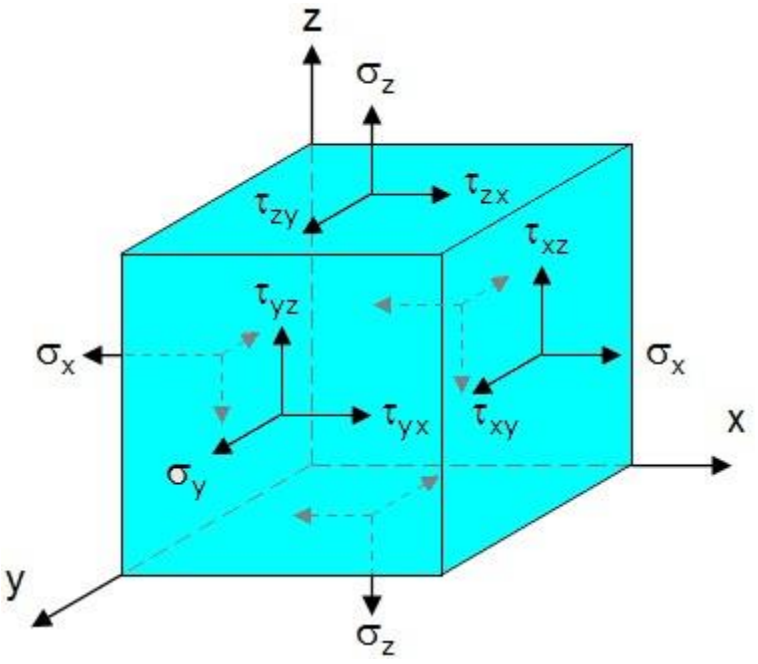

Figure 1: Stress tensor block.

Assuming insignificant accelerations and summing the net forces in each principal direction, the force-displacement equilibrium equations are obtained with help of Figure 1 (Cheng, 1993; Wang, 2000). The body force is expressed as gravitational force $\bar{F} = (0, 0, -\rho g)$.

In engineering notation, the three force-displacement equilibrium equations are represented as

$$\sum_{n=1}^{3} \frac{\partial \sigma_{ij}}{\partial x_i} = -F_i \tag{2.37}$$

$$\left[\frac{\partial \sigma_{xx}}{\partial x} + \frac{\partial \sigma_{yx}}{\partial y} + \frac{\partial \sigma_{zx}}{\partial z}\right] = F_x \tag{2.38}$$

$$\left[\frac{\partial \sigma_{xy}}{\partial x} + \frac{\partial \sigma_{yy}}{\partial y} + \frac{\partial \sigma_{zx}}{\partial z}\right] = F_y \tag{2.39}$$

$$\left[\frac{\partial \sigma_{xz}}{\partial x}+\frac{\partial \sigma_{yz}}{\partial y}+\frac{\partial \sigma_{zz}}{\partial z}\right]=F_z \tag{2.40}$$

Now substituting constitutive equations developed in the previous section into above force equilibrium equations lead to three partial differential equations relating the six quantities of strain to pore pressure and overall body forces. A more convenient set of unknowns is the structural displacements. The displacement is related to the strain (using indicial notation) through

$$\left[G\nabla^2 u+\frac{G}{1-2v}\left(\frac{\partial^2 u}{\partial x^2}+\frac{\partial^2 v}{\partial x \partial y}+\frac{\partial^2 w}{\partial x \partial z}+\right)\right]=F_X-\alpha\ \frac{\partial P}{\partial x} \tag{2.41}$$

$$\left[G\nabla^2 v+\frac{G}{1-2v}\left(\frac{\partial^2 u}{\partial x \partial y}+\frac{\partial^2 v}{\partial y^2}+\frac{\partial^2 w}{\partial x \partial z}+\right)\right]=F_y-\alpha\ \frac{\partial P}{\partial x} \tag{2.42}$$

$$\left[G\nabla^2 w+\frac{G}{1-2v}\left(\frac{\partial^2 u}{\partial x \partial y}+\frac{\partial^2 v}{\partial x \partial y}+\frac{\partial^2 w}{\partial z^2}+\right)\right]=F_z-\alpha\ \frac{\partial P}{\partial x} \tag{2.43}$$

Where in case small deformations, the strains can be defined equivalently with index notation in terms of derivatives of displacement,

$$\varepsilon_{ij}=\frac{1}{2}\left[\frac{\partial u_i}{\partial x_j}+\frac{\partial u_j}{\partial x_i}\right] \tag{2.44}$$

The volumetric strain is the sum of the longitudinal strains as expressed by the divergence of displacement

$$\varepsilon_{ij}=\varepsilon_{kk}=\varepsilon_{xx}+\varepsilon_{yy}+\varepsilon_{zz}=\frac{\partial u}{\partial x}+\frac{\partial v}{\partial y}+\frac{\partial w}{\partial z} \tag{2.45}$$

Fluid Flow Relations

Darcy's Law (1856) governs the flow of the fluid in porous material, it is an energy transport equation, which links fluid flow rates to pressure gradients and elevation gradients:

$$q = -\frac{k}{\mu}\nabla(p + \rho_f gz) \tag{2.46}$$

where q is fluid flux, k is the intrinsic permeability, μ is the viscosity of fluid, ρ_f is the fluid density, g is the acceleration of gravitational, and z is the elevation potential.

Since Darcy's law is an energy transport equation and the fluid flow because of potential energy expressed as "The frictional forces between fluid and solid matrix will balance the driving force due to the potential gradients." As result, seepage velocity should be expressed as an average linear velocity between the fluid and the solid matrix displacements Wang (2000):

$$v = \frac{\partial u_{fluid}}{\partial t} - \frac{\partial u_{solid}}{\partial t} = \frac{1}{\emptyset} q \tag{2.47}$$

In defining the increment of fluid content, Biot and Willis (1941) defined this quantity as

$$\zeta = -\varphi\nabla.(u_{fluid} - u_{solid}) \tag{2.48}$$

Biot assumes the porosity is constant, so the porosity term drops out of this fluid continuity equation by taking the time derivative and substituting in the relative seepage velocity:

$$\frac{\zeta}{\partial t} = -\varphi\nabla.\left(\frac{1}{\emptyset} q\right) = -\nabla. q \tag{2.49}$$

By substituting in Darcy's law for the fluid flux, into Biot and Wills (1957) increment of the fluid, we arrive at following:

$$\frac{\zeta}{\partial t} = -\varphi\nabla.\left(\frac{1}{\emptyset}q\right) = -\nabla.q \tag{2.50}$$

Finally, substituting the seventh constitutive relation between increment of fluid content and strain and pressure from pervious section see Equation 2.36:

$$\zeta = \alpha\left(\varepsilon_{xx} + \varepsilon_{yy} + \varepsilon_{zz}\right) + \frac{\alpha}{K_u B}P \tag{2.51}$$

We get:

$$\left[\alpha\frac{\partial}{\partial t}\left(\varepsilon_{xx}+\varepsilon_{yy}+\varepsilon_{zz}\right)+\frac{\alpha}{K_u B}\frac{\partial P}{\partial t}\right] - \nabla.\left[\frac{k}{\mu}\nabla(p+\rho_f gz)\right] = QS \tag{2.52}$$

Then, substitute the relation between strain and deflection:

$$\varepsilon_{xx} + \varepsilon_{yy} + \varepsilon_{zz} = \frac{\partial u}{\partial x} + \frac{\partial v}{\partial y} + \frac{\partial w}{\partial z} \tag{2.53}$$

And substitute storage coefficient as following:

$$s_\alpha = \frac{\alpha}{K_u B} \tag{2.54}$$

We get:

$$S_\alpha\frac{\partial p}{\partial t} - \nabla.\left[\frac{K}{\mu}\nabla(p+\rho_f gz)\right] = Q_s - \alpha\frac{\partial}{\partial t}(\nabla.u \tag{2.55}$$

2.2 Summary of Poroelastic Equation to Solve Hydro-Mechanical Model

In this chapter, a set of Biot's poroelastic equation were developed to describe the Hydro-mechanical coupling between structural deformation and fluid flow. Constitutive and governing

equations and their poroelastic parameters were presented. This chapter showed the physical important coefficient needed to describe the coupling behavior such as compressibility of fluid, Biot's coefficient and Skempton's factors. It can be concluded that Poroelastic equations is linked structural displacement equations with fluid flow equation as the following:

2.2.1 Structure equation:

$$\left[G\nabla^2 u+\frac{G}{1-2v}\left(\frac{\partial^2 u}{\partial x^2}+\frac{\partial^2 v}{\partial x\partial y}+\frac{\partial^2 w}{\partial x\partial z}+\right)\right]=F_X-\alpha\ \frac{\partial P}{\partial x} \tag{2.56}$$

$$\left[G\nabla^2 v+\frac{G}{1-2v}\left(\frac{\partial^2 u}{\partial x\partial y}+\frac{\partial^2 v}{\partial y^2}+\frac{\partial^2 w}{\partial x\partial z}+\right)\right]=F_y-\alpha\ \frac{\partial P}{\partial x} \tag{2.57}$$

$$\left[G\nabla^2 w+\frac{G}{1-2v}\left(\frac{\partial^2 u}{\partial x\partial y}+\frac{\partial^2 v}{\partial x\partial y}+\frac{\partial^2 w}{\partial z^2}+\right)\right]=F_z-\alpha\ \frac{\partial P}{\partial x} \tag{2.58}$$

2.2.2 Fluid flow equations

$$S_\alpha\frac{\partial p}{\partial t}-\nabla.\left[\frac{K}{\mu}\nabla\left(p+\rho_f gz\right)\right]=Q_s-\alpha\frac{\partial}{\partial t}(\nabla.u) \tag{2.59}$$

3. VALIDATION OF HYDROMECHANICAL MODEL FOR POROUS MATERIALS

3.1 Introduction

Numerical models based on the Biot's poroelasticity formulation are presented in this chapter. Biot's poroelastic equations are used to couple the relation between fluid flow and deformation. The goal in this chapter is to validate number of numerical models by using COMSOL simulation software (2012). This will be accomplished by using numerical models based on the Biot's poroelasticity formulation, and more specifically, using Biot's poroelastic equations to couple the relation between fluid flow and deformation Poroelastic equations developed in Chapter 2 can be found under COMSOL's poroelasticity package.

Zheng et al. (2003) provide a complete detailed account of reservoir models based on the Biot's poroelastic theory. Zhang developed the finite element model, and then validates his results with Biot's analytical solution. Here, the goal is to gain a better understanding of COMSOL software and show the ability to obtain results that agree with Zhang's solution.

3.2 Uniaxial-Constrained Hydro-Mechanical Model:

3.2.1 Introduction

The first model was carried out by Zheng et al (2003) to describe the behavior of a 2D rock sample. A schematic of the model simulation is shown in Figure 2. The dimension of the sample is 2 m × 3 m. The rock density is 2000 kg m^{-3}. The rock sample is filled with oil. The displacement of the bottom boundary is set to zero, the sides displacement are confined by mechanical roller constraints. The vertical displacement at top boundary is free to move. The parameters of this rock sample are given in the Table 1.

In this model, poroelasticity equations for single flow are used. These equations illustrate the effect of the flow of fluid in the stress-strain of the rock sample, as well the geomechnical deformations effect on the fluid flow. The poroelasticity equations implemented in COMSOL, which were developed in Chapter 2 to describe the coupling between fluid and deformation can be formulated as following:

$$\frac{1}{M}\frac{\partial p}{\partial t} - \nabla\left(\frac{k}{\mu}(\nabla p - \rho fg\nabla z)\right) = -\alpha\frac{\partial(\nabla . u)}{\partial t} \tag{3.1}$$

where M, Biot's Modulus is defined as:

$$\frac{1}{M} = \frac{\alpha - \varphi}{k_s} + \frac{\varphi}{k_f} \tag{3.2}$$

where Ks is the soil-grain modulus. However, the Ks can be interpreted as the bulk modules of soil phase K_f is the bulk modulus of fluid; φ is the porosity of porous material; α is Biot-Willis coefficient.

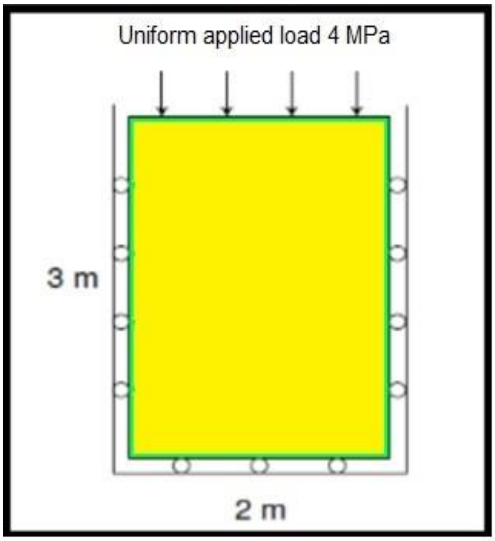

Figure 2: 2m × 3m sample under a load Zheng et al (2003).

Table 1: List of parameters of rock simple Zhang el al (2003).

Young's Modules	$1.44x\ 10^4$ M Pa
Poisson's Ratio	0.2
Biot's Coefficient	0.79
Biot's Modules	$1.23x10^4$ M Pa
Rock Density	2000 Kg/m^3
Oil Density	940 kg/m^3
Porosity	0.2
Permeability	$2x10^{-13}$ m^2
Kinematic viscosity	$1.3x10^{-4}$ m^2/s

3.2.2 Test Setup and simulation

The rock sample simulation is done in two stages. In the first stage, the sample is subjected to uniform load where no pore pressure will dissipate from sample boundaries. The applied uniform load is 4 M Pa. The pore pressure is constant during first stage; the pore pressure is 1.64 M Pa. The vertical displacement and pore pressure obtained from COMSOL shows a good agreement with Zhang's analytical and numerical solution. This agreements is shown in Figures 3 and 4.

In the second stage, the top boundary of the rock sample is opened so water can flow out of the sample. The applied uniform load remains constant at 4 M Pa. Time-Displacement plots shows excellent agreement with Zhang results.

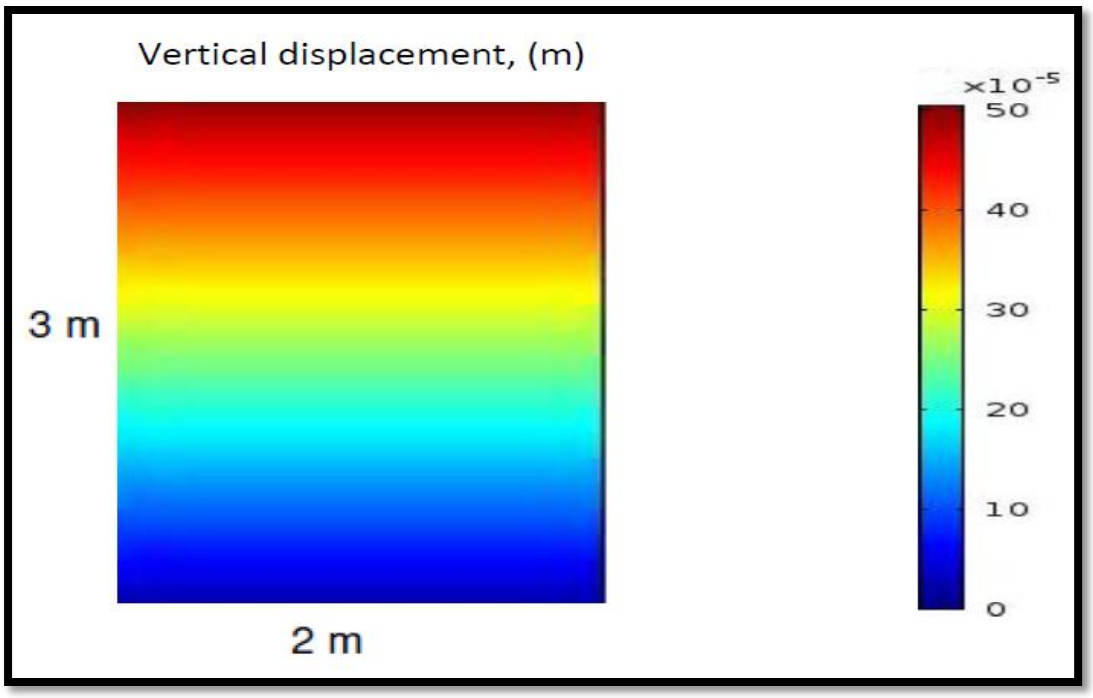

Figure 3: Vertical Displacement for the rock sample for undrained condition Ahmad (2013).

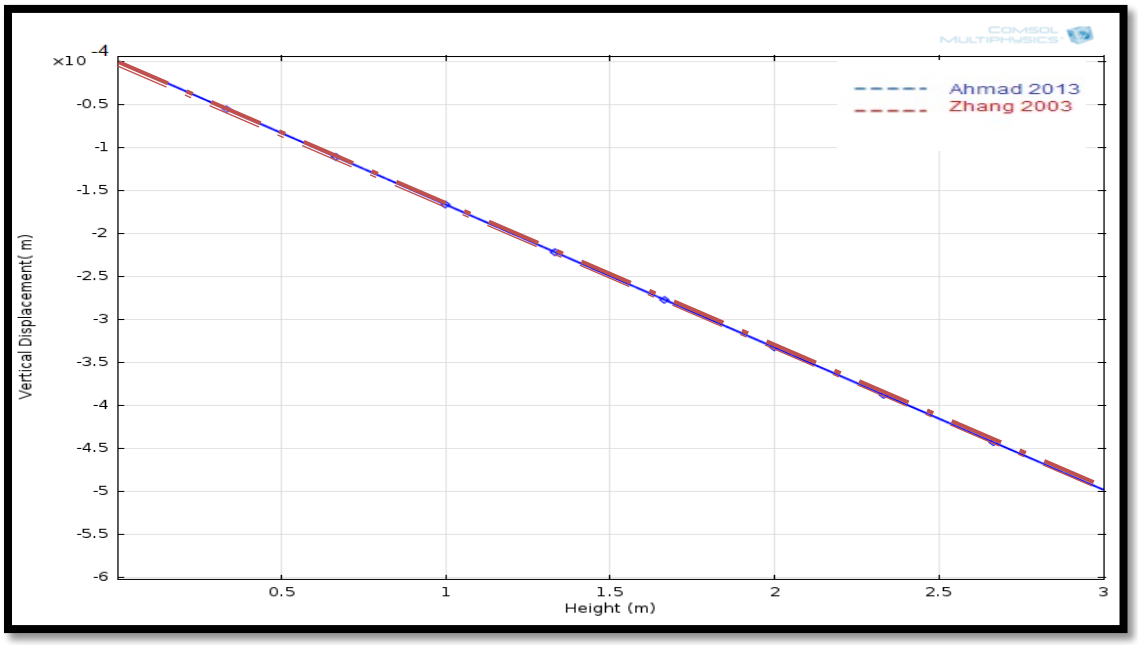

Figure 4: Vertical displacement vs height of the sample with undrained boundaries by Ahmad (2013).

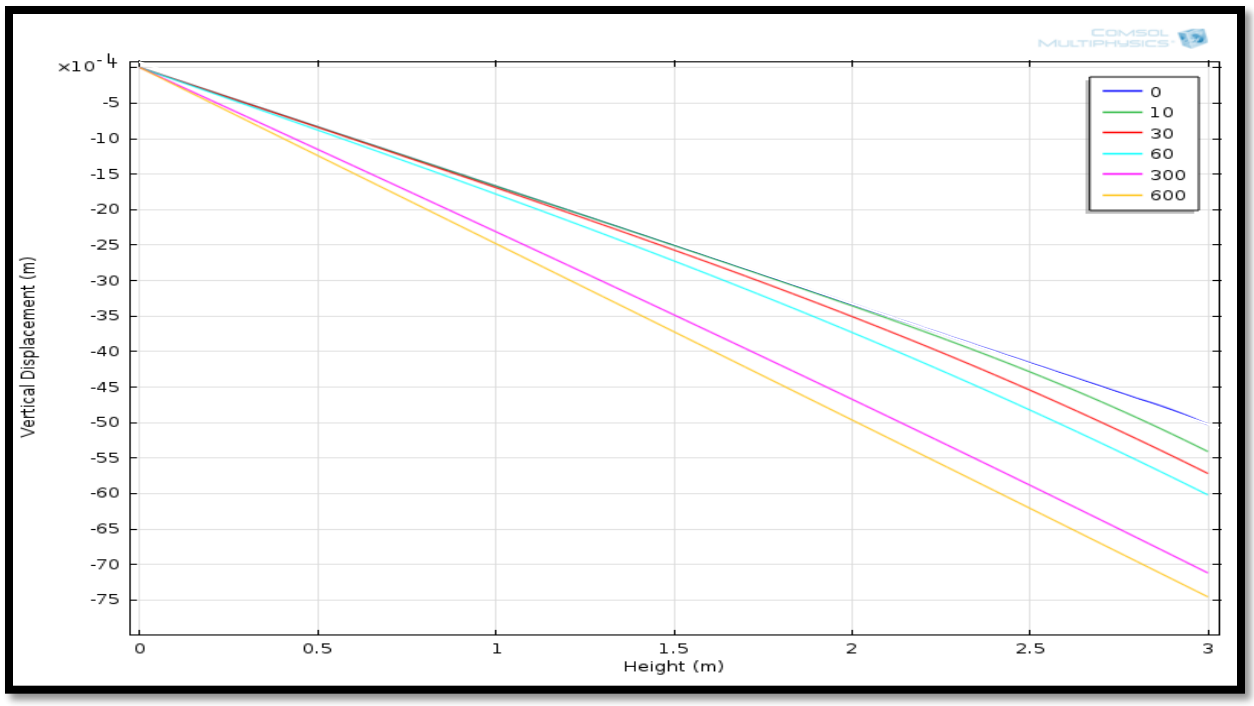

Figure 5: Vertical displacements plotted in different time intervals for the second stage by Ahmad (2013).

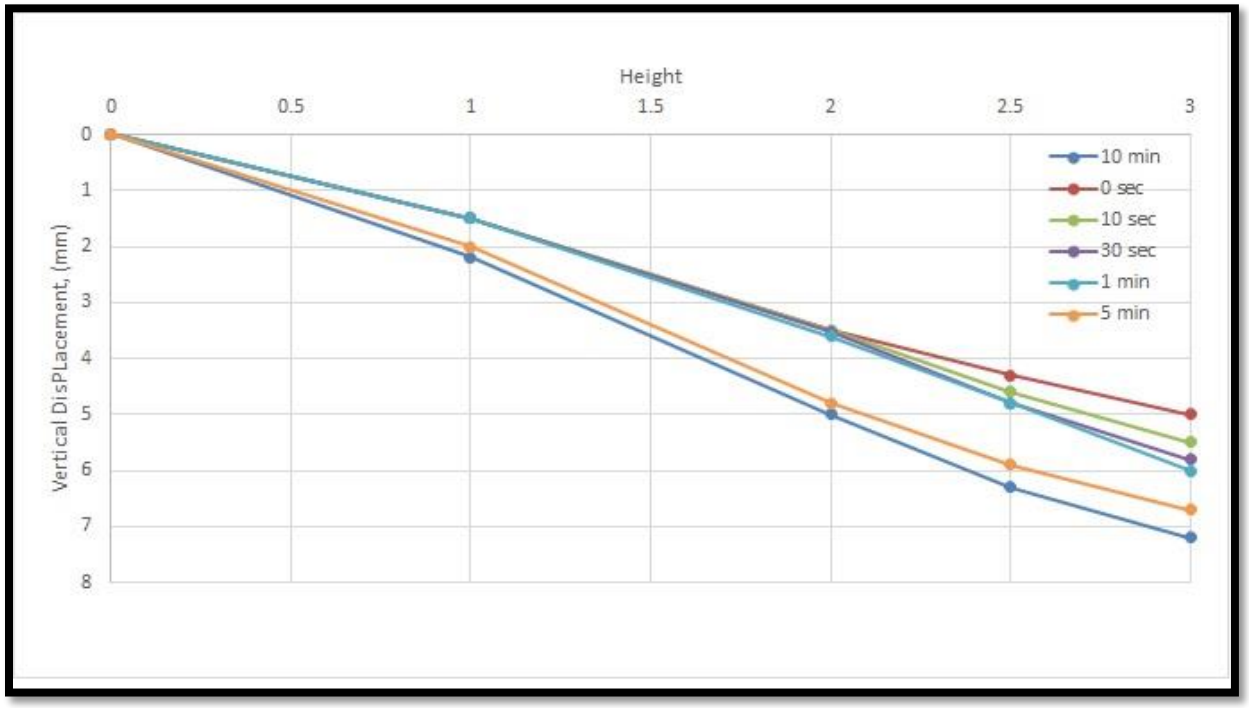

Figure 6: Vertical displacements plotted in different time intervals for the second stage by Zheng.(2003).

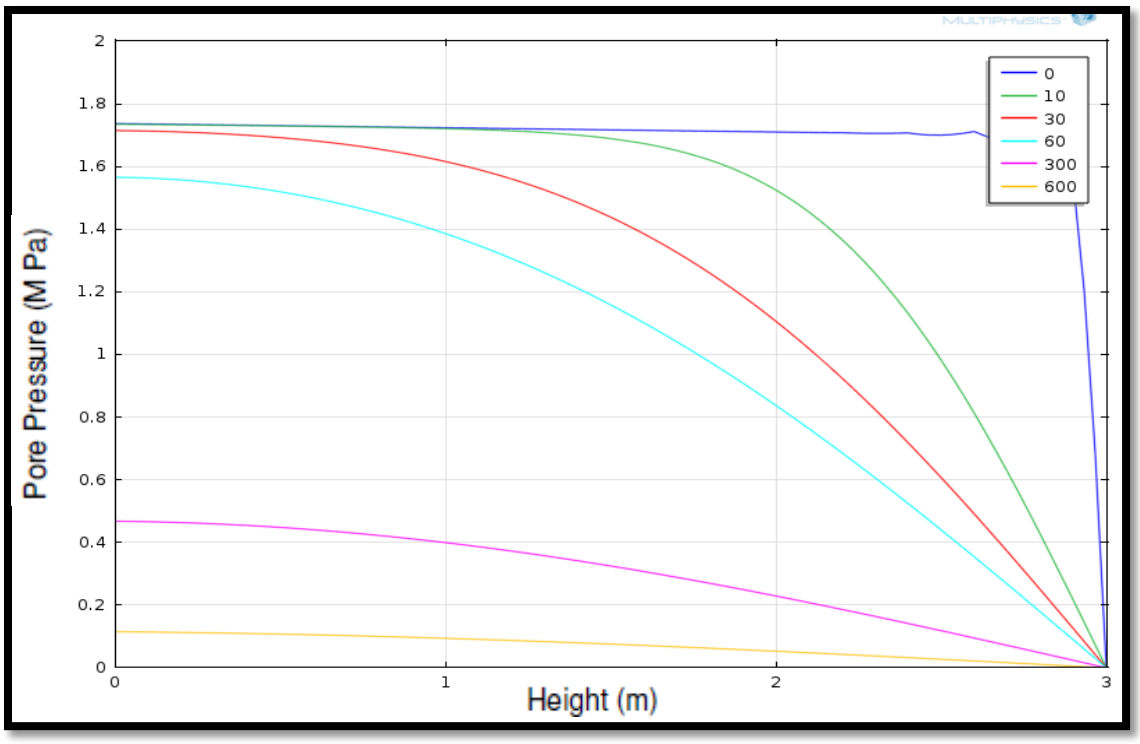

Figure 7: Pore pressure plotted in different time intervals by Ahmad (2013).

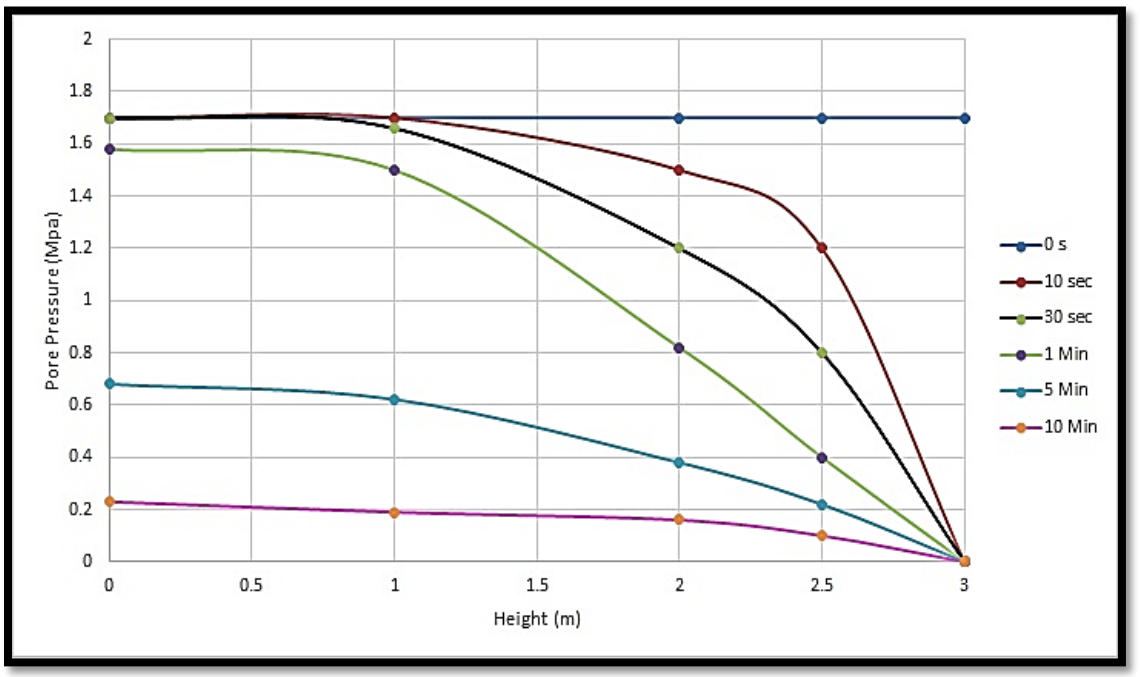

Figure 8: Pore pressure plotted in different time by Zheng (2003).

3.3 Results and Discussion

3.3.1 Undrained Condition

The vertical displacements resulting from the applied stress for undrained condition are shown in Figure 3. Figure 4 compares the vertical displacements along the height of rock sample calculated from the Zheng simulation to Comsol's solution. As we can see from Figure 4 the vertical displacement is 5×10^{-4} m for Zheng's solution and the same results for vertical displacement are obtained by Comsol simulation.

3.3.2 Drained condition

In this setup, the water is allowed to move freely from the top of rock sample. Vertical displacement along the height of the rock sample will be measured. In addition, the change in water pressure over time inside the rock sample will be calculated. Figure5 and 6 show vertical displacement with time, as we can see there is an excellent agreement between Zheng solutions and Comsol's solution. Both figures shows that maximum displacement occurs after 10- minutes .The change in pore pressure inside the rock sample over time is shown in Figure 7 and 8. Both figures shows excellent agreement between Zheng's solution and Comsol's results.

4. SENSITIVITY STUDY

4.1 Background

Hydro-mechanical description of poroelastic material is ubiquitous in several fields ranging from geology, petroleum and hydrogeology Hydro-mechanical behavior of porous materials is significantly influenced by the poroelastic parameters of porous media The purpose of carrying out a sensitivity study for rock sample is to explore the influence of various poroelastic parameters on the behavior of Hydro-mechanical coupling of porous material. Biot (1941) stated that the magnitude of coupling depends mostly on solid compressibility, fluid flow and porosity of porous material. The objective here is to detail how the rock sample is responds to various poroelastic parameters inputs. More specifically this section will demonstrate, which poroelastic parameters has significant impact on the behavior of Hydro-mechanical coupling of porous material.

4.2 Approach

The effect of poroelastic parameters on the Hydro-mechanical coupling behavior of 2-D rock sample under a constant applied pressure is presented in this chapter. In order to show the correlation between poroelastic parameters and the response of porous media for 2-D rock sample, numerical models for various poroelastic parameters are carried out on COMSOL multiphysics software 4.2.

It can be concluded that the compressibility of framework is a very important factor influencing the deformation of porous material .The compressibility can be defined as the ratio of volume change with respect to a pressure change. Biot’s theory (1941) introduce modules of

compressibility, the equation below shows that compressibility of framework is influenced by Biot coefficient and bulk modules of the solid.

$$\frac{1}{M} = \frac{\alpha}{K_u B} \tag{4.1}$$

In addition, this chapter investigate the effect of pore pressure on the behavior of porous material is investigated. The basic concept of poroelastic theory indicates that magnitude of coupling is affected by pore pressure of fluid material. Biot's theory (1944) stated 'Fluid-to-solid coupling occurs when a change in fluid pressure will produce change in volume of poroelastic material".

All the above shows that the behavior of coupling of porous material is less straightforward to predict. The goal here is to investigate the effects of Biot's coefficient, porosity and pore pressure on porous material. In order to explore the effect of poroelastic parameters, sensitivity study is carried out in this Chapter for different geomechnical models. Sensitivity study simulation is carried out with COMSOL software. In each simulation, the geomechnical parameters of the porous material are inputs into the system.

4.3 Sensitivity Analysis Description

In this section, a sensitivity analysis for 2-D rock sample.is carried out. As part of this analysis study, a fully coupled Hydro-mechanical model based on COMSOL Multiphysics is developed. In each model run, the geomechnical parameters of the porous material are inputs into the system. The boundary condition is constant for all models. The top boundary of rock sample will be free to move, horizontally and the bottom will be constrained.

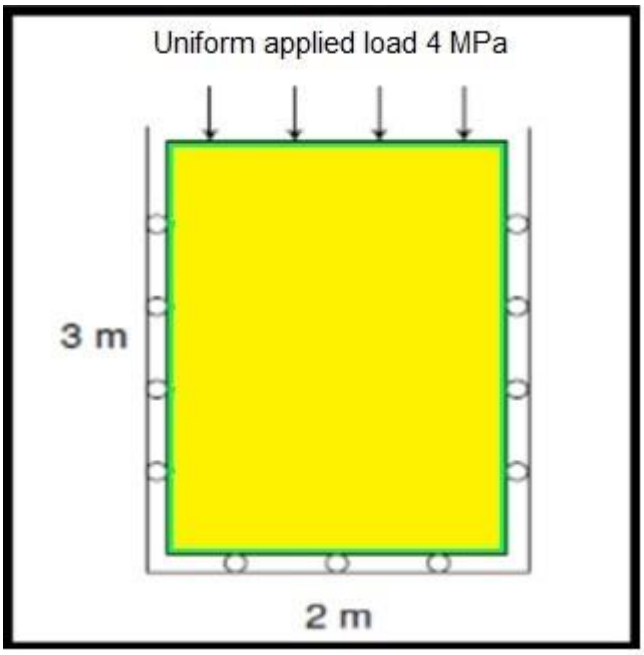

Figure 9: 2-D Rock sample dimensions.

A set of poroelastic parameters are required to develop a sensitivity analysis of 2-D rock sample. As mentioned on Chapter two poroelastic parameters are primarily determined from drained moduli E, υ, K and K_u. These parameter are sufficient to compute Biot's coefficient α and compressibility of the framework. Detournay and Cheng (1993) provided a table of several values for sandstone rock parameters. Detournay and Cheng (1993) parameters will be used as an entry inputs for each simulation case. In each model run, vertical displacement and pore pressure change with time for rock sample will be determined.

The following poroelastic parameters will be used in each simulation run

1. Constant Parameters:

- Material type: Sandstone rock sample from Detournay and Cheng (1993).
- Dimensions of the sample: 2×3 m.

- Rock Density: 2000 Kg/m3
- The applied uniform load :4 M Pa
- Oil Density : 940Kg/m3

2. Controlling parameters:

- Range of Porosity: 0.22, 0.2, 0.18
- Biot's coefficient : 0.83, 0.79, 0.74
- Initial pore pressure: 2, 1.8, 1.6 M Pa.

In summary, the correlation between poroelastic parameters and the response of 2D rock sample will be studied for various poroelastic parameters. In the next section, nine models for different controlling parameters are presented

4.4 Sensitivity analysis and discussion

4.4.1 Effects of Biot's Coefficients on Pore Pressure and Displacement

To explore the effects of Biot's coefficient on the behavior of 2-D rock sample, the vertical displacement and pore pressure changes over time for a range of Biot's coefficient values α= (0.83, 0.79, and 0.74) are presented in detail in this section. Table 2 summarizes the list of parameters for the three Biot's coefficient values. It should be noted that average parameters values were used to calculate Biot's coefficient. In the next section, the results of the effects of the three Biot's coefficient values will be shown. In order to illustrate the role of Biot's coefficient for a specific point on the rock sample, a compiled figure for vertical displacement and pore pressure change with time for point at (x=0, y=3) will be presented

Table 2: List of parameters for Effects of Biot's Coefficients

Effects of Biot's Coefficients on Pore Pressure and Displacement			
Case 1-Biot's coefficient α=0.83			
Constant parameters		Measurements	
Average Young's Modules	1.47E04 Mpa	Change in pore pressure with time	$\frac{\partial p}{\partial t}$ –
Average Poisson's Ratio	0.18	Vertical displacement	$\frac{\partial(\nabla . \mathrm{u})}{\partial \mathrm{t}}$
Porosity	0.2	$\frac{1}{\mathrm{m}} \frac{\partial \mathrm{p}}{\partial \mathrm{t}} - \nabla \left(\frac{\mathrm{k}}{\mu} (\nabla \mathrm{p} - \rho \mathrm{fg} \nabla \mathrm{z}) \right) = - \alpha \frac{\partial(\nabla . \mathrm{u})}{\partial \mathrm{t}}$	
Average Biot's module	1.30E04 Mpa		
Case 2-Biot's coefficient α=0.79			
Constant parameters		Measurements	
Average Young's Modules	1.47E04 Mpa	Change in pore pressure with time	$\frac{\partial p}{\partial t}$ –
Average Poisson's Ratio	0.18	Vertical displacement	$\frac{\partial(\nabla . \mathrm{u})}{\partial \mathrm{t}}$
Porosity	0.2	$\frac{1}{\mathrm{m}} \frac{\partial \mathrm{p}}{\partial \mathrm{t}} - \nabla \left(\frac{\mathrm{k}}{\mu} (\nabla \mathrm{p} - \rho \mathrm{fg} \nabla \mathrm{z}) \right) = - \alpha \frac{\partial(\nabla . \mathrm{u})}{\partial \mathrm{t}}$	
Average Biot's module	1.30E04 Mpa		
Case 3-Biot's coefficient α=0.74			
Constant parameters		Measurement	
Average Young's Modules	1.47E04 Mpa	Change in pore pressure with time	$\frac{\partial p}{\partial t}$ –
Average Poisson's Ratio	0.18	Vertical displacement	$\frac{\partial(\nabla . \mathrm{u})}{\partial \mathrm{t}}$
Porosity	0.2	$\frac{1}{\mathrm{m}} \frac{\partial \mathrm{p}}{\partial \mathrm{t}} - \nabla \left(\frac{\mathrm{k}}{\mu} (\nabla \mathrm{p} - \rho \mathrm{fg} \nabla \mathrm{z}) \right) = - \alpha \frac{\partial(\nabla . \mathrm{u})}{\partial \mathrm{t}}$	
Average Biot's module	1.30E04 Mpa		

Biot's coefficient α=0.83 results

Figure 10 illustrates the vertical displacement at ground surface (x=0, y=3m) after 10 minutes from when the water starts to move out of the top boundary. Figure 13 shows the pressure distribution inside the rock sample. It can be concluded that pressure is almost zero after 10 minutes which corresponds to the creep settlement. Additionally, a 3-D mesh map for the rock sample is presented to show displacement along the height of rock sample plotted in different time intervals.

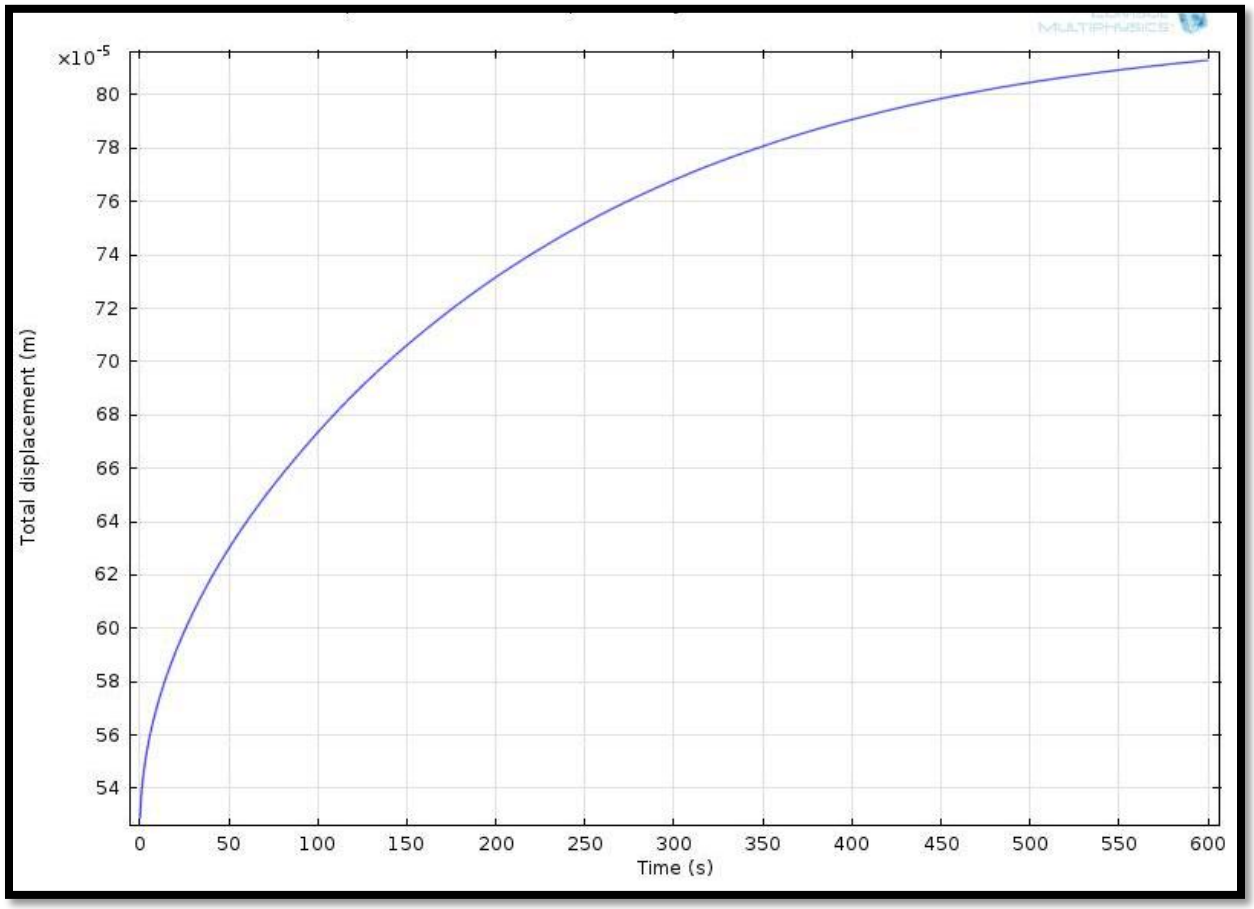

Figure 10: Vertical displacement (m) at point (x=0, y=3) of the rock sample vs. time (α=0.83).

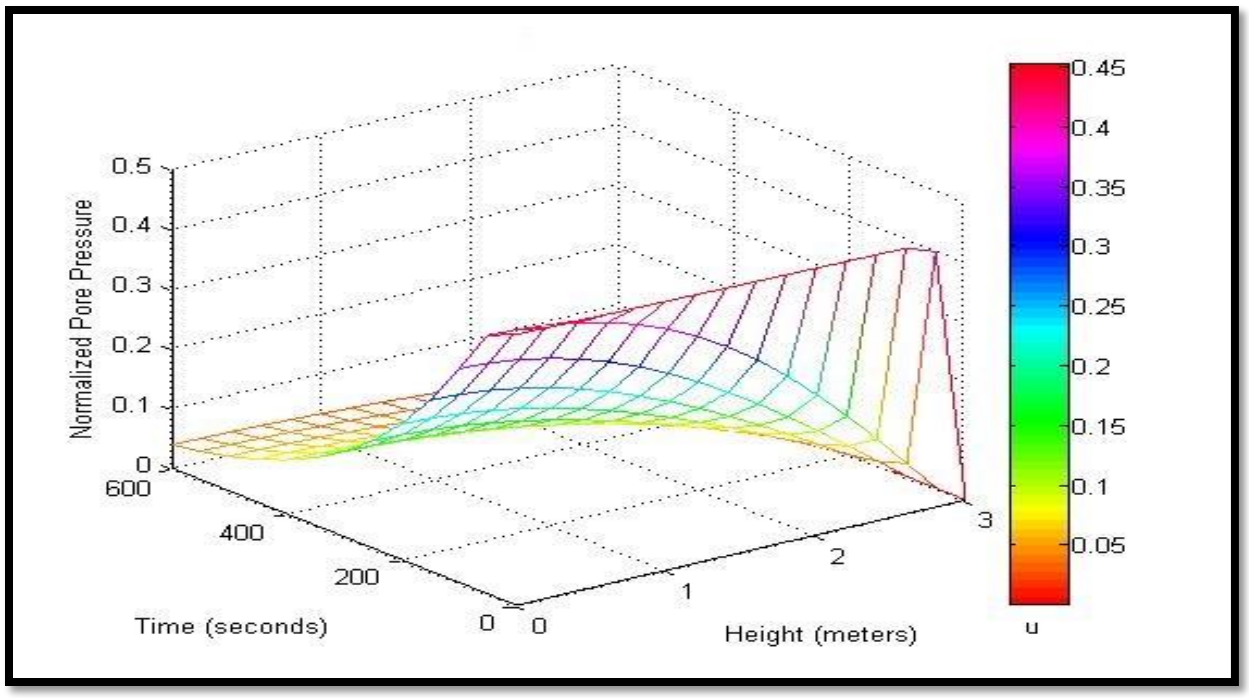

Figure 11 : 3-D mesh for Pore pressures inside the sample plotted in different time intervals (α=0.83).

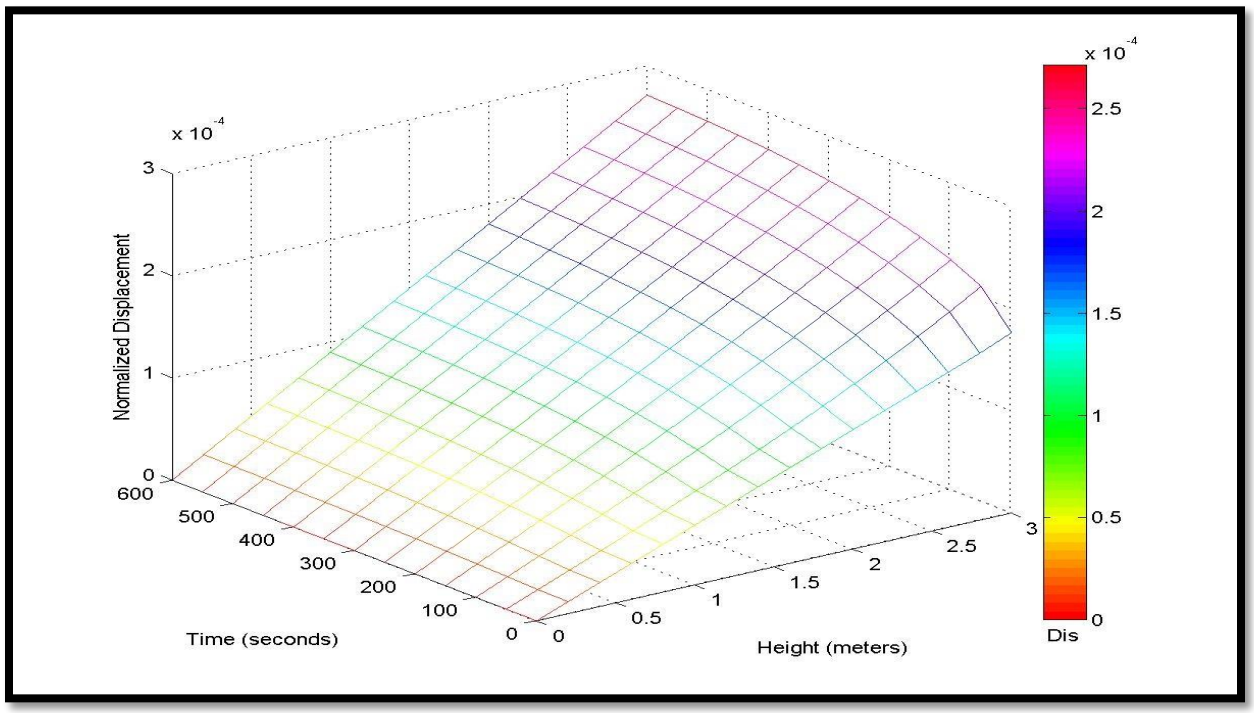

Figure 12: 3-D mesh map for displacement along the height of the sample (α=0.83).

Biot's coefficient α=0.79 results

Figure 13 shows the vertical displacement for point at ground surface (x=0, y=3m). Figure 14 shows the normalized pore pressure distribution for Biot's coefficient (0.79) plotted in different time intervals. It can be concluded that pore pressure dissipation from the top boundary of the rock still have same trend as the previous Biot's coefficient (0.83), however, the amount of dissipation is higher in case of Biot's coefficient of (0.83) Figure 15 shows 3-D displacement map to demonstrate displacement rate along the height of rock with time.

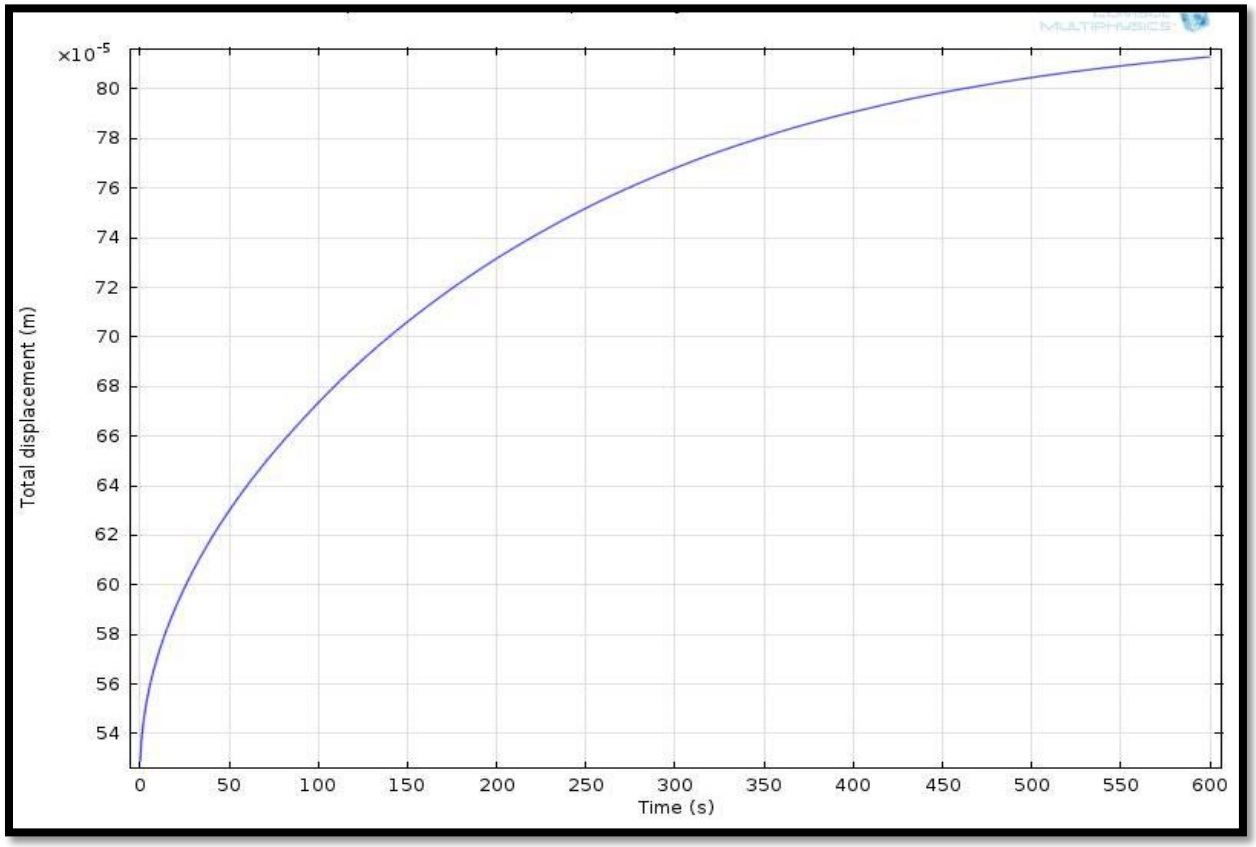

Figure 13: Vertical displacement (m) at point (x=0, y=3) of the rock sample vs. time (α=0.79).

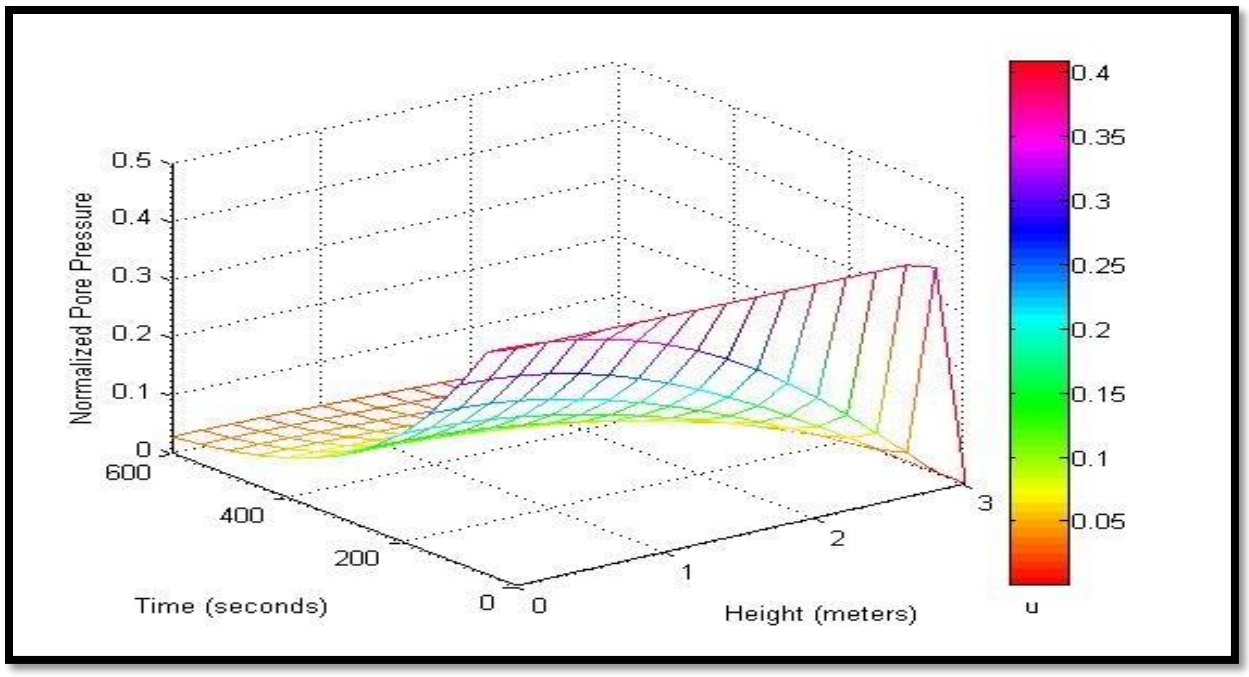

Figure 14: 3-D mesh for Pore pressures inside the sample plotted vs time (α=0.79).

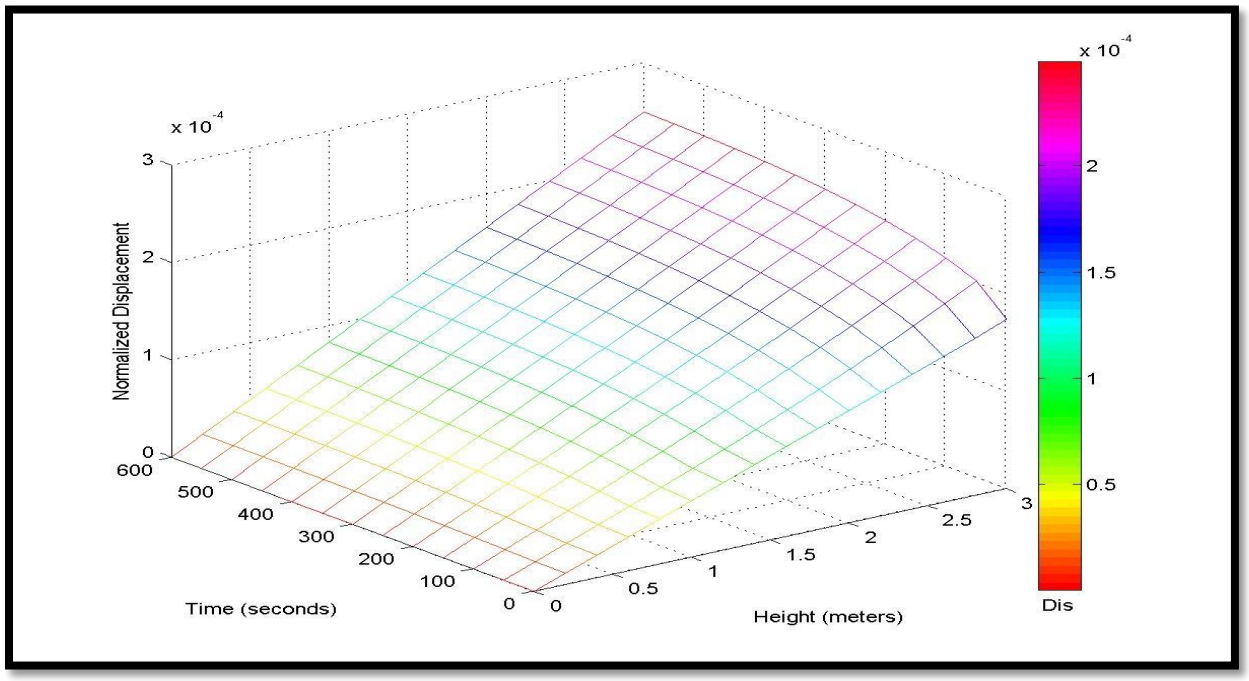

Figure 15: 3-D mesh map for displacement along the height of the sample (α=0.79).

Biot's coefficient α=0.74 results

Figure 16 illustrates the vertical displacement at ground surface (x=0, y=3m) after 10 minutes from when the water starts to move out of the top boundary. Figure 17 shows the pressure distribution inside the rock sample. It can be concluded that pressure is almost zero after 10 minutes which corresponds to the creep settlement. Figure18 shows 3-D for normalized displacement map to demonstrate displacement rate along the height of rock with time.

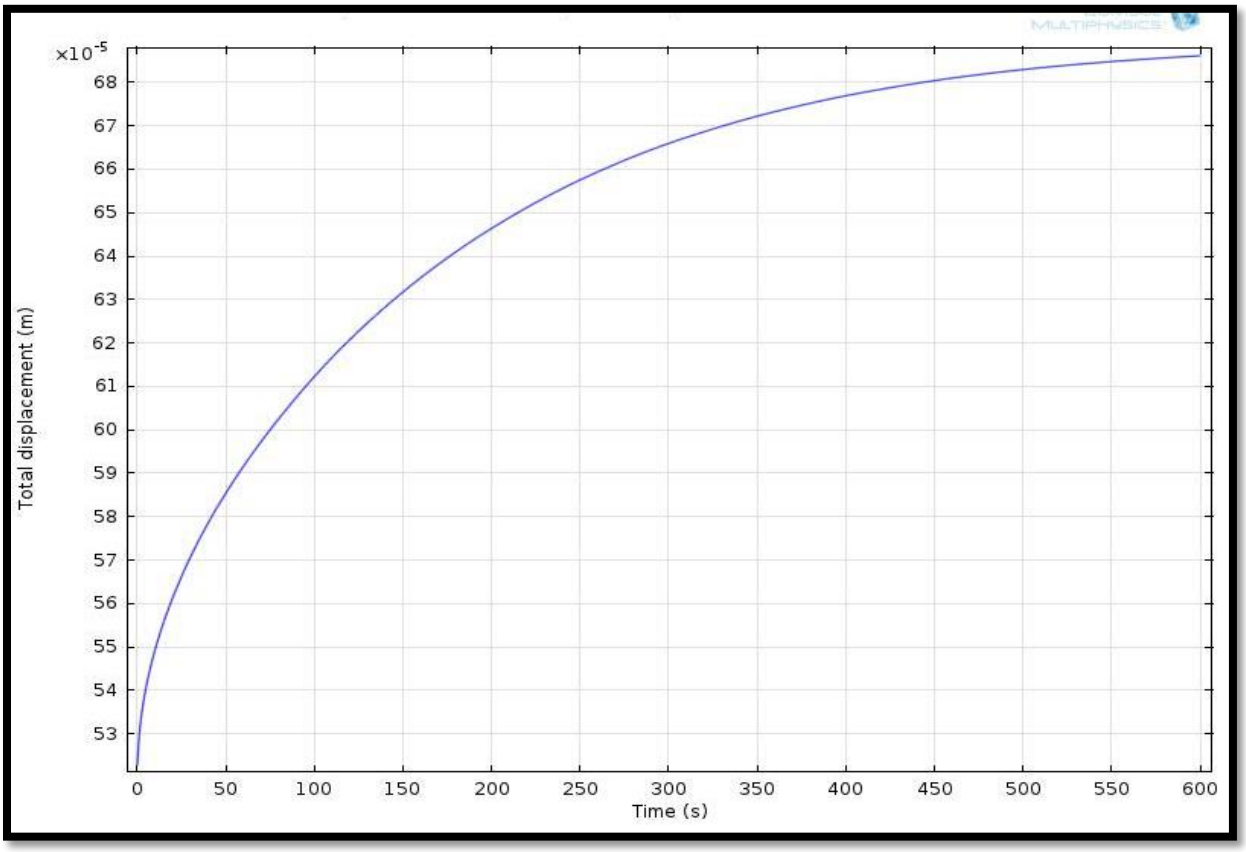

Figure 16: Vertical displacement (m) at point (x=0, y=3) of the rock sample vs. time (α=0.74).

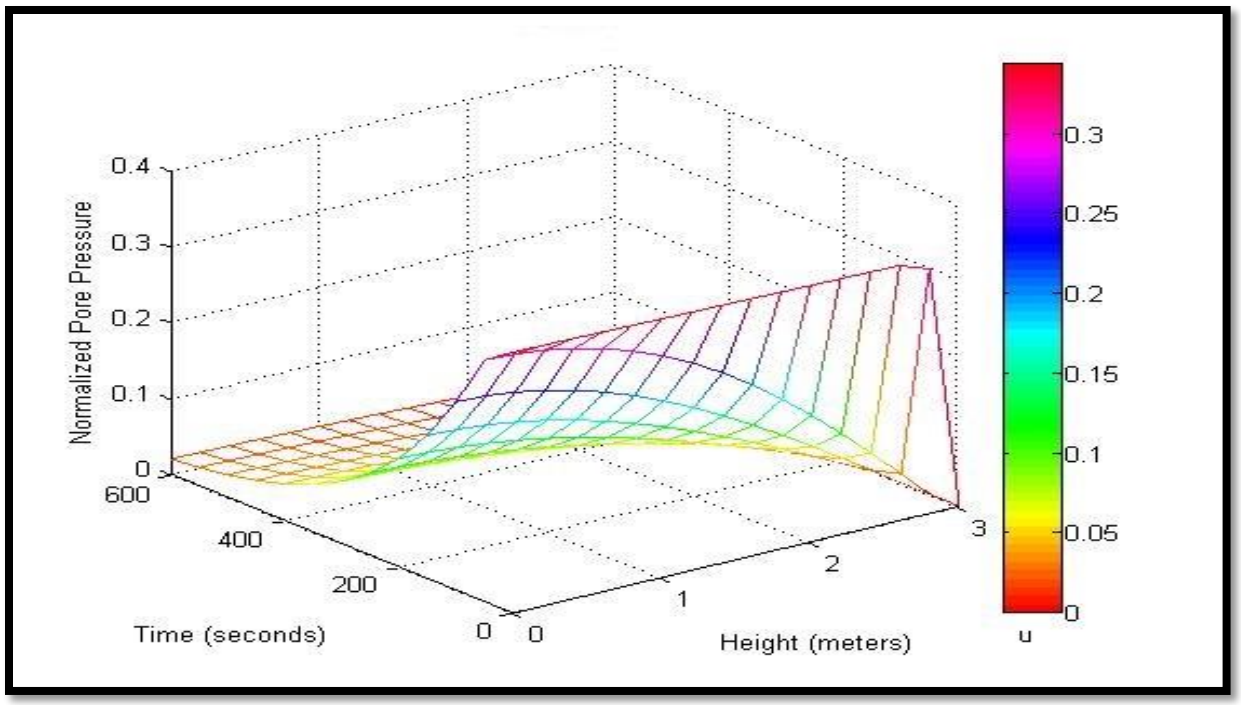

Figure 17: 3-D mesh for Pore pressures inside the sample plotted vs time (α=0.74).

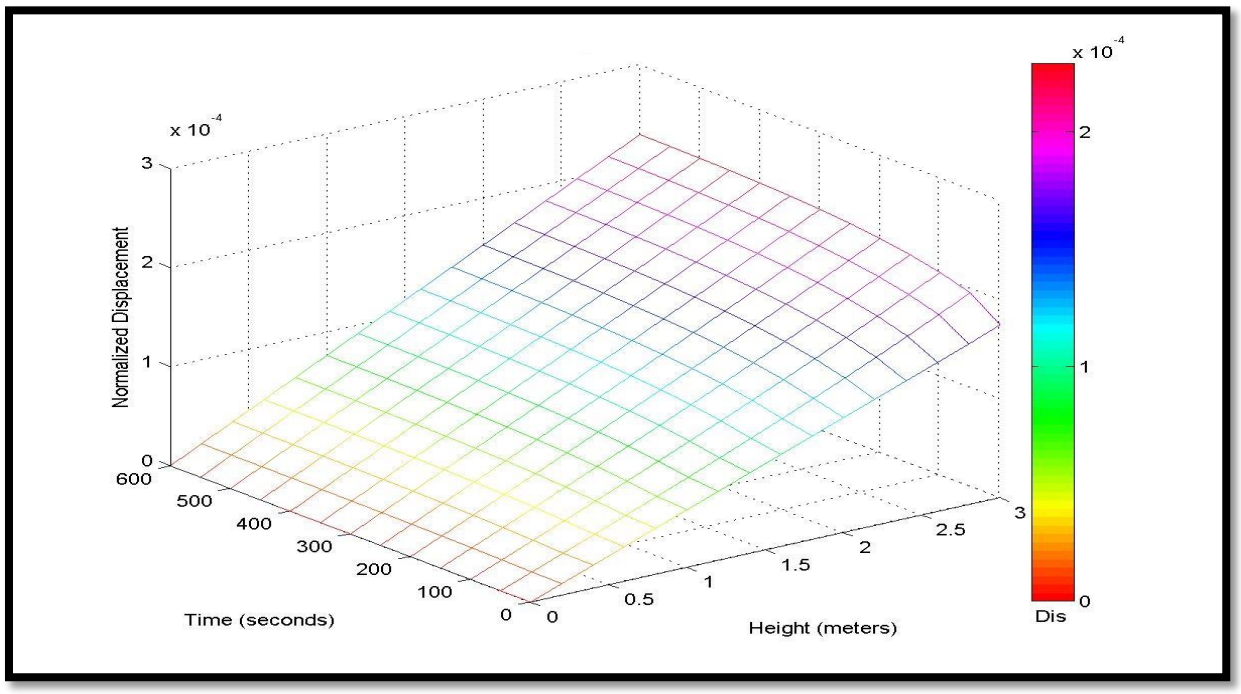

Figure 18: 3-D mesh map for displacement along the height of the sample (α=0.74).

Summary of the Effects of Biot's Coefficient on Rock Sample Behavior

To show the role of Biot's coefficient (α) on the behavior of rock sample under the same load, changes on vertical displacement and pore pressure for range of Biot's coefficient are shown on Figure 19 and Figure 20 . It can be concluded from Figure 20 that reducing Biot's coefficient, the final vertical displacement are more sensitive. However, at the initial run of model for different Biot's coefficient values (0.83, 0.79 and 0.74)) the displacement has same values. It can be concluded that by increasing the Biot's coefficient value the final displacement will be increased.as well. Despite the fact that Biot's coefficient influence the displacement, the pore pressure is less effected by Biot's coefficient as shown in Figure 20.

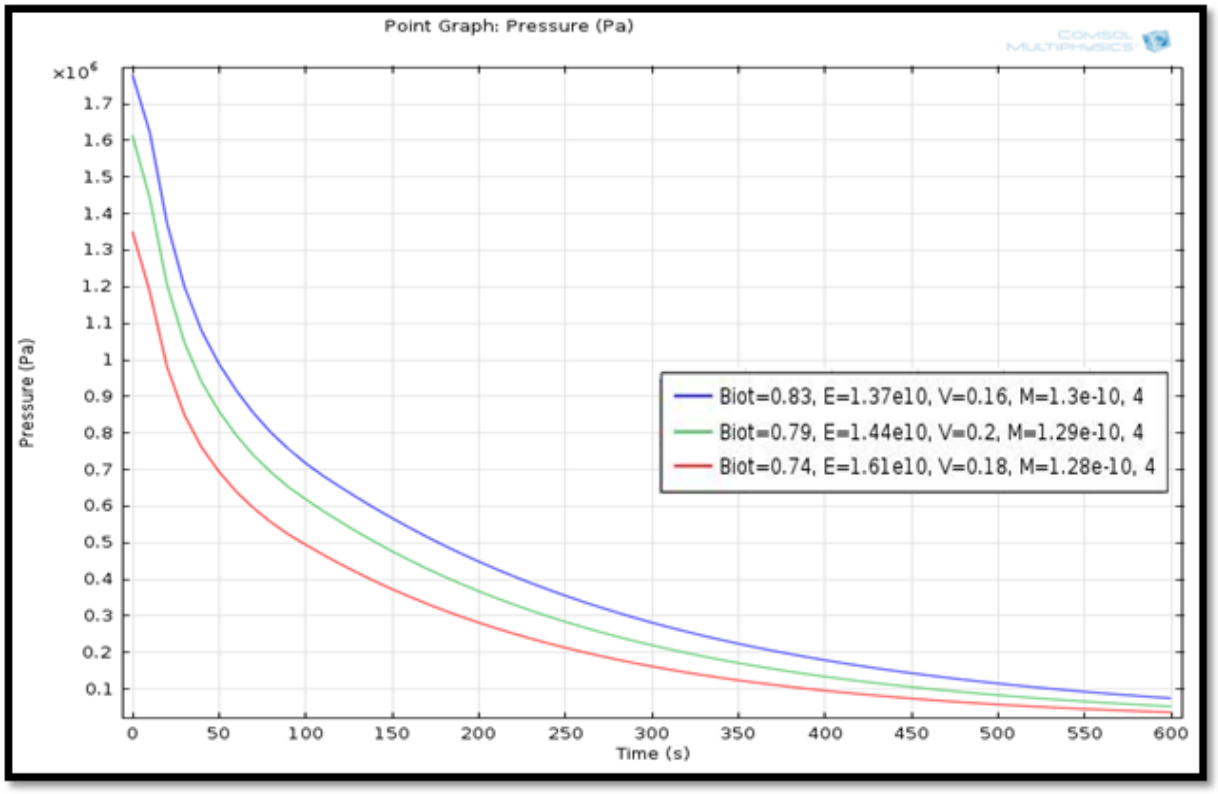

Figure 19: Pore pressure Vs time for point (x=0,y=3) for different Biot's values.

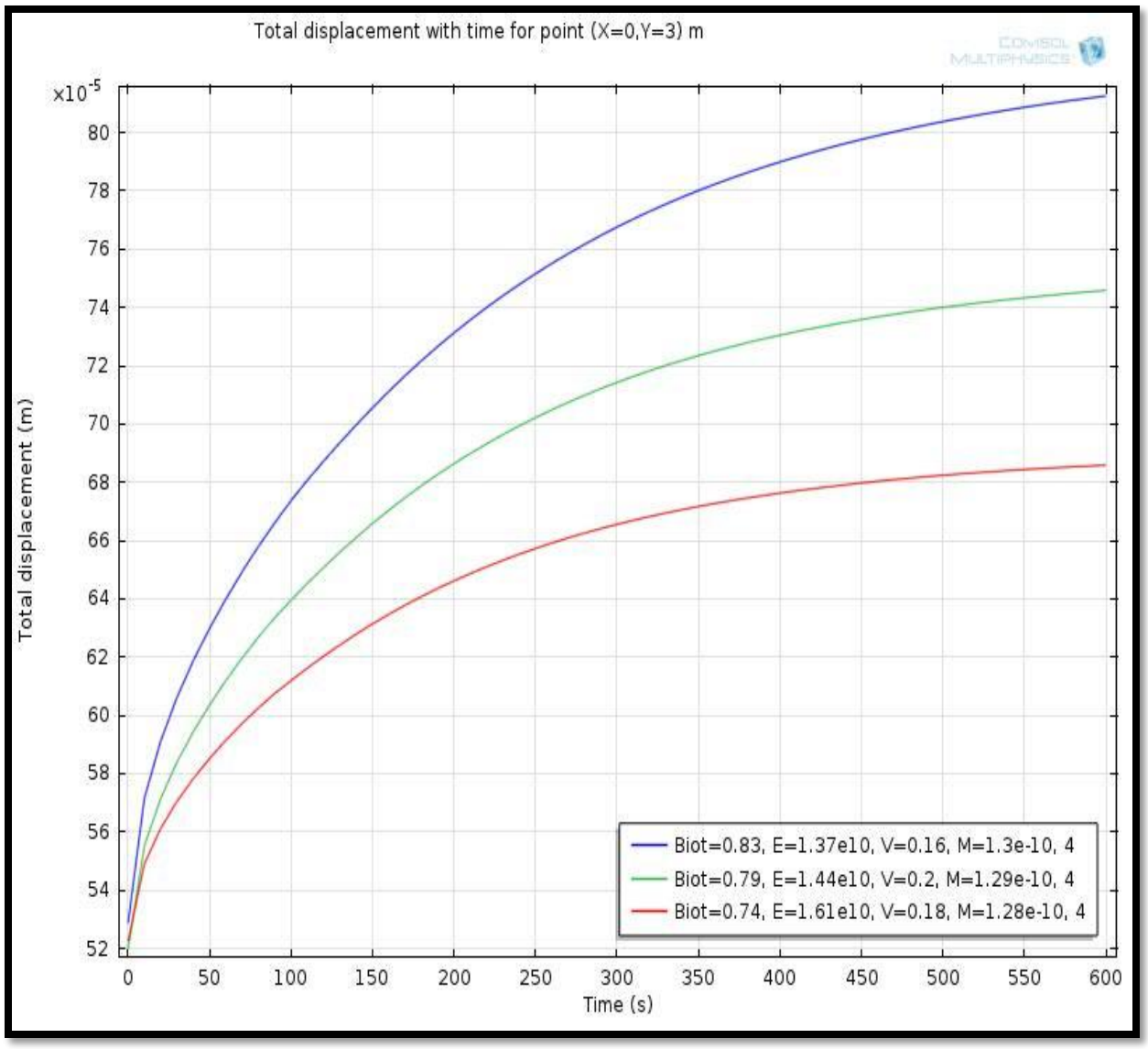

Figure 20: Vertical Displaement Vs time for point (x=0,y=3) for different Biot's values.

4.4.2 Effects of Initial pore pressure on Pore Pressure changes and Displacement

In this study, we examined the effect of the initial fluid pressure on the behavior of 2-D rock sample. In each model run, a range of pore pressure values are introduced to show the respond of the rock sample. Table 3 summarizes the list of parameters for the different pore pressure values. Initial pore pressure values presented in this study are taken so that Skempton's coefficient B will not change dramatically. In order to determine the role of initial pore pressure on the behavior of rock sample , a compile figure for vertical displacement and pore pressure change with time for point at (x=0, y=3) will be presented

Table 3: poroelastic paramters for different initial pore pressure.

Effects of Pore Pressure on Rock sample			
Case 1.Initial pore pressure :2E06 Mpa			
Constant parameters		Measurements	
Young's Modules	1.47E04 MPa	Change in pore pressure with time	$\frac{\partial p}{\partial t}$ –
Poisson's Ratio	0.2	Vertical displacement	$\frac{\partial(\nabla . u)}{\partial t}$
Porosity	0.2	$\frac{1}{m}\frac{\partial p}{\partial t} - \nabla\left(\frac{k}{\mu}(\nabla p - \rho f g \nabla z)\right) = -\alpha\frac{\partial(\nabla . u)}{\partial t}$	
Biot's coefficient	0.79		
Case 2.Initial pore pressure :1.6e6 Mpa			
Constant parameters		Measurements	
Young's Modules	1.47E04 MPa	Change in pore pressure with time	$\frac{\partial p}{\partial t}$ –
Poisson's Ratio	0.2	Vertical displacement	$\frac{\partial(\nabla . u)}{\partial t}$
Porosity	0.2	$\frac{1}{m}\frac{\partial p}{\partial t} - \nabla\left(\frac{k}{\mu}(\nabla p - \rho fg\nabla z)\right) = -\alpha\frac{\partial(\nabla . u)}{\partial t}$	
Biot's coefficient	0.79		
Case 3.Initial pore pressure :1.2e6 Mpa			
Constant parameters		Measurement	
Young's Modules	1.47E04 MPa	Change in pore pressure with time	$\frac{\partial p}{\partial t}$ –
Poisson's Ratio	0.2	Vertical displacement	$\frac{\partial(\nabla . u)}{\partial t}$
Porosity	0.2	$\frac{1}{m}\frac{\partial p}{\partial t} - \nabla\left(\frac{k}{\mu}(\nabla p - \rho fg\nabla z)\right) = -\alpha\frac{\partial(\nabla . u)}{\partial t}$	
Biot's coefficient	0.79		

Initial pore pressure 2e6 Mpa results

Figure 21 demonstrates the relation between vertical displacement versos time at the ground surface (x=0, y=3m) after for initial pore pressure value of 2e6 Mpa. Figure 22 shows the normalized displacement along the height of the rock sample. It can be concluded that displacement trend has the maximum value at 10 minutes. Figure 23 shows 3-D mesh map for pore pressure distribution along the height plotted in different time intervals

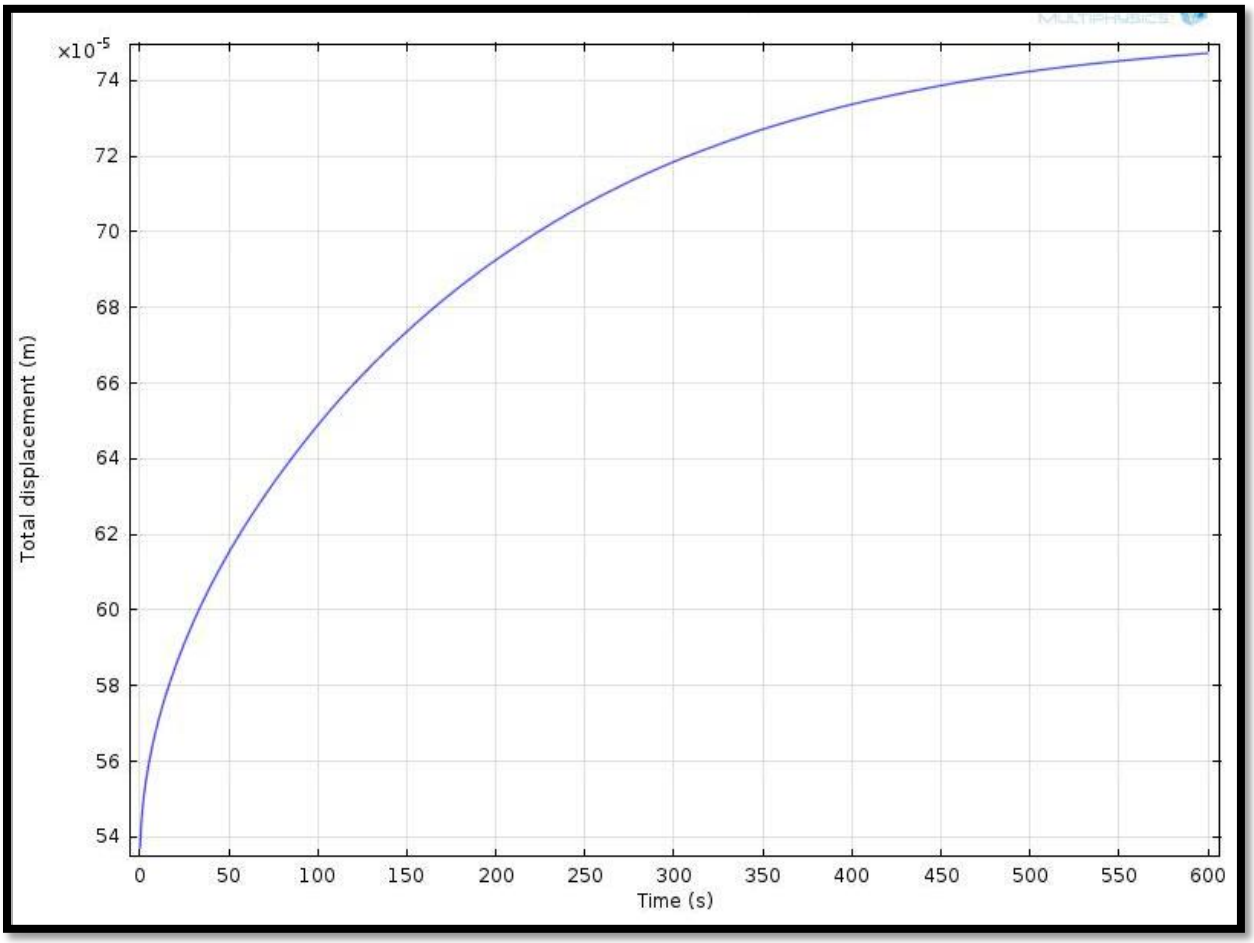

Figure 21: Vertical displacement (m) at point (x=0, y=3) of the rock sample vs. time (p_0=2e6 Mpa).

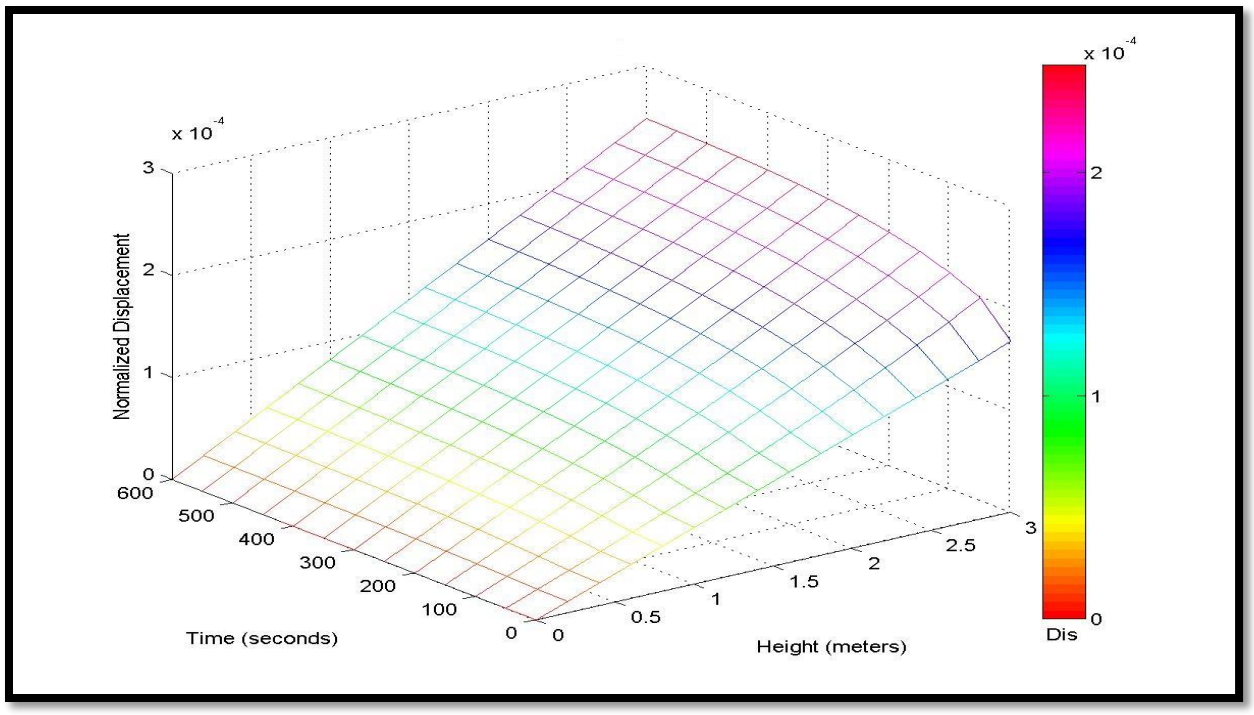

Figure 22: 3-D mesh map for displacement along the height of the sample (p_0=2e6 Mpa).

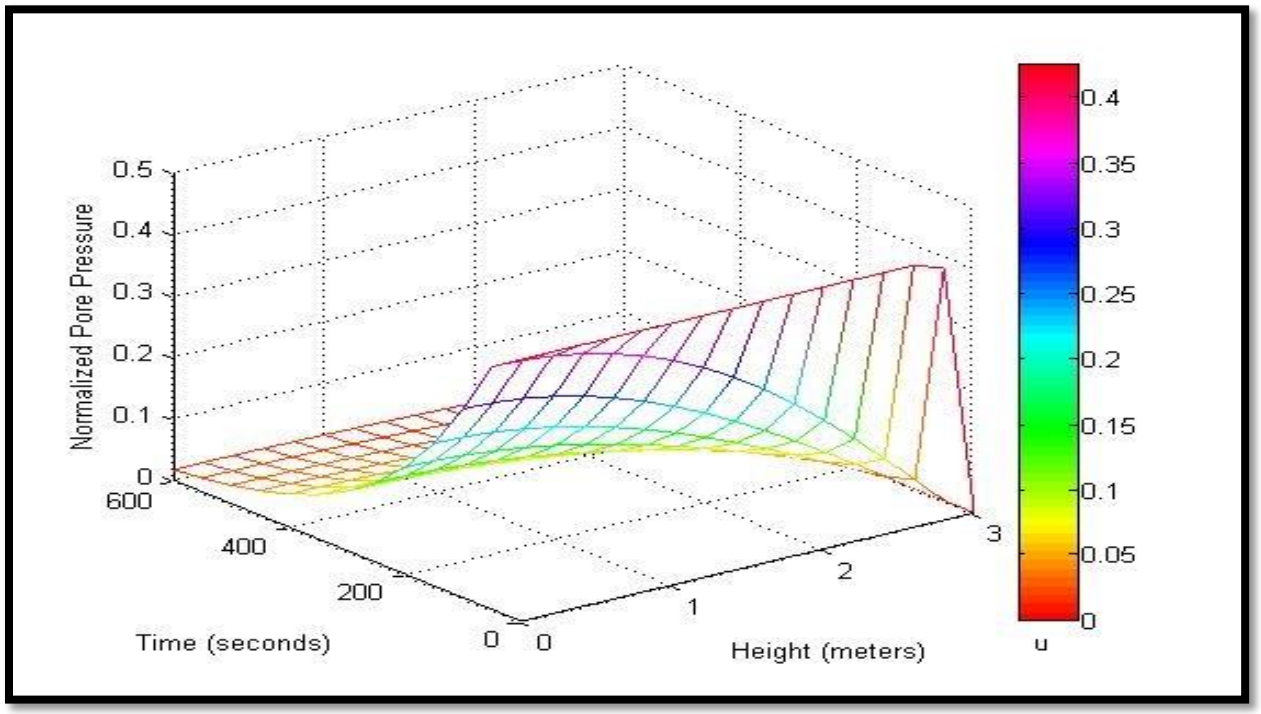

Figure 23: 3-D mesh map for pore pressure distrubtion along the height plotted (p_0=2e6 Mpa)

Initial pore pressure 1.8e6 Mpa results

Results for initial pressure with 1.8e6 Mpa value is presented in this section. The correlation between displacement and initial pore pressure is shown in Figure 24. Despite the decrease of the initial pore pressure compared with previous case, it can be seen from the Figure 24 that the vertical displacement value is not affected by changing initial pore pressure value. Figure 25 illustrate the vertical displacement in 3-D of the rock sample plotted in different time intervals. Figure 26 shows the pressure distribution along the height of the rock sample.

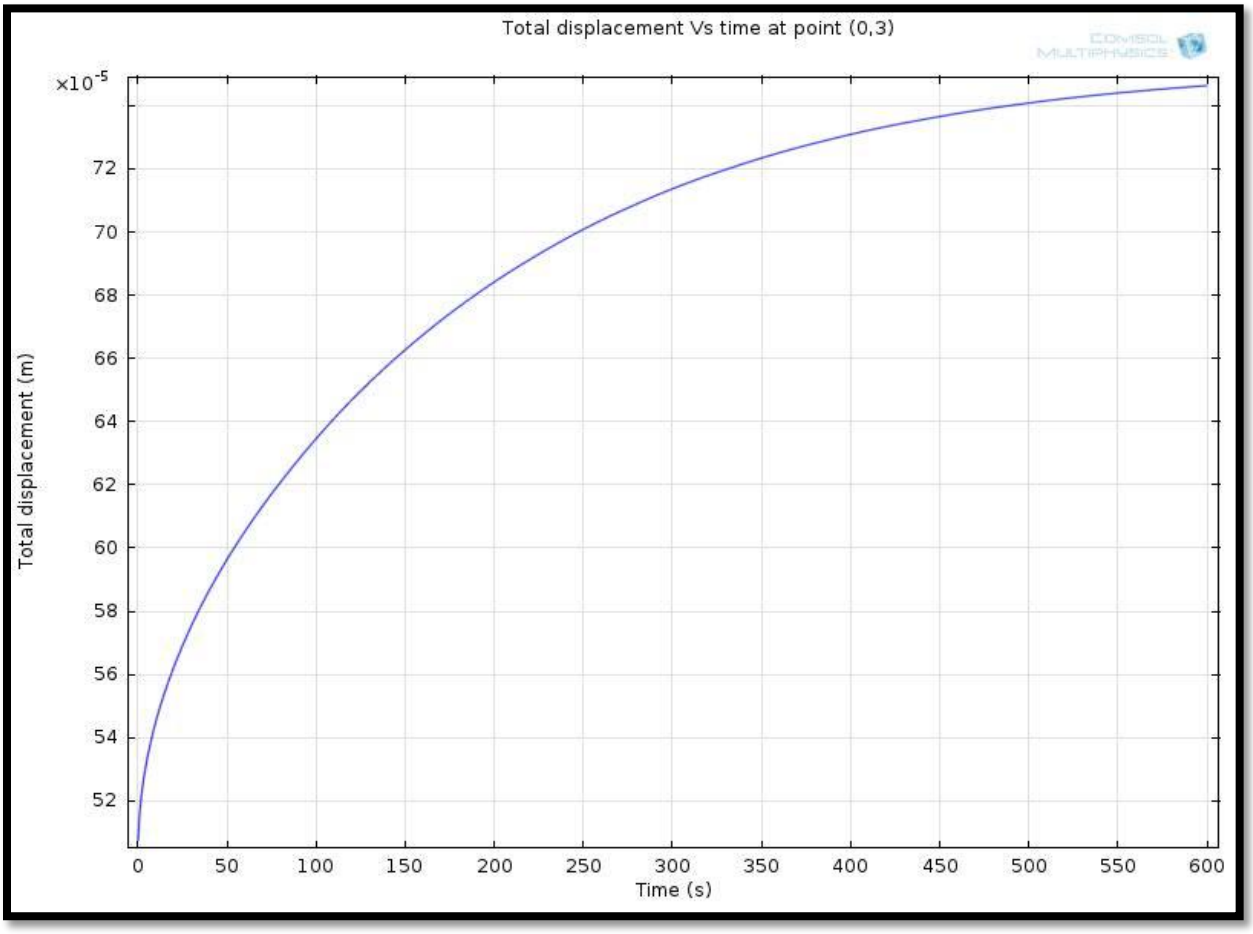

Figure 24: Vertical displacement (m) at point (x=0, y=3) of the rock sample vs. time (p_0=1.8e6 Mpa).

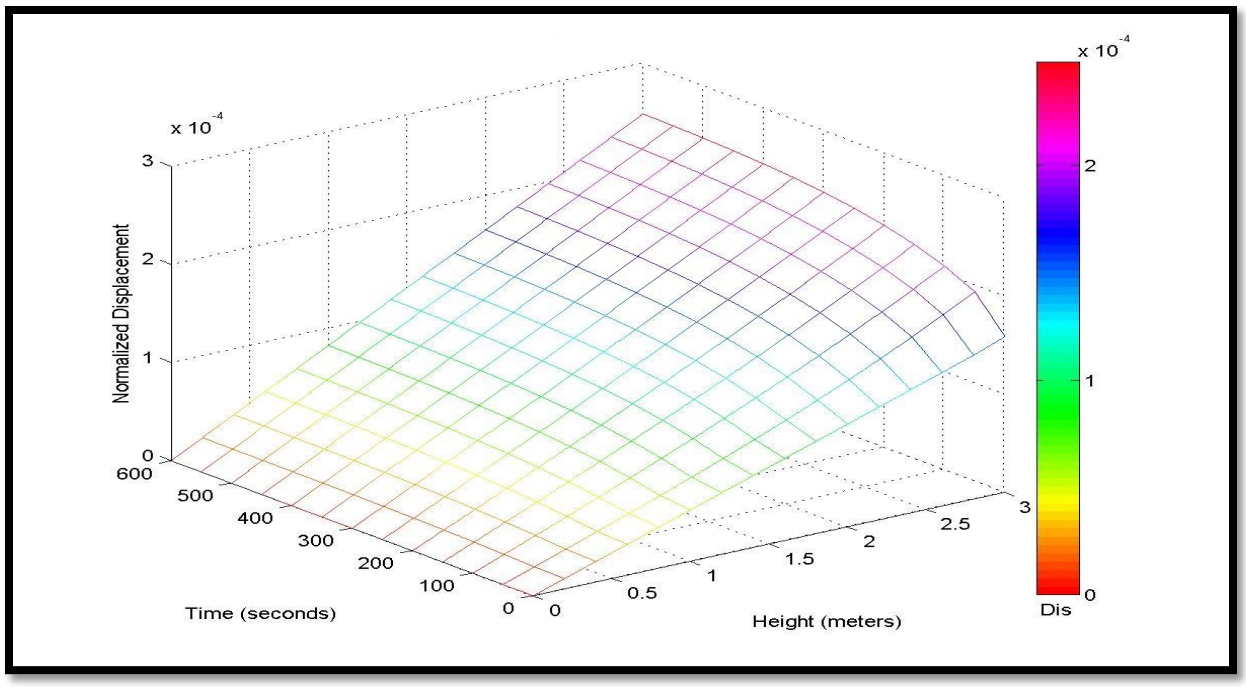

Figure 25: 3-D mesh map for displacement along the height of the sample (p_0=1.8e6 Mpa).

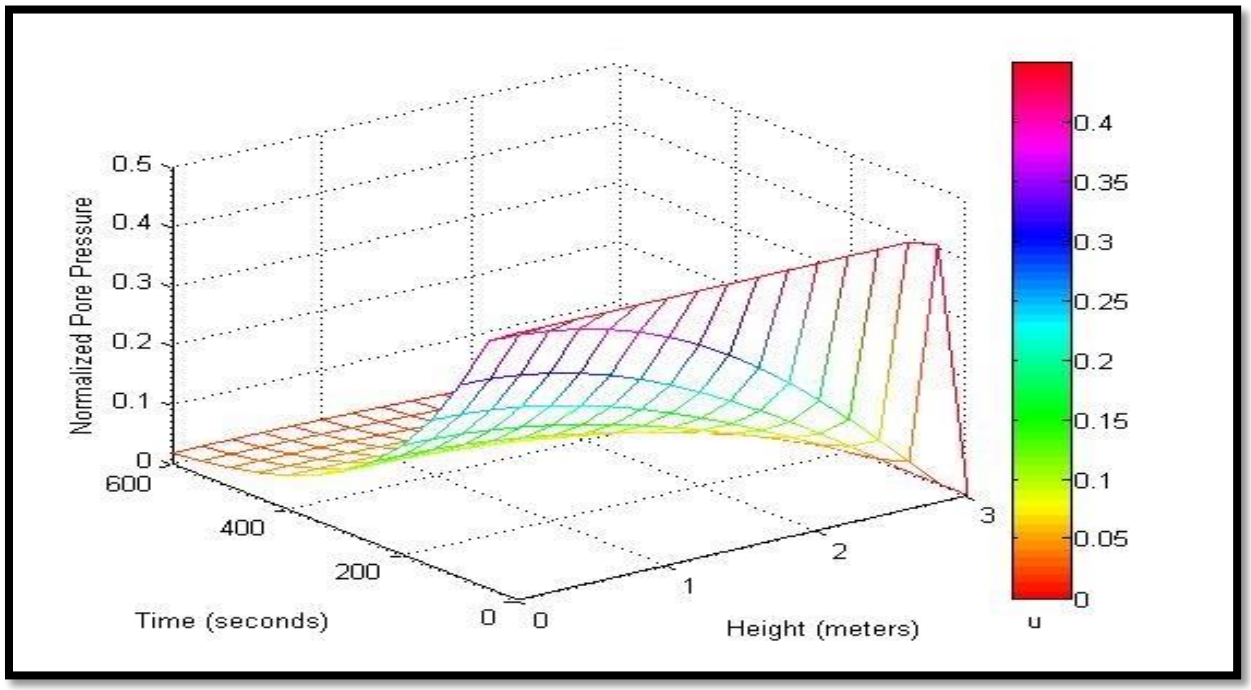

Figure 26: 3-D mesh map for pore pressure distrubtion along the height plotted (p_0=1.8e6 Mpa).

Initial pore pressure 1.6e6 Mpa results

Figure 27 illustrates the vertical displacement at ground surface (x=0, y=3m) after 10 min from water starts to move out the top boundary. Figure 28 illustrate the vertical displacement along the height of rock sample plotted in different time intervals. Figure 29 shows the pressure distribution inside the rock sample. It can be concluded that pressure is almost zero after 10 minutes which corresponding to the creep settlement.

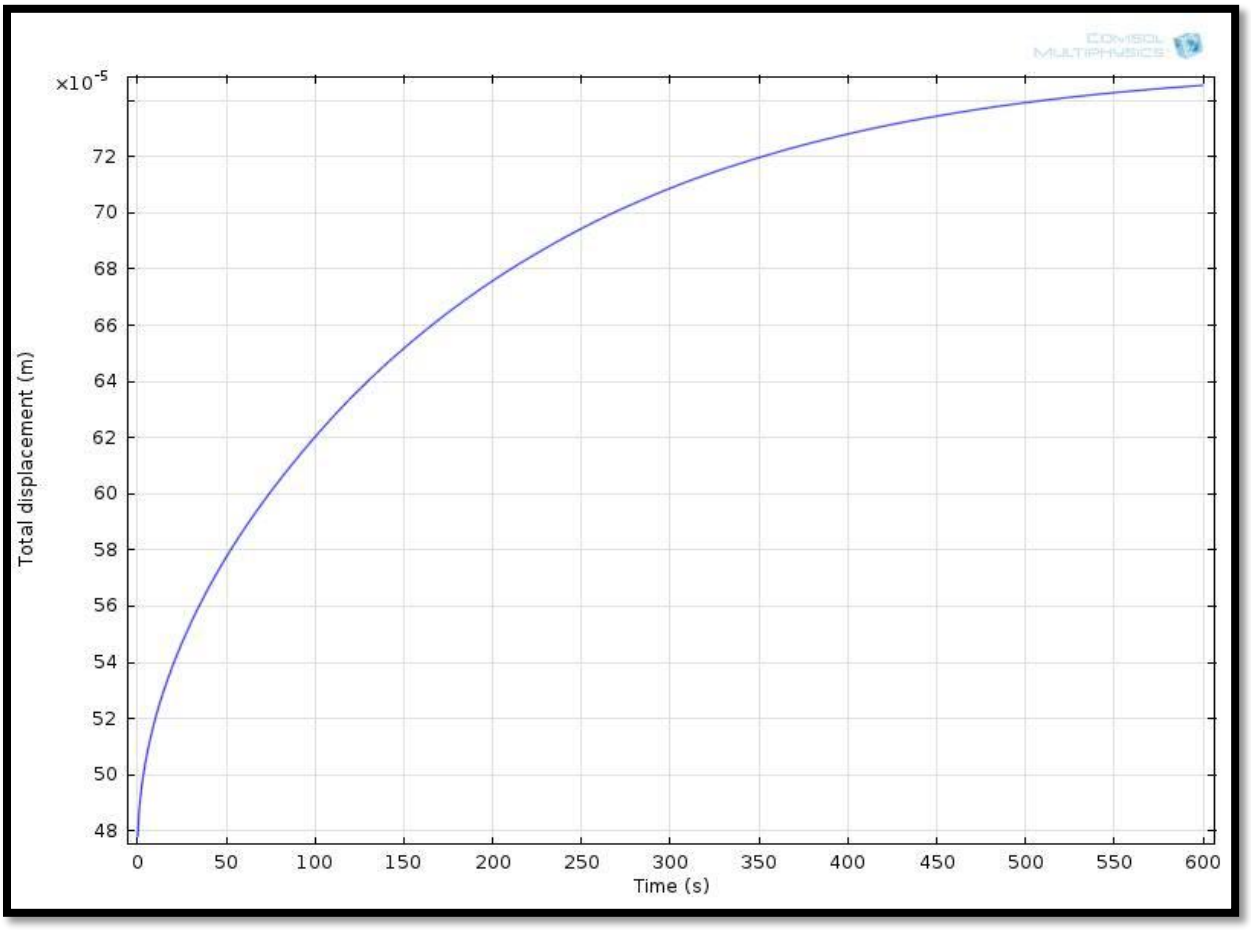

Figure 27: Vertical displacement (m) at point (x=0, y=3) of the rock sample vs. time (p_0=1.6e6 Mpa).

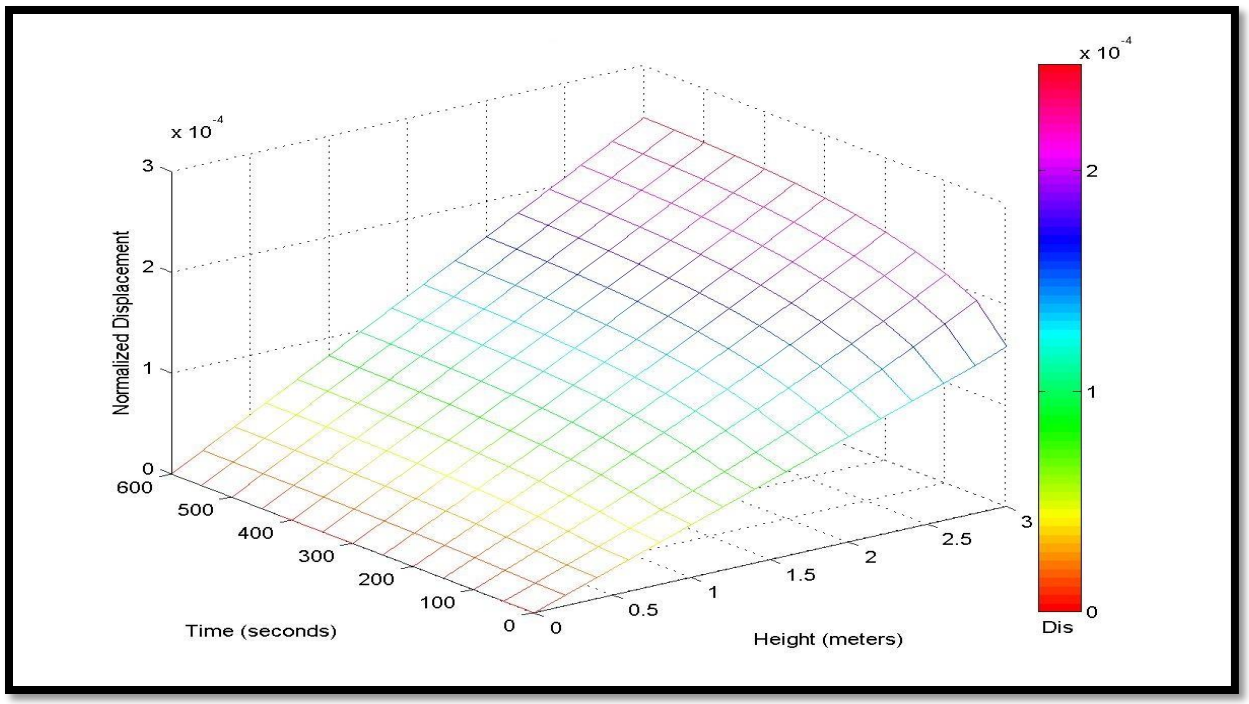

Figure 28: 3-D mesh map for displacement along the height of the sample (p_0=1.6e6 Mpa).

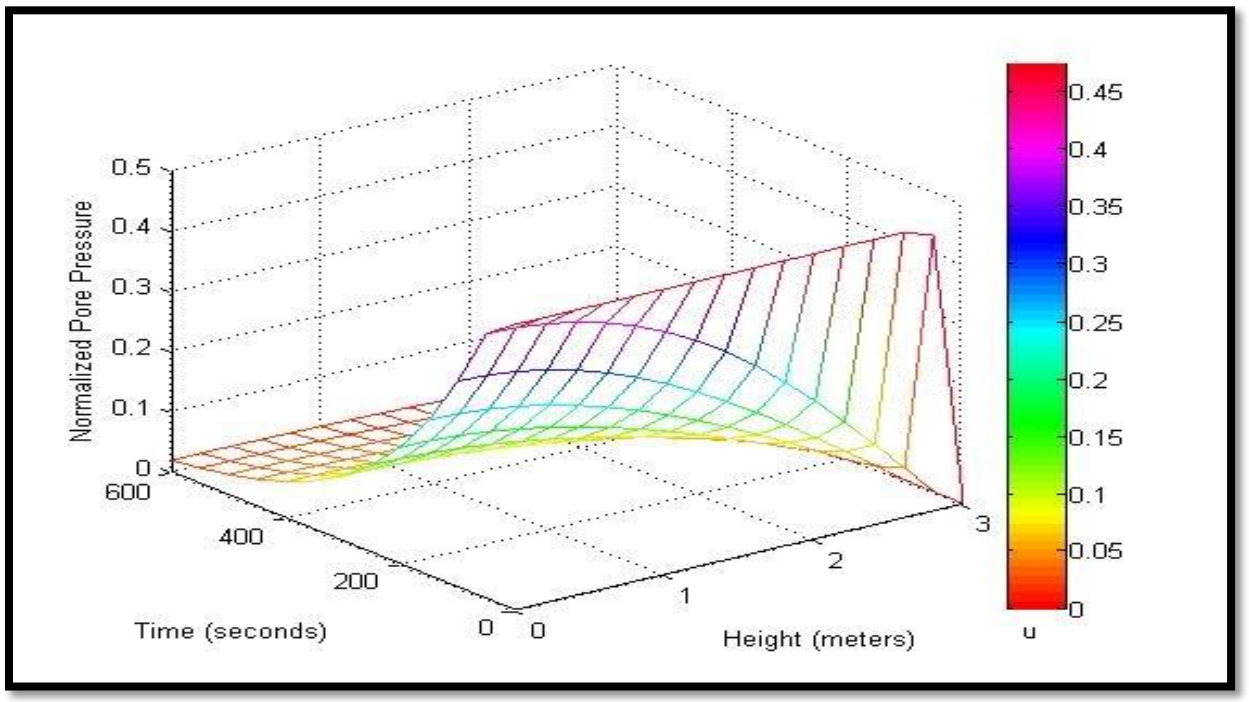

Figure 29: 3-D mesh map for pore pressure distrubtion along the height plotted (p_0=1.6e6 Mpa).

Summary of the Effects of Initial Pore Pressure Value on Rock Sample Behavior

The premise of this study is to show the impact of initial pore pressure values on the behavior of rock sample while holding other poroelastic parameters constant. The initial values of pore pressure are inputs to model to with a special attention to the value of Skempton's coefficient (B). It can be noted from Figure 30 that displacement of rock sample is less sensitive to initial pore pressure changes Despite the fact that the magnitude of total displacement corresponding to pore pressure change for three cases is not large , their effect on the initial displacement are quite significant Figure 31. Shows that water pressure is almost the same after 5 minutes.

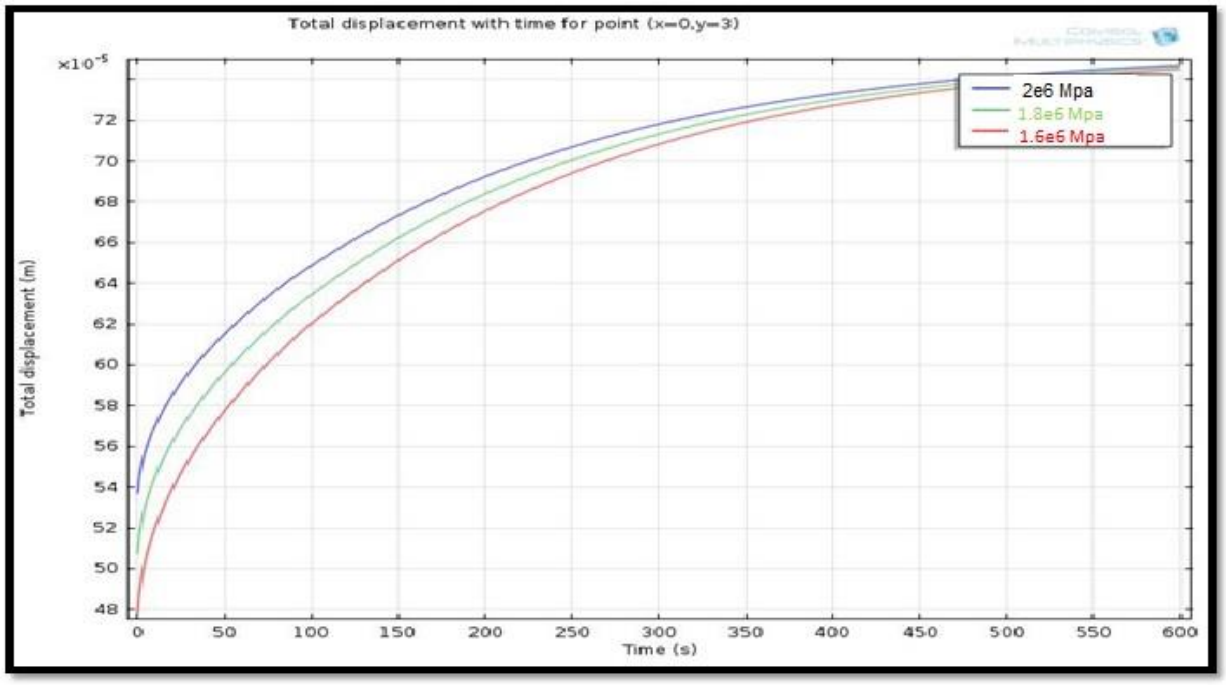

Figure 30: Vertical displacement pressure Vs time for point (x=0,y=3) for different initial pore pressure.

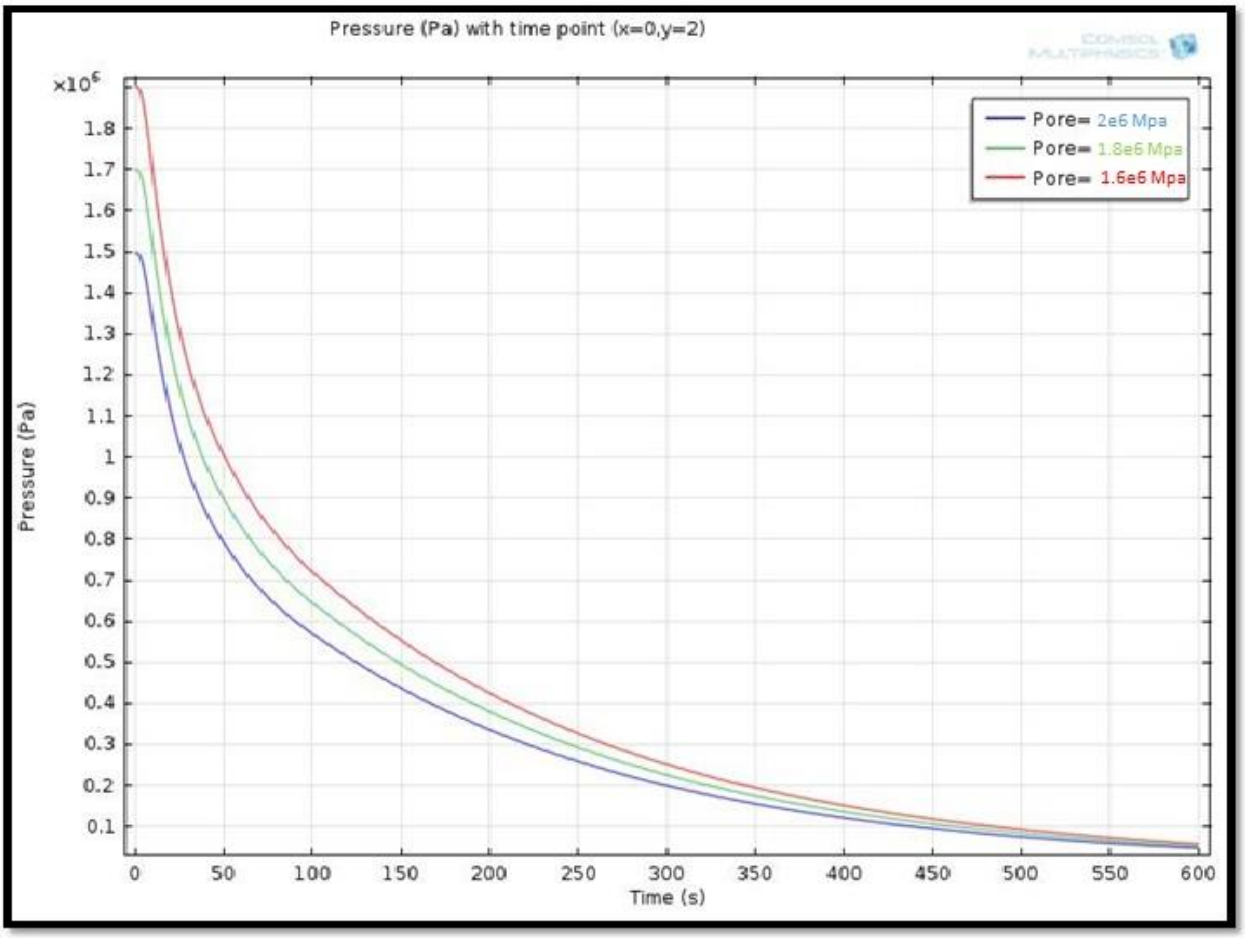

Figure 31: Pore pressure Vs time for point (x=0,y=3) for different initial pore pressure.

4.4.3 Effects of porosity on Pore Pressure changes and Displacement

In this section, we studied the effect of different porosity values on the behavior of 2-D rock sample. In each model run, a range of porosity values are introduced to show the sensitivity of the rock sample to these values. Table 4 summarizes the list of parameters for the different pore pressure values. In order to carry out the sensitivity study the effect of changing porosity values on Biot's modulus is neglected .Initial pore pressure value presented in this study is equal to 1.6e6 Mpa, so Skempton's coefficient B is constant throughout the model run.

Table 4: Poroelastic paramters for different Porosities values

Effects of porosity on Pore Pressure on Pore Pressure and Displacement change			
Case 1.Porosity(0.22)			
Constant parameters		Measurements	
Young's Modules	1.47E04 MPa	Change in pore pressure with time	$\frac{\partial p}{\partial t} -$
Poisson's Ratio	0.2	Vertical displacement	$\frac{\partial(\nabla . \mathrm{u})}{\partial \mathrm{t}}$
Biot's coefficient	0.79	$\frac{1}{\mathrm{m}} \frac{\partial \mathrm{p}}{\partial \mathrm{t}} - \nabla \left(\frac{\mathrm{k}}{\mu} (\nabla \mathrm{p} - \rho \mathrm{fg} \nabla \mathrm{z}) \right) = - \alpha \frac{\partial(\nabla . \mathrm{u})}{\partial \mathrm{t}}$	
Biot's module	1.30E04 Mpa		
Case 2-Porosity (0.20)			
Constant parameters		Measurements	
Young's Modules	1.47E04	Change in pore pressure with time	$\frac{\partial p}{\partial t} -$
Poisson's Ratio	0.2	Vertical displacement	$\frac{\partial(\nabla . \mathrm{u})}{\partial \mathrm{t}}$
Biot's coefficient	0.79	$\frac{1}{\mathrm{m}} \frac{\partial \mathrm{p}}{\partial \mathrm{t}} - \nabla \left(\frac{\mathrm{k}}{\mu} (\nabla \mathrm{p} - \rho \mathrm{fg} \nabla \mathrm{z}) \right) = - \alpha \frac{\partial(\nabla . \mathrm{u})}{\partial \mathrm{t}}$	
Biot's module	1.30E04 Mpa		
Case 3. Porosity (0.18)			
Constant parameters		Measurement	
Young's Modules	1.47E04	Change in pore pressure with time	$\frac{\partial p}{\partial t} -$
Poisson's Ratio	0.2	Vertical displacement	$\frac{\partial(\nabla . \mathrm{u})}{\partial \mathrm{t}}$
Biot's coefficient	0.79	$\frac{1}{\mathrm{m}} \frac{\partial \mathrm{p}}{\partial \mathrm{t}} - \nabla \left(\frac{\mathrm{k}}{\mu} (\nabla \mathrm{p} - \rho \mathrm{fg} \nabla \mathrm{z}) \right) = - \alpha \frac{\partial(\nabla . \mathrm{u})}{\partial \mathrm{t}}$	
Biot's module	1.30E04 Mpa		

Porosity value of (0.22) Results

In Figure 32, the change in displacement from time 0 to 10 minutes for porosity value of (0.22). The plot shows upward trend of vertical displacement with time for point at (x=0, y=3m) after 10 min. Figure 33 shows 3-D map for the pressure distribution inside the rock sample. It can be concluded that pressure is value of 0.1 Mpa after 10 minutes. Figure 34 demonstrate the vertical displacement along the height of rock sample plotted in 3-D mesh.

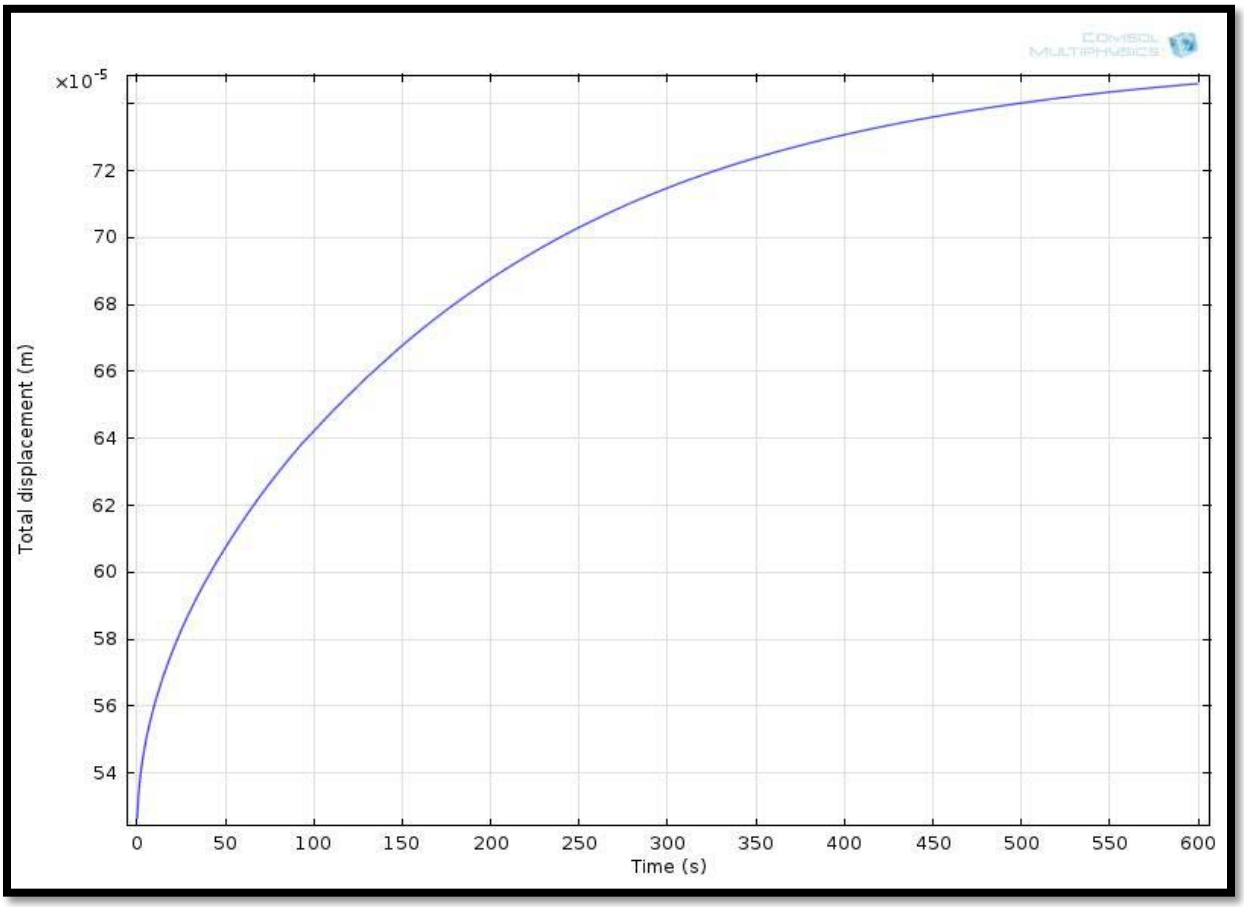

Figure 32: Vertical displacement (m) at point (x=0, y=3) of the rock sample vs. time for Porosity(0.22).

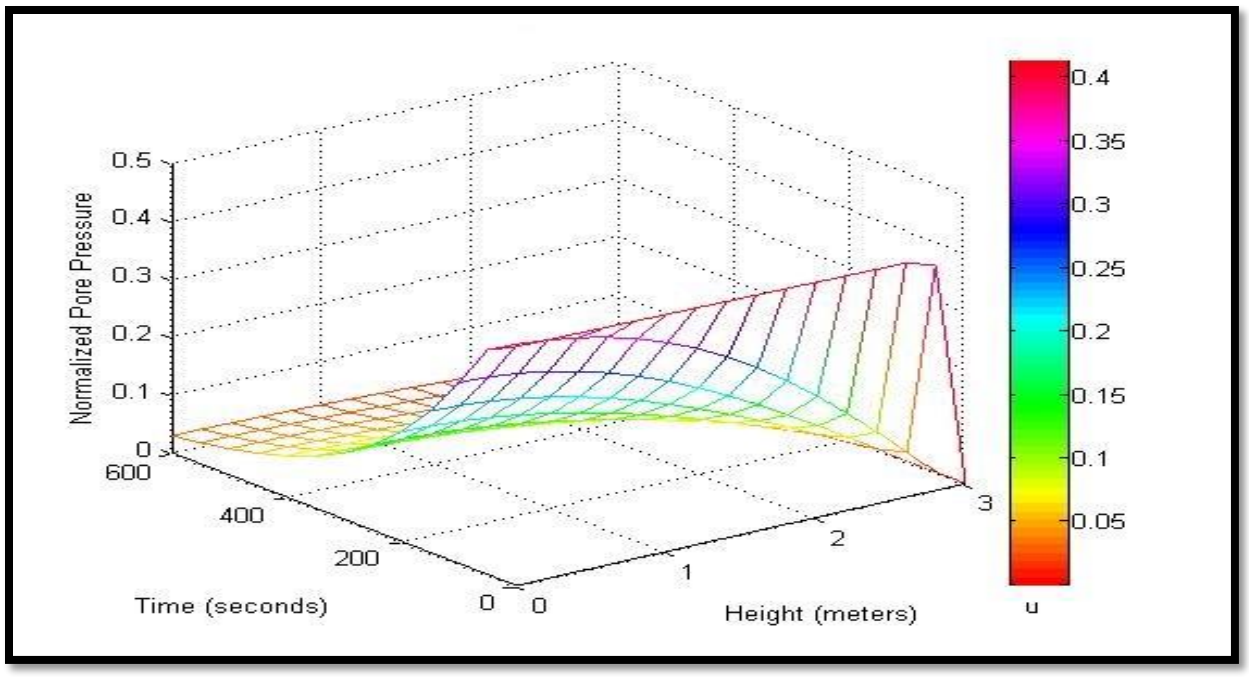

Figure 33: 3-D mesh for Pore pressures inside the sample plotted vs time for Porosity(0.22).

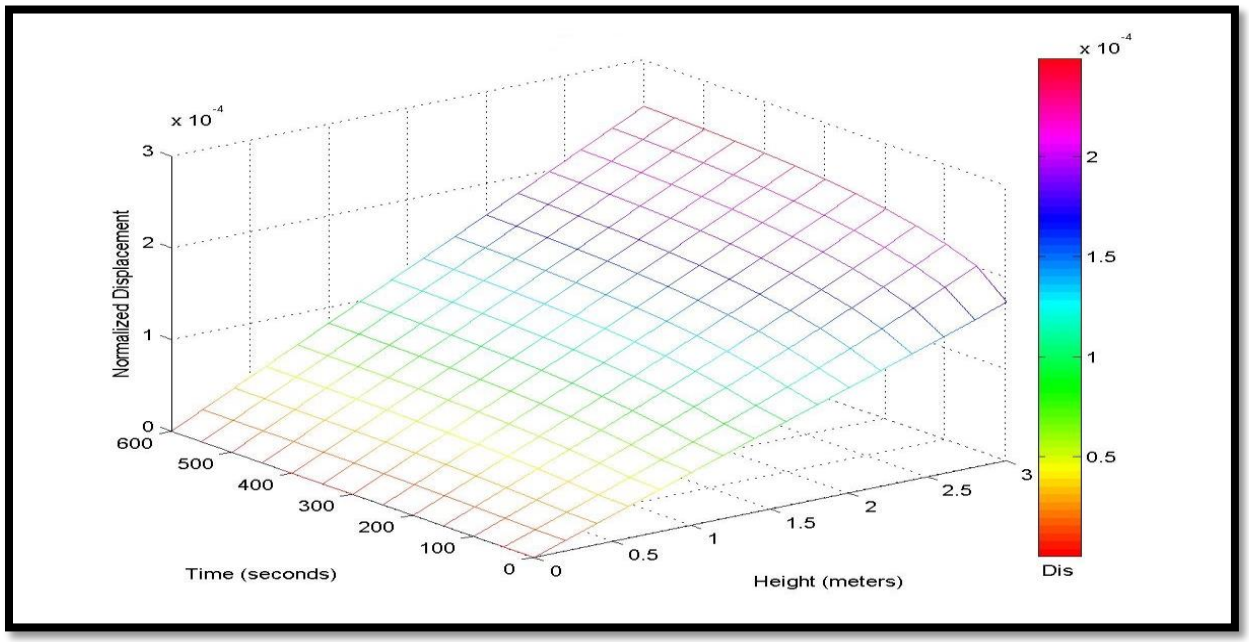

Figure 34 : 3-D mesh for vertical displacement (m) of the rock sample vs. time.for Porosity(0.22).

Porosity of value (0.2) Results

Figure 35 shows the respond of rock sample for porosity value of (0.20). The Plot shows upward trend of vertical displacement with time for point at (x=0, y=3m) after 10 min. Figure 36 shows 3-D map for the pressure distribution inside the rock sample. It can be concluded that pressure is value of 0.1 M Pa after 10 minutes. Figure 37 demonstrate the vertical displacement along the height of rock sample plotted in different time intervals.

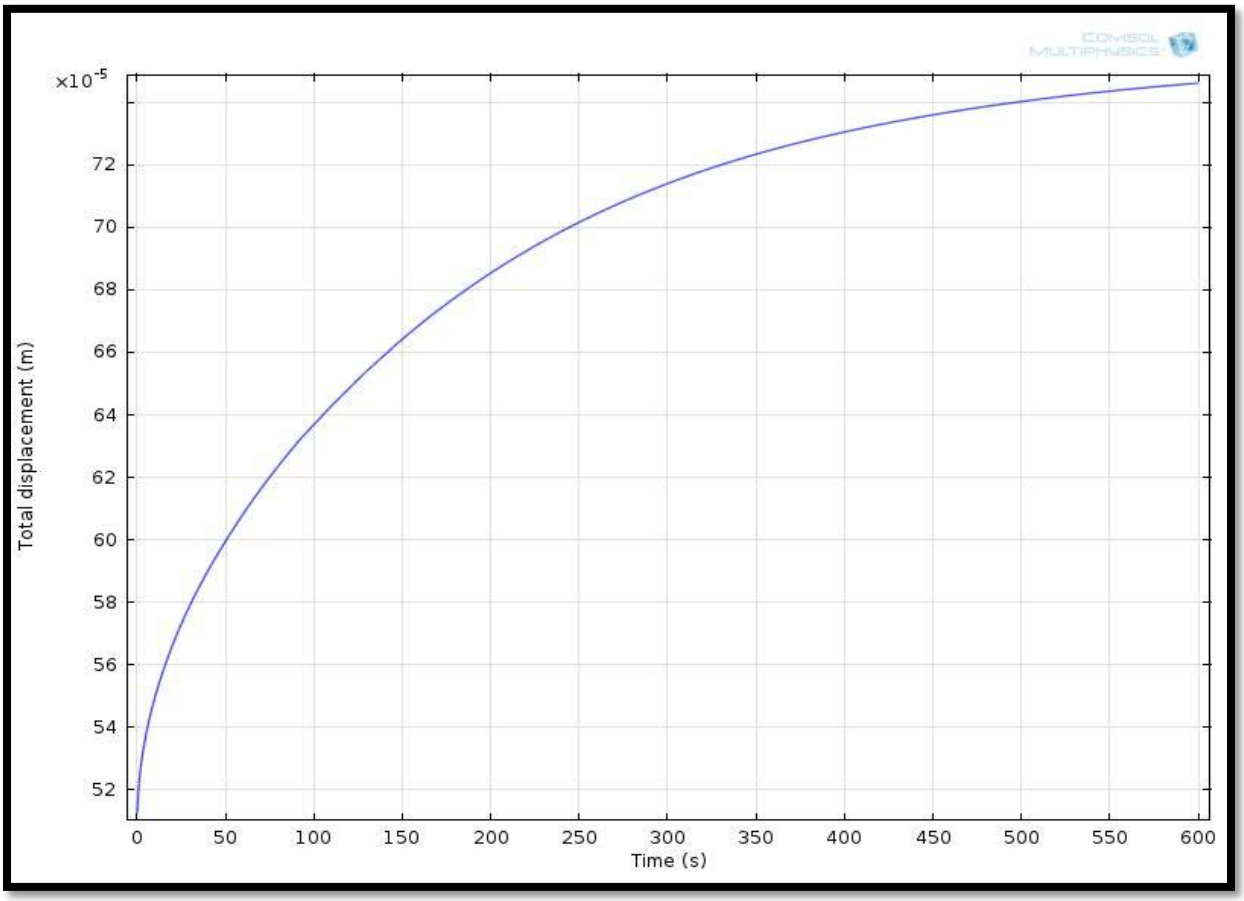

Figure 35: Vertical displacement (m) at point (x=0, y=3) of the rock sample vs. time for Porosity(0.20).

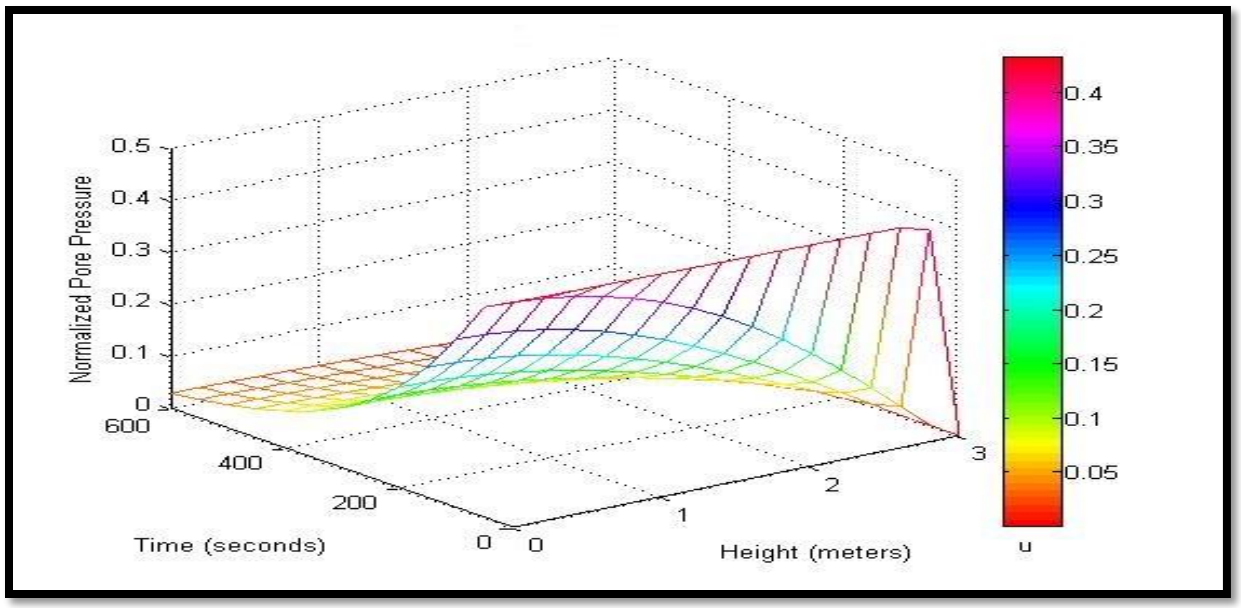

Figure 36: 3-D mesh for Pore pressures inside the sample plotted vs time intervals for Porosity(0.20).

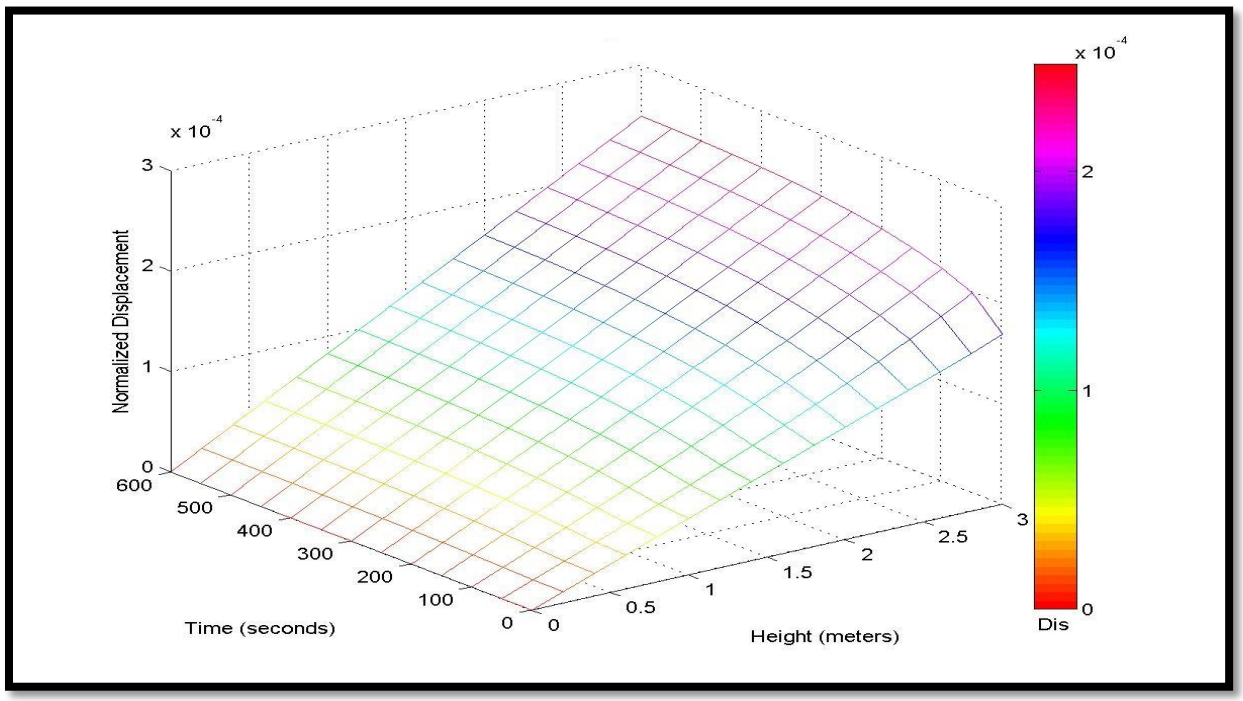

Figure 37: 3-D mesh for vertical displacement (m) of the rock sample vs. time.for Porosity(0.20).

Porosity value of (0.18) Results

Figure 38 shows the respond of rock sample for porosity value of (0.18). The Plot shows upward trend of vertical displacement with time for point at (x=0, y=3m) after 10 min. Figure 39 shows the pressure distribution inside the rock sample. It can be concluded that pressure is value of 0.1 M Pa after 10 minutes. Figure 40 demonstrate the vertical displacement along the height of rock sample plotted in different time intervals.

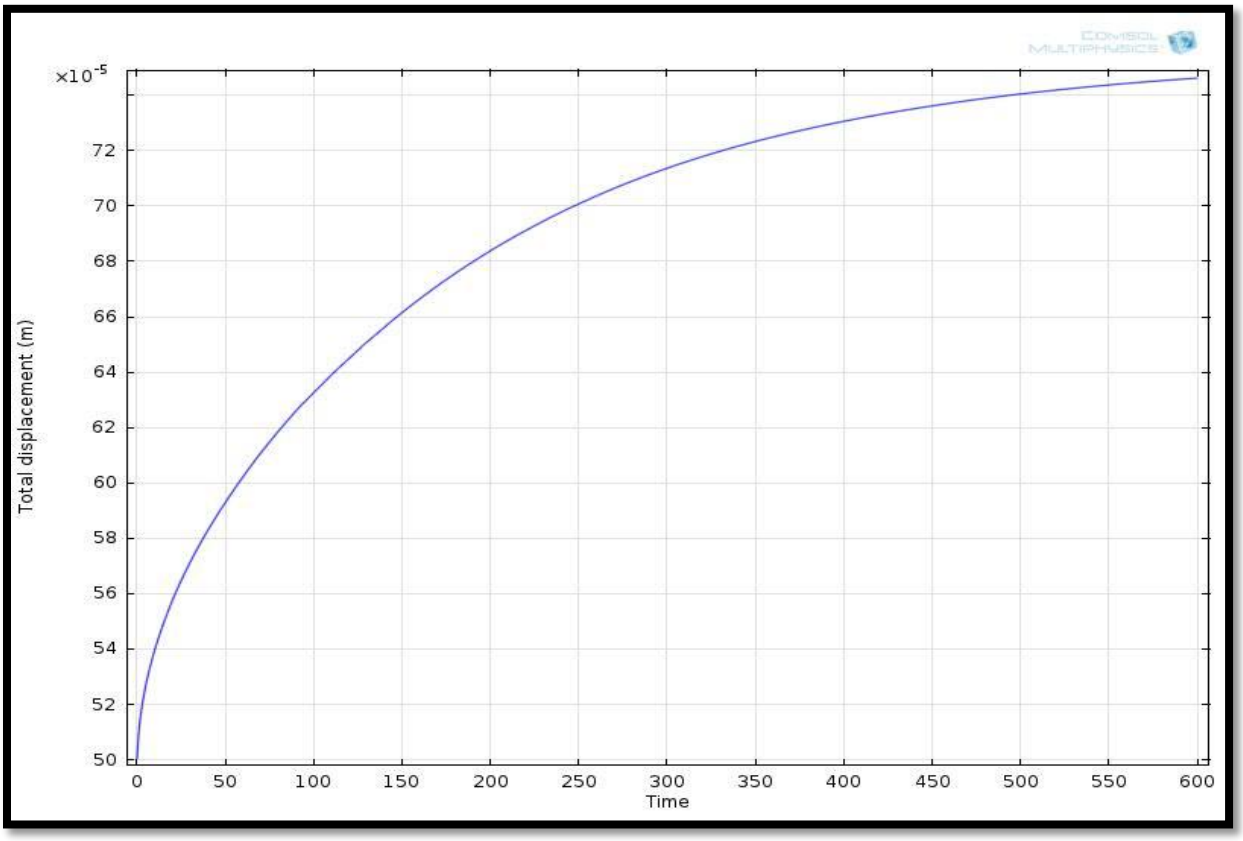

Figure 38: Vertical displacement (m) at point (x=0, y=3) of the rock sample vs. time for Porosity(0.18).

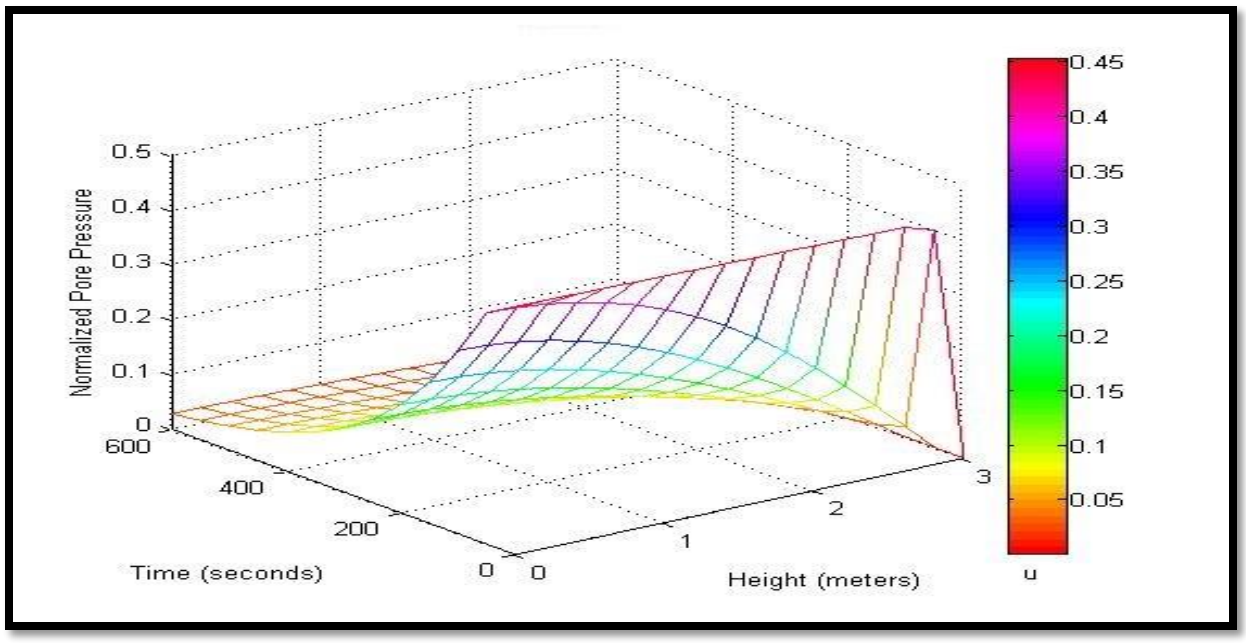

Figure 39: 3-D mesh for Pore pressures inside the sample plotted vs time for Porosity(0.18).

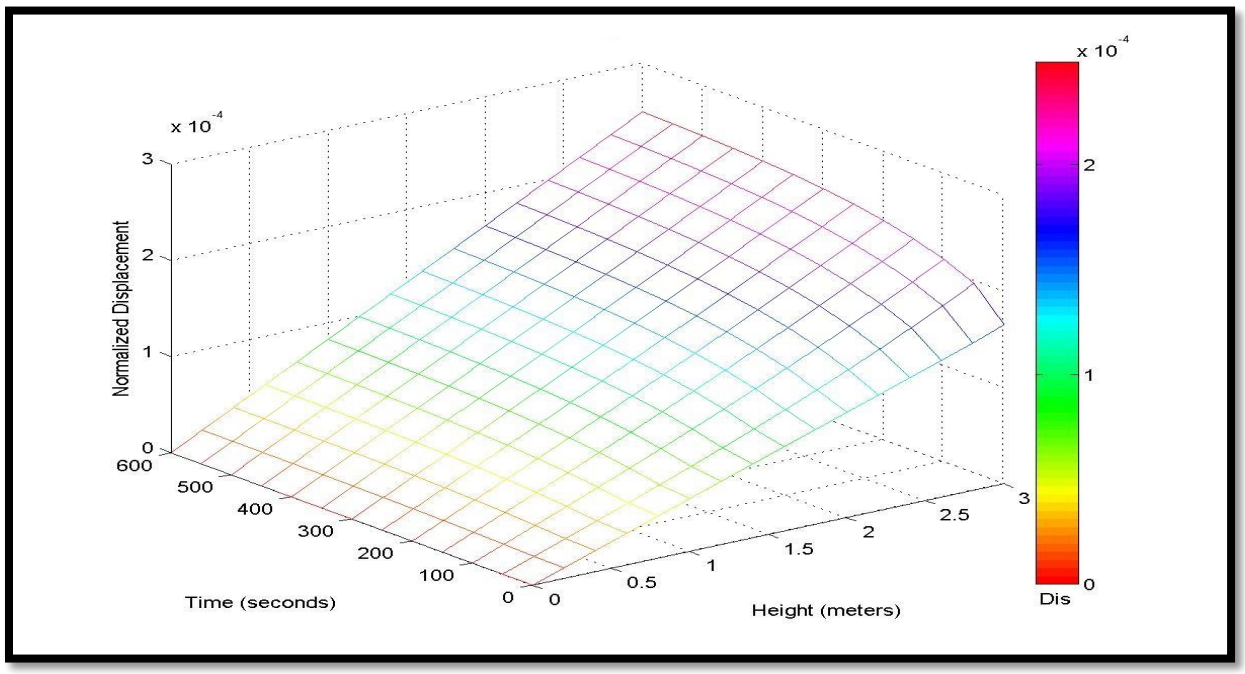

Figure 40 : 3-D mesh for vertical displacement (m) of the rock sample vs. time. for Porosity(0.18).

Summary of the Effects of Porosity on Rock Sample Behavior

In this model, the displacement of rock sample with time for different porosity values are studied. Figure 41 shows that changing porosity value has no effect on the total displacement of the rock sample. However, porosity has effect on the initial displacement on the rock sample as shown in Figure 41. The pore pressure dissipation also has the significant values at the beginning of the run, then after 5 minutes all porosities values have the same pore pressure dissipation trend. It can be concluded that poroelastic parameters are less sensitive to porosity change of range of (+/- 0.2%).

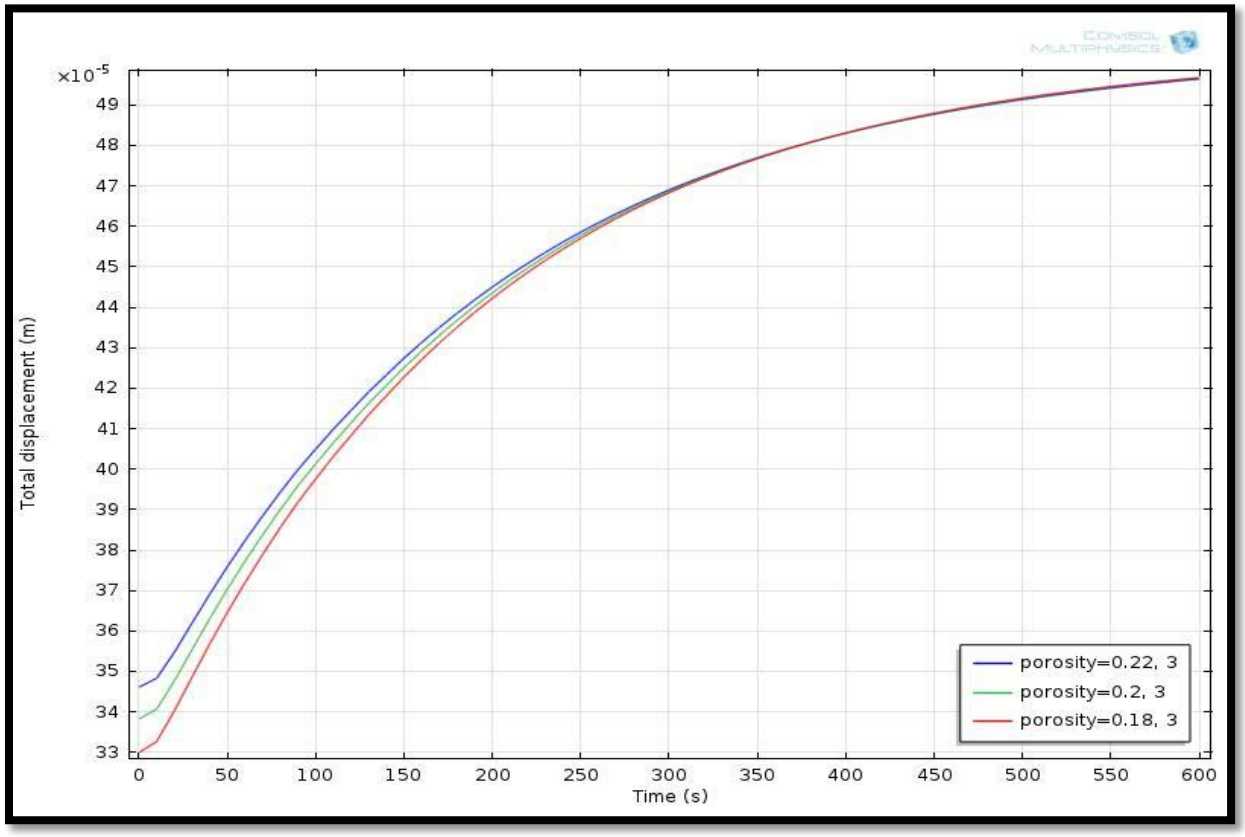

Figure 41: Vertical displacement Vs time for point (x=0,y=3) for diffrenet poristies

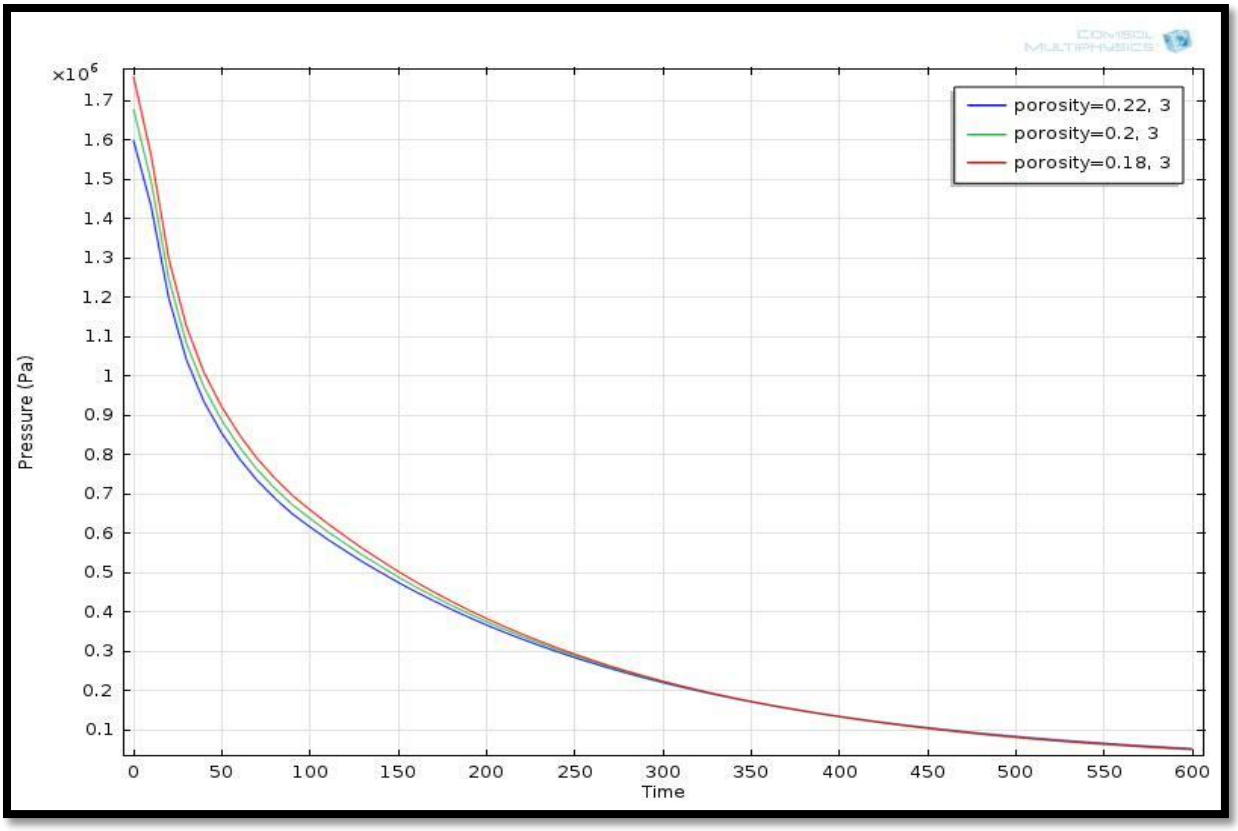

Figure 42: Pore pressure Vs time for point (x=0,y=3) for range of porosities.

5. EMBANKMENT

5.1 Motivation

The objective of this chapter is to develop a coupled Hydro-mechanical model finite element model for a real-world example of embankment settlement using Comsol Multiphysics. Settlement of soil under embankment is considered one of the major challenges encountered in maintaining roadway facilities. Current methods for predicting consolidation settlement stages under embankment are based on the theory of elasticity such as Schmertmann' method (Sallam, 2009). Also constitutive models are typically used to estimate soil settlement under embankment such as Mohr Coulomb (MC) model and Modified Cam Clay model. The goal of this study is to predict the settlement of embankment by using coupled Hydro-mechanical finite element model and to compare the results with a real field measurements data of embankment published by Sallam et al (2009).

5.2 Approach

The goal of this study is to analyze and compare numerical and field results of Lake Jessup embankment in Central Florida presented by Sallam et al (2009) with developed hydromechanical coupling model. Sallam (2009) performed Finite Element Analysis (FEA) to estimate time dependent settlement due construction stages of the embankment; FEA was carried out by using Mohr-Coulomb and Soft Soil Creep models using the software program PLAXIS (2006). Hydromechanical model developed in this section is created by using COMSOL software. The subsoil, groundwater level, and boundary loading of the embankment are defined by using poroelasticity model on COMSOL software.

5.3 Background

The embankment is located in Seminole County on Florida as shown in Figure (43). The embankment height is 8 m and constructed on three stages, in the first month, a 2.3 m high embankment was constructed, then a 5 m high mechanically stabilized earth (MSE) was constructed in three months, and a 1.2 m high earth embankment was constructed in one month.

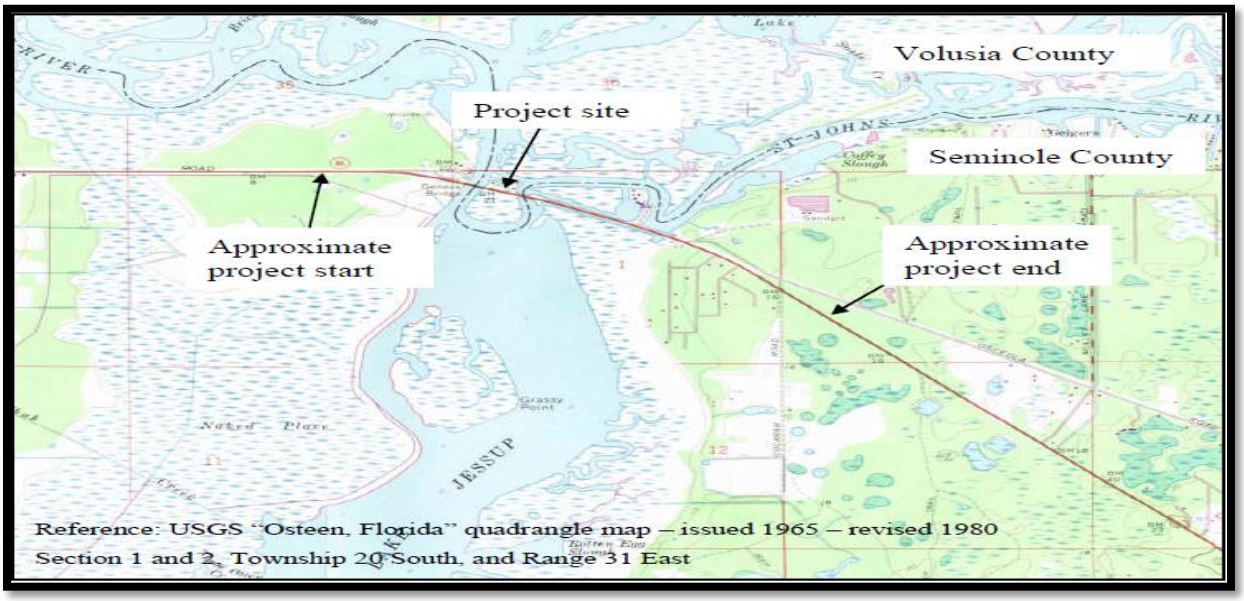

Figure 43: Project location adopted from Sallam et al (2009)

5.4 Mohr-Coulomb Model (Sallam)

Sallam el al (2010) performed FEM model for Lake Jessup embankment based on Mohr-Coulomb (MC) theory to describe the behavior of subsoil condition during construction stages of the embankment. To define the stress-strain relation of the subsoil condition under the embankment, a set of soil parameters are required to describe the behavior of (MC) model which are modulus of elasticity (E) and Poisson ratio (ν) for elasticity, cohesion (c) and angle of shearing resistance (φ) for plasticity, and dilation angle (ψ) for dilatancy.

Table 11 shows the soil properties for the subsoil condition. Figure 44 shows the geometry and subsoil layers at the end of embankment construction.

Table 5: Soil parameters for the Mohr-Coulomb model

Property	Units	Embankment	Sand I	Clay I	Sand II	Clay II	Sand III	Sand IV	Sand V
		Drained	Drained	Undrained	Drained	Undrained	Drained	Drained	Drained
γ_{unsat}	KN/m^3	17.75	16.97	18.22	16.97	18.22	17.75	18.85	23.25
γ_{sat}	KN/m^3	20.42	19.95	18.38	19.95	18.38	20.42	20.89	23.40
K_X	m/day	0.91	1	8.53E-05	1	8.53E-05	0.3	0.3	1
K_Y	m/day	0.91	1	8.53E-05	1	8.53E-05	0.3	0.3	1
E_{ref}	Mpa	13.8	11.5	23.94	11.5	23.94	13.8	16.85	30.6
υ	N/A	0.3	0.3	0.3	0.3	0.3	0.3	0.3	0.3
C_{ref}	Kpa	2.4	2.4	65.6	2.4	65.6	0.5	0.5	0.5
Φ	degree	33	32	0	32	0	33	35	40
Ψ	degree	0	0	0	0	0	0	0	0

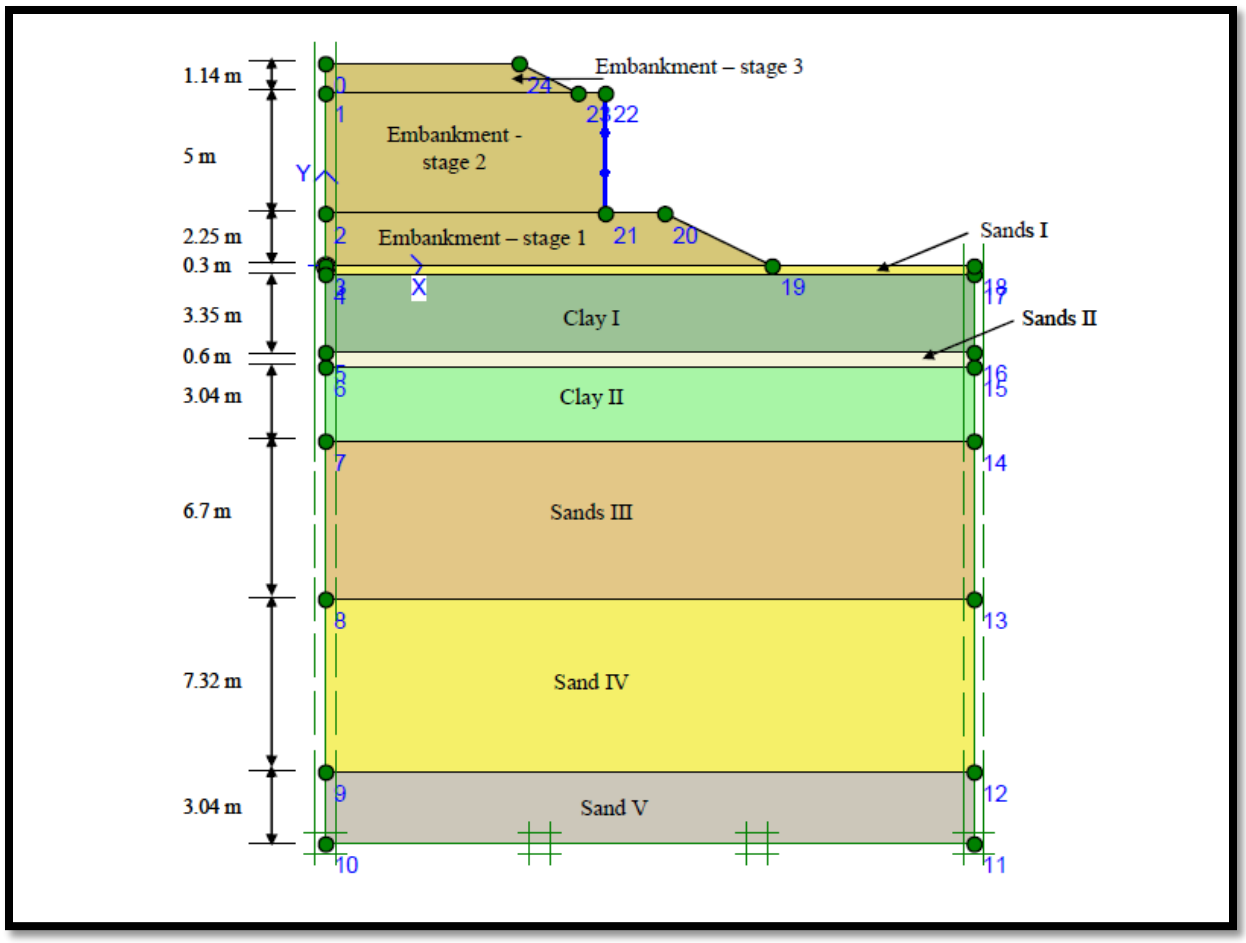

Figure 44: Mohr-Coulomb Model geometry adpoted from Sallam.et al (2009).

Sallam results shows time dependent settlement during construction stages of the embankment. The loads from the embankment were applied gradually to represent a construction stages. Figure 45 shows vertical settlement contours estimated for the modeled stages. Figure 46 shows the settlement time relationship for Point A at ground surface, which shows that maximum settlement is 0.14 m after 5 months. As part of this study, eight settlement plates were installed to monitor the actual settlement under the embankment, the results from monitored program shows total average value of about 0.22 m as compared to a total settlement of about 0.14 using FEA at about 220 days.

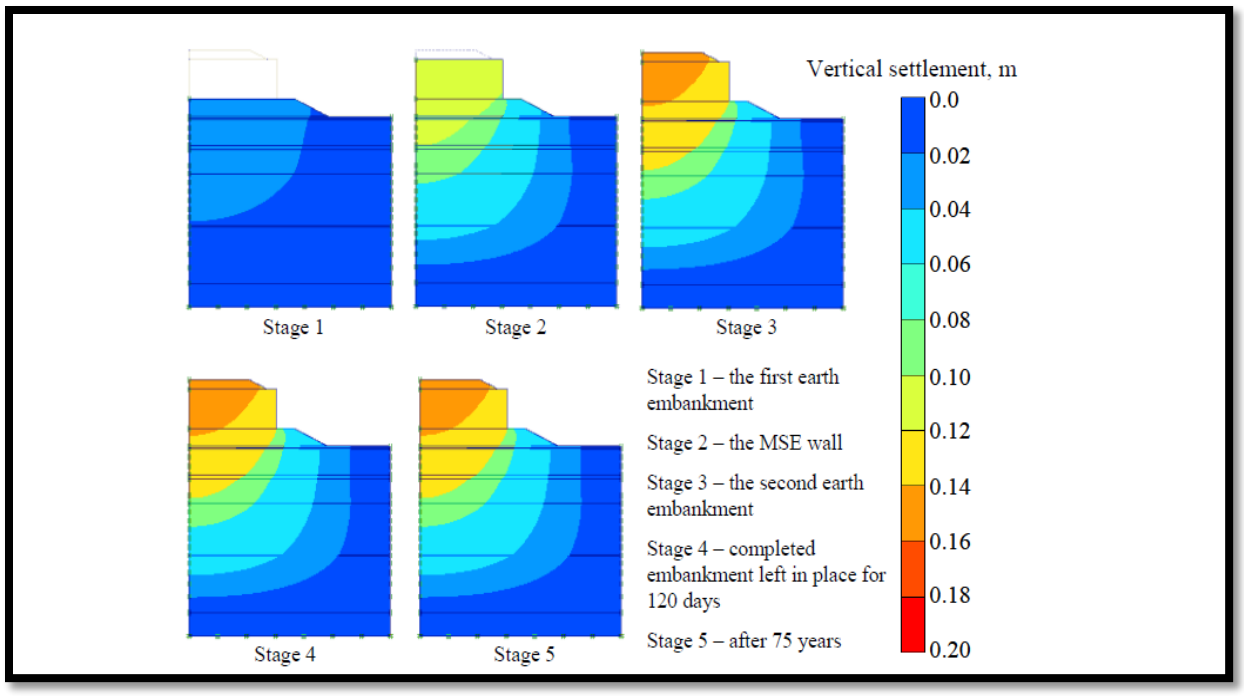

Figure 45: MC analysis for settlement contours for construction stages adopted from Sallam (2009).

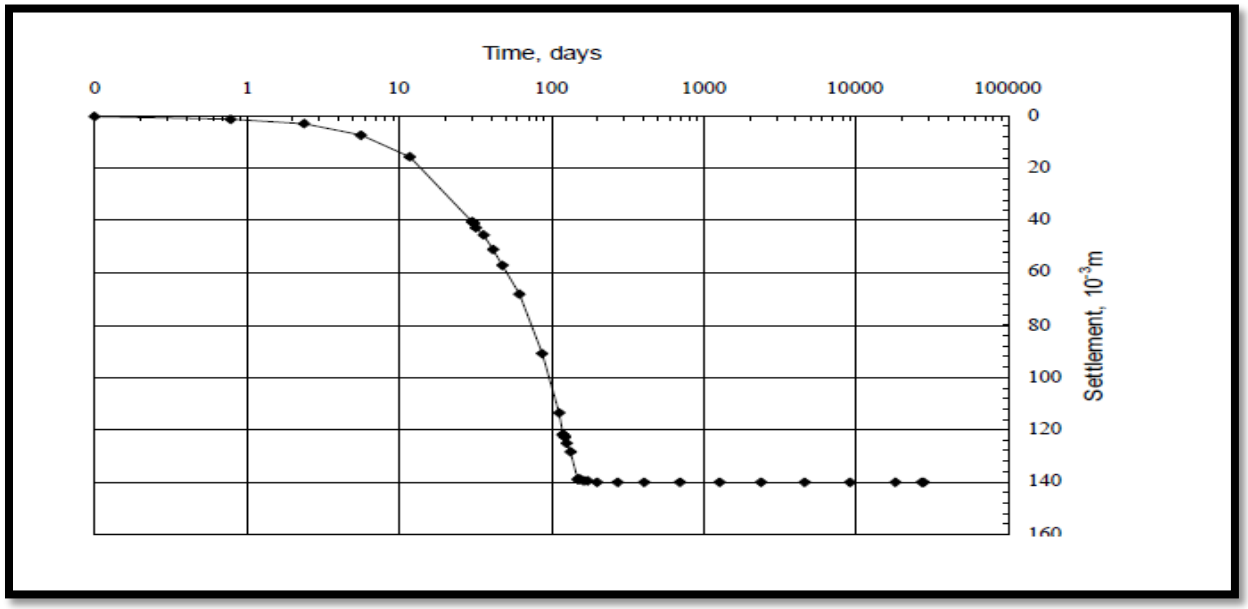

Figure 46: MC analysis for Settlement log-time relationship for at a ground point by Sallam (2009).

5.5 Hydro- mechanical Model

5.5.1 Background

In this section, Hydro-mechanical coupling model is developed to capture the behavior of the subsoil condition during construction stages of the embankment. The aim of this study is to demonstrate the ability of Hydro-Mechanical model to predict the vertical settlement of the embankment by comparing the results with field data measurements.

Embankment is simulated and analyzed by using COMSOL software version 4.2.The soil parameters obtained from laboratory test presented by Sallam (2009) are used to estimate poroelastic parameters; Poroelastic parameters are needed to create Hydro-mechanical model. Table 12 summarized poroelastic parameters used to predict the vertical settlement due embankment construction.

5.5.2 Hydro-mechanical coupling description

Geometry

In order to create Hydro-mechanical model, first the geometry of embankment and subsoil condition should be defined. The geometry model of the subsoil condition under the embankment is consist of six layers of soil is shown in Figure 47. In addition, there are three layers of the construction stages of the embankment are modeled starting from the ground level and continued until reached the maximum height of eight meters. For each model run, calculation of settlement is carried out by activating the corresponding construction stage for specific time.

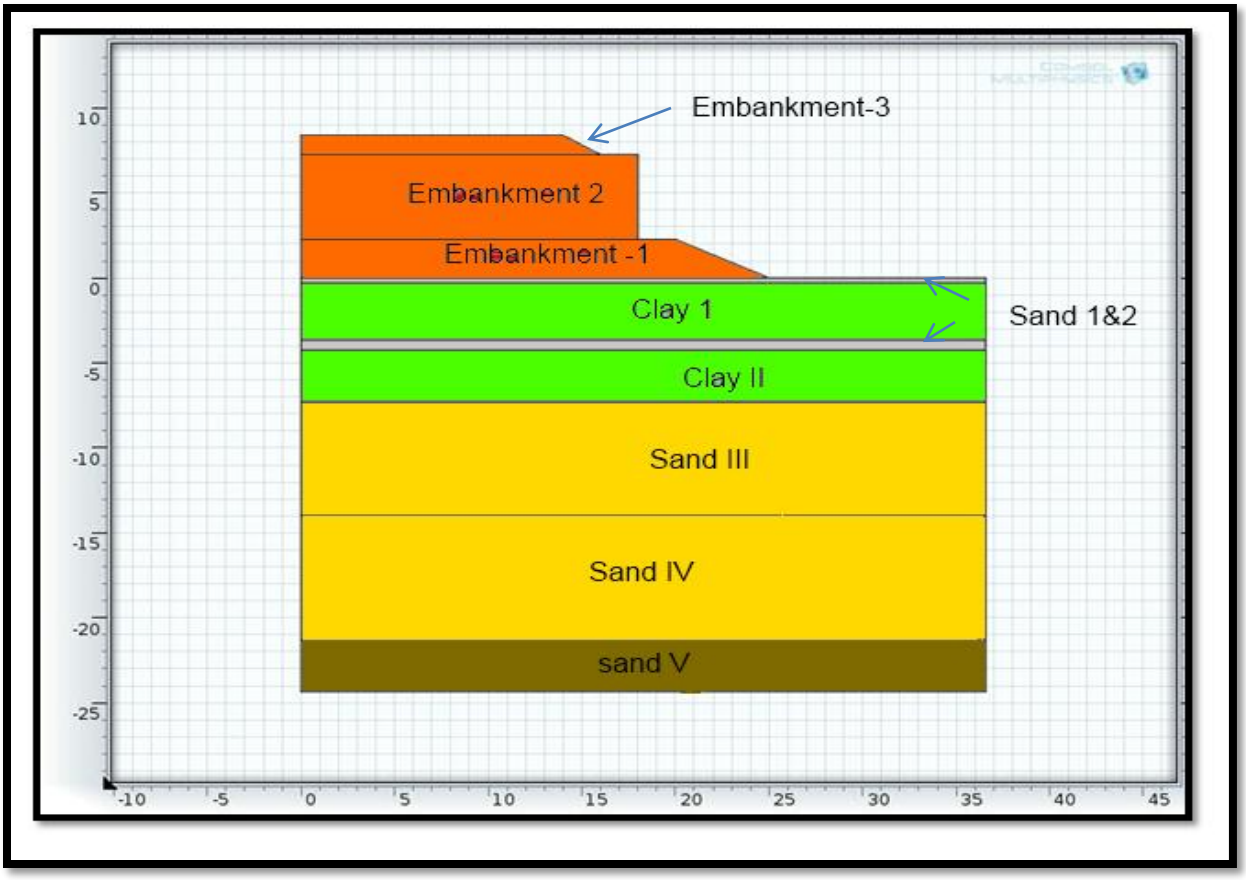

Figure 47: Hydro-Mechnical Model geometry.

Hydro-mechanical parameters

In this section, calculations of Hydro-mechanical model parameters are presented. Correlations between Mohr-Coulomb (MC) parameters and Poroelastic parameters are needed to use the Hydro-mechanical model. It should be noted that Hydro-Mechanical coupling equations contain two important coefficients, which are Biot's coefficient and Biot's modulus. Table 6 summaries Hydro-Mechanical parameters for subsoil layers.

Table 6: Summary of soil properties for Hydro-mechnical model

Property	Units	Embankment	Sand I	Clay I	Sand II	Clay II	Sand III	Sand IV	Sand V
		Drained	Drained	Undrained	Drained	Undrained	Drained	Drained	Drained
γ_{unsat}	KN/m^3	17.75	16.97	18.22	16.97	18.22	17.75	18.85	23.25
γ_{sat}	KN/m^3	20.42	19.95	18.38	19.95	18.38	20.42	20.89	23.40
k_X	m/day	0.91	1	8.53E-05	1	8.53E-05	0.3	0.3	1
k_Y	m/day	0.91	1	8.53E-05	1	8.53E-05	0.3	0.3	1
E_{ref}	Mpa	13.8	11.5	23.94	11.5	23.94	13.8	16.85	30.6
υ	N/A	0.3	0.3	0.3	0.3	0.3	0.3	0.3	0.3
α	N/A	1	1	1	1	1	1	1	1
μ	m^2/s	1E-03	1E-03	1E-03	1E-03	1E-03	1E-03	1E-03	1E-03
k_f	Pa	4E03	4E03	4E03	4E03	4E03	4E03	4E03	4E03

It should be noted that Biot's coefficient is assumed to be equal to 1 as recommended by Biot for fully saturated soil. The poroelasticity equations to describe the coupling between fluid and deformation can be formulated as following:

$$\frac{1}{M}\frac{\partial p}{\partial t} - \nabla\left(\frac{k}{\mu}(\nabla p - \rho fg\nabla z)\right) = -\alpha\frac{\partial(\nabla . u)}{\partial t} \tag{5.1}$$

where M, Biot's Modulus is defined as:

$$\frac{1}{M} = \frac{\alpha - \varphi}{k_s} + \frac{\varphi}{k_f} \tag{5.2}$$

where, the Ks can be interpreted as the bulk modules of soil phase K_f is the bulk modulus of fluid; φ is the porosity of porous material; α is Biot-Willis coefficient. The Bulk modules of soil is interpreted from the following relation:

$$K_s = \frac{E}{3(1-2\nu)} \tag{5.3}$$

where E is the Young's modules and ν, Poisson's ratio, are measured under drained conditions.

Settlement Calculation

The embankment construction is divided into three phases. After the first construction phase of the embankment, a consolidation of 60 day is introduced to allow the pore pressure to dissipate. Subsequently, construction of the second phase for Mechanically Stabilized Earth (MSE) will take place. However, it should be noted that the construction of MSE is assumed to be carried out in ten steps for COMSOL Software. In each step, 50 cm of MSE height will be introduced until reach the maximum height of the MSE. After the second construction stage another consolidation time will be introduced to allow water to dissipate. Finally, the last stage of embankment construction

takes place, the duration of construction in this stage is 30 days. Next, the third construction stage a consolidation period of 225 days is introduced to allow water to dissipate.

Results

In this study, point A at the ground level of the embankment is selected to investigate the displacement versus time. The results of the embankment settlement during construction stages is shown in Figure 49. Figure 49 clearly illustrates settlement estimation for the three construction stages, which include; first embankment (30 days), MSE wall (60 days), second embankment (10 days). It can be concluded from settlement–time relationship for Point A that the maximum settlement occurs after 7 months of construction, then the settlement is stabilized at value of 0.19 m settlement. Figure 50 shows the pore pressure dissipation at Points B at the middle of the clay layer which showed the excess pore pressure mostly dissipate after about 10 moths.

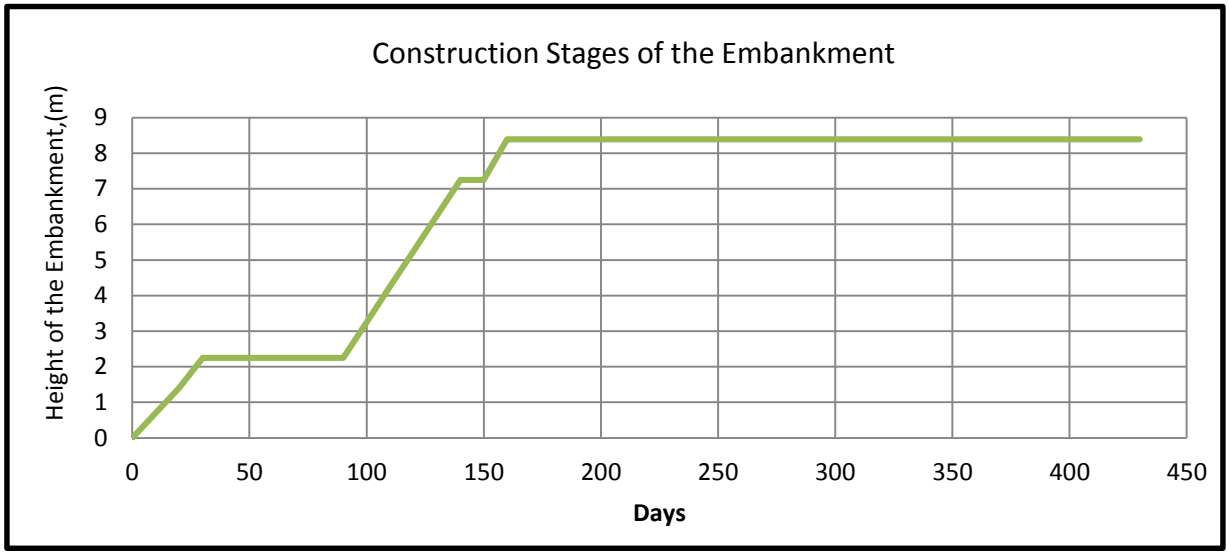

Figure 48: Construction stages of the Lake Jessup embankment.

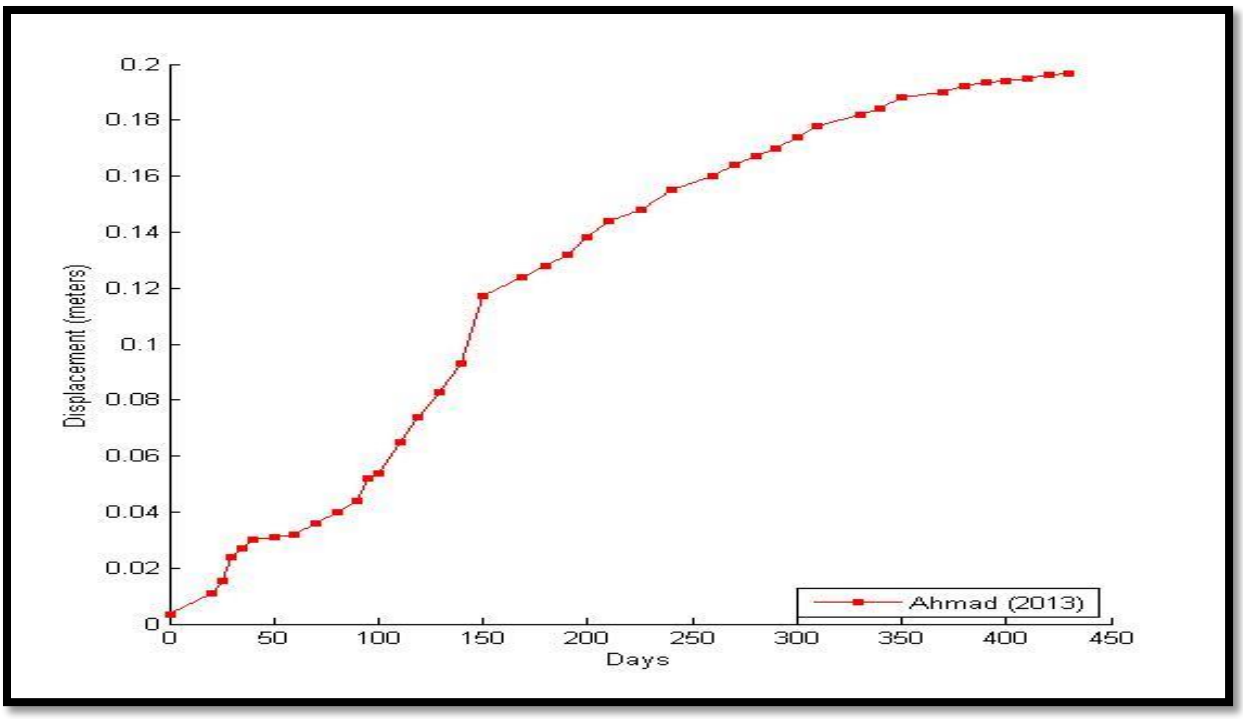

Figure 49: Settlement profile at ground level from H-M model COMSOL.

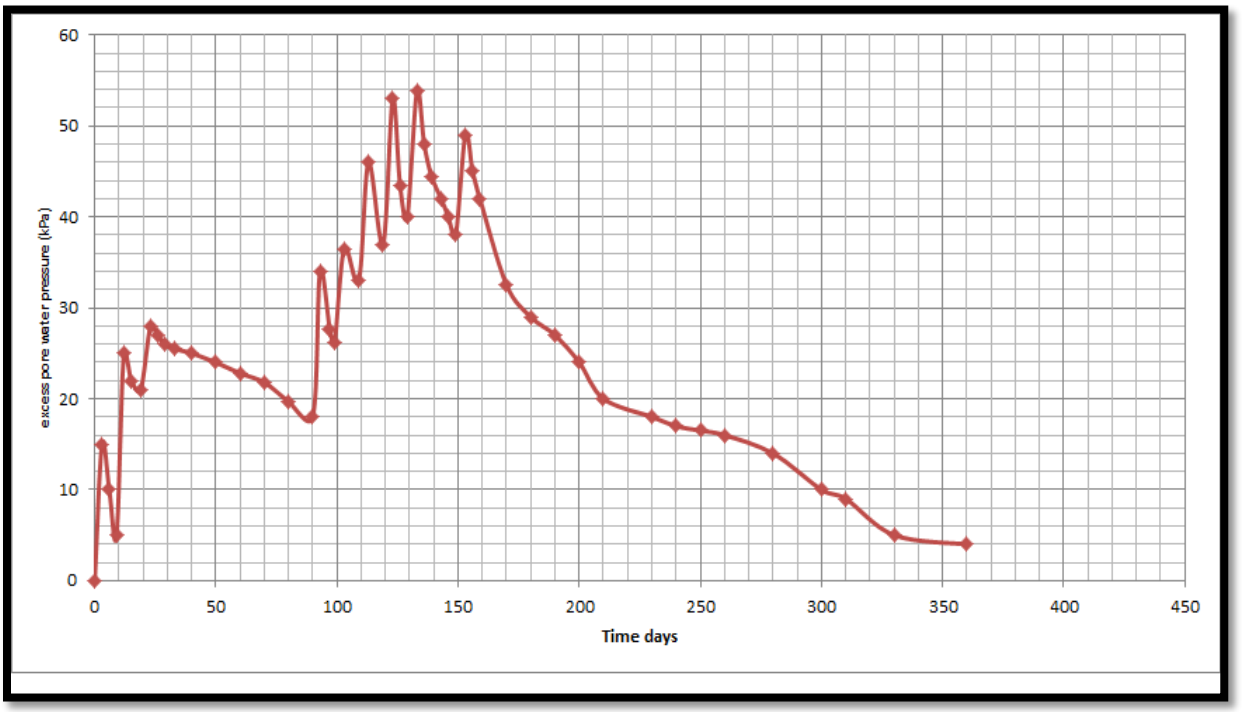

Figure 50: Pore pressure distrubtion at point A.

5.6 Comparison between model results and field data

In this section, FEM models and field results are compared and analyzed. In order to verify and confirm the settlement estimated from Hydro-Mechanical model, the settlement results of Hydro-Mechanical (H-M) model are compared with filed data and Mohr-Coulomb (MC) results presented by Sallam (2009). Figure 51 shows results of filed data for eight settlement plates, MC model results and H-M model results.

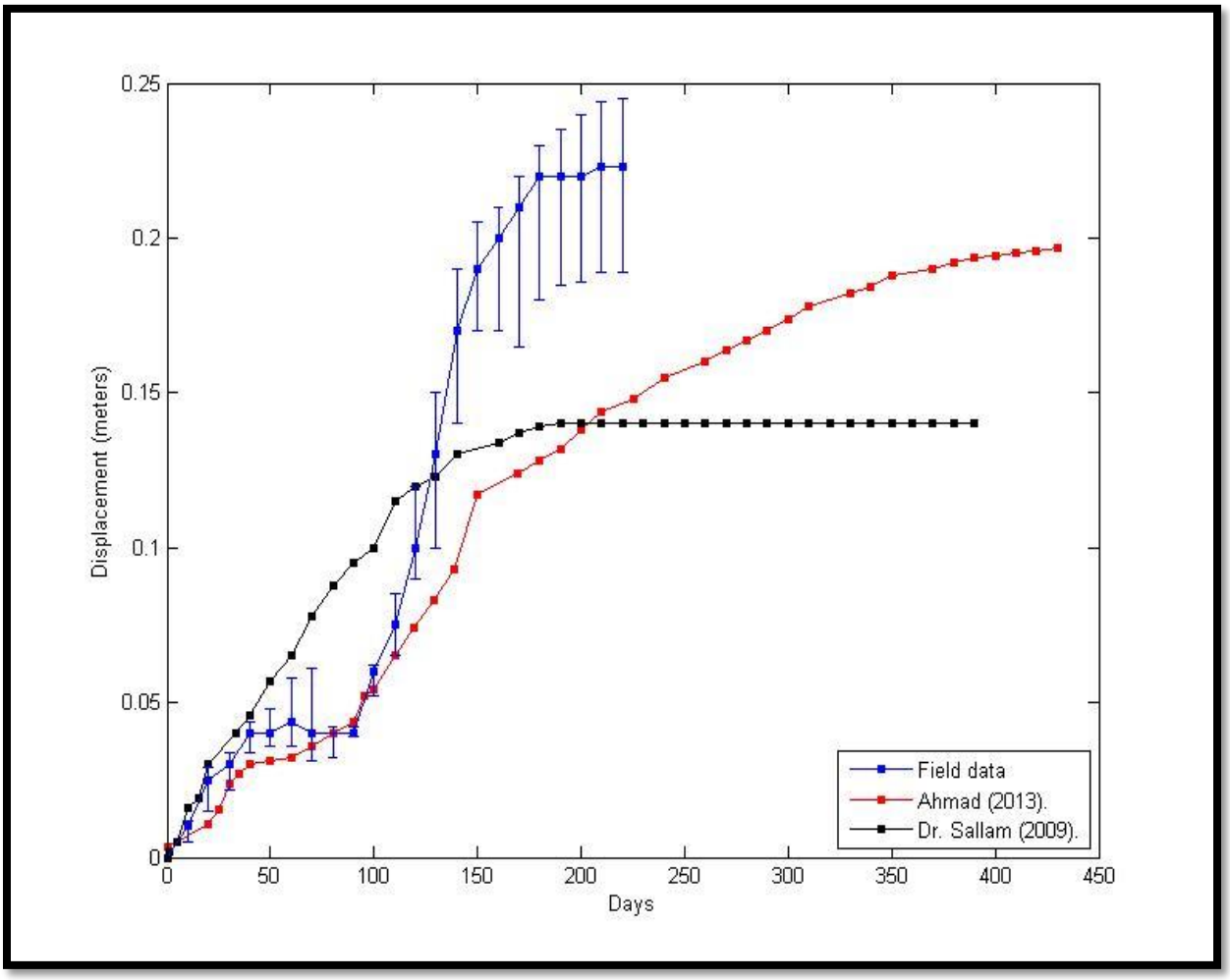

Figure 51: Plot of settlement versus time under the embankment .

It can be concluded from figure 51 that (H-M) model have general agreements with field data. Figure 51 shows a settlement in order of 0.22 m after 8.5 months measured by settlement plates while H-M model predict a settlement of 0.19 m after 10 months. In other hand, (MC) model estimate only 0.14 m after 7.5 months. It should be noted that (H-M) model was able to capture the delay on construction for the first 90 days. Both the filed data and (H-M) model shows a settlement of 0.05 m for the first 90 days. It should be noted that there were less information about the loading stags for the second stage which could be the reason for different in settlement calculated by (H-M) model. It can be said that (H-M) model is more accurate for settlement analysis of embankment construction compared by (MC) model.

6. CONCLUSIONS

6.1 Summary

The main focus of this thesis study was to demonstrate the importance of modeling multiphysical effects to describe the real realistic coupled behavior of porous materials. The advantages of using hydromechanical coupling to estimate deformation and pore water pressure dissipation of porous materials was demonstrated in this research. The followings are major findings from this study:

1. Extensive literature survey was conducted about hydro-mechanical models based on Biot's poroelastic concept. Derivation of the Biot's poroelastic equations was presented based on the Wang's approach (2000).
2. Sensitivity analyses were conducted to correlate the effect of poroelastic parameters on the behavior of porous material. The results of the sensitivity analysis showed that the porosity and Biot's coefficient have dominant contribution to porous material behavior.
3. It can be concluded by implementing and developing a numerical model of poroelastic rock materials that the hydromechanical coupling are paramount in estimating the deformation of porous material. The numerical models developed in this thesis were created by using COMSOL, a commercialized multiphysics finite element software package. The results of these models were compared with the analytical model developed by Zheng (2000).
4. To validate the fully hydromechanical model developed in this study, the model was compared with the settlement data collected from a realistic filed embankment site. The H-M model results were also compared with (MC) results embankment was presented.

The simulation results of hydromechanical models showed general agreement with field and MC model measurements of embankment settlement.

6.2 Recommendations of future works

1. Heat transfer in porous material are important factors in many engineering disciplines, such as geotechnical engineering and petroleum engineering. To study the behavior of porous material under thermal, fluid and/or mechanical loading, Thermo hydro mechanical coupling techniques should be developed.
2. Biot's theory for hydromechanical coupling were developed only for saturated soil However, unsaturated soils problems appears to be gaining general acceptance by geotechnical engineers. Thus, Biot's theory should be extended to describe the behavior of unsaturated soil.
3. Biot's assumed a small deformation occur to the soil skeleton, this carries the assumption that porosity is constant. One should investigate the effect of porosity on the overall behavior of porous material.

LIST OF REFERENCES

A. M. Sallam, and S.E. Jammal (2009). Finite Element Analysis of Time Dependent Settlement of Lake Jessup Bridge Embankment in Central Florida.

Assessment, N. (1998). Prediction of Embankment Dam Breach Parameters, (July).

Bear, J. and Corapcioglu, M. Y. (1981). A mathematical mode1 for consolidation in elastic aquifer due to hot water injection of pumping. Water Recourses Res. 17, 723-736.

Bear,J. and Bachmat,Y. (lggO), Introduction to Modelling of THM Phenomena in Porous Media. Kluwer Academic Publishers, London

Biot, M., 1941, General Theory of Three-Dimensional Consolidation. Journal of Applied Physics, 12(2): 155-164.

Biot, M., 1955, Theory of Elasticity and Consolidation for a Porous Anisotropic Solid. Journal of Applied Physics, 26(2): 182-185.

Biot, M.A. and Willis, D.G., 1957, The Elastic Coefficients of the Theory of Consolidation. J. Appl. Mech., 24: 594-601.

Biot, M.A., 1962, Mechanics of Deformation and Acoustic Propagation in Porous Media. Journal of Applied Physics, 33(4): 1482-1498.

Booker, J.R. and Sawidou,C. (l984), Consolidation around a point heat source. Int.J- Numer. Anal. Method Gwmech. 9, 173-184-.

Bowen, R M. (1983). Compressible porous media models by use of the theory of mixtures. Int- J. Eng. Sci. 20, 697-735.

Brooks, R. and Corey, A., 1966, Properties of Porous Media Affecting Fluid Flow, J. Irrigation and Drainage Div., Proc. Am. Soc. Civil Eng.(IR2), 92: 61-88.

Carey, G.F., 1989. Parallel Supercomputing: Methods, Algorithms and Applications. Wiley, New York, USA, 298pp.

Chen, C., Pei, S. and Jiao, J., 2003, Land Subsidence Caused by Groundwater Exploitation in Suzhou City, China. Hydrogeology Journal, 11(2): 275-287.

Chen, H., Teufel, L. and Lee, R., 1995, Coupled Fluid Flow and Geomechanics in Reservoir Study- I. Theory and Governing Equations. Society of Petroleum Engineers Journal (SPE 30752): 507-519.

Chen, W., Tan, X., Yu, H., Wu, G., & Jia, S. (2010). A fully coupled thermo-hydro-mechanical model for unsaturated porous media. Journal of Rock Mechanics and geotechnical Engineering, 2010(1), 31–40. doi:10.3724/SP.J.1235.2009.00031

Chijimatsu, M., Fujita, T., Kobayashi, A., Nakano, M., 2000. Experiment and validation of numerical simulation of coupled thermal, hydraulic and mechanical behavior in the engineered buffer materials. International Journal of Numerical and Analytical Methods in Geomechanics 24, 403–424.

Chin, L. Y., Raghavan, R., Thomas, L. K., & Co, P. P. (2000). Fully Coupled Geomechanics and Fluid-Flow Analysis of Wells with Stress-Dependent Permeability, (July 1999), 2–6.

Comsol Multiphysics 4.2a (2012), a commercial finite element modeling software.

De Boer, R., 2005. Trends in Continuum Mechanics of Porous Media: Theory and Applications of Transport in Porous Media. Springer, Heidelberg, Germany, 282pp.

Dean, R. H., Systems, S., Gai, X., Texas, U., Stone, C. M., Laboratories, S. N., Minkoff, S. E., et al. (2006). A Comparison of Techniques for Coupling Porous Flow and Geomechanics, (March).

Detournay, E., & Cheng, A. H. (1993). Fundamentals of Poroelasticity 1, II, 113–171.

Doughty, C., Pruess, K., 2004. Modeling supercritical carbon dioxide injection in heterogeneous porous media. Vadose Zone Journal 3, 837–847.

E. Detournay, A.H.-D. Cheng, Fundamentals of Poroelasticity, Chap. 5 in Comprehensive Rock Engineering: Principles, Practice and Projects, Vol. II, Analysis and Design Method, C.

Ehlers, W., Bluhm, J., 2002. Porous Media: Theory, Experiments and Numerical Applications. Springer, Berlin, Germany, 459pp.

Farhat, C., Roux, F., 1991. A method of finite element tearing and interconnecting and its parallel solution algorithm. International Journal for Numerical Methods in Engineering 32 (6), 1205–1227.

Fayer, M. J. (2000). Unsaturated Soil Water and Heat Flow Model Theory, User Manual, and Examples, (June).

Freeman, T. T., Chalaturnyk, R. J., & Bogdanov, I. I. (2008). Fully Coupled Thermo-Hydro-Mechanical Modeling by COMSOL Multiphysics, with Applications in Reservoir Geomechnical Characterization.

Gambolati, G., Teatini, P., Bau, D., & Ferronato, M. (2000). Importance of poroelastic coupling in dynamically active aquifers of the river basin, Italy, 36(9), 2443–2459.

Gens, A., & Olivella, S. (2011). Revue Française de Génie Civil THM phenomena in saturated and unsaturated porous media THM phenomena in saturated and unsaturated porous media, (July 2012), 37–41.

Gutierrez, M. and H. Hansteen, Fully-Coupled Analysis of Reservoir Compaction and ubsidence, in SPE 28900. 1994: London.

Gutierrez, M., N. Barton and A. Makurat 1995. Compaction and subsidence in North Sea hydrocarbon fields. In Intl. Workshop on Rock Foundations of Large Structures.

J. Sulem, P. Lazar, I. Vardoulakis, Thermo-Poro-Mechanical Properties of Clayey

Kim, J. (2004). Fully coupled poroelastic governing equations for groundwater flow and solid skeleton deformation in variably saturated true anisotropic porous geologic media, 8(3), 291–300.

Liu, Q., Zhang, C., Liu, X., 2006. A practical method for coupled THM simulations of the Yucca Mountain and FEBEX case examples for task D of the DECOVALEX- THMC project. In: Proceedings of GEOPROC 2006, 2nd International Sympo- sium on Coupled THMC Processes in Geosystems and Engineering. HoHai University, Nanjing, China, pp. 220–225.

Liu, X., Wang, S., & Wang, E. (2006). Coupled thermo-hydro-mechanical (THM) processes of high slopes in the Nuozhadu hydropower project on Lancang river in Yunnan province , China, (754), 1–11.

Liu, Z., & Yu, X. (2011). Coupled thermo-hydro-mechanical model for porous materials under frost action: theory and implementation. Acta Geotechnica, 6(2), 51–65. doi:10.1007/s11440-011-0135-6

Lopes, M. G. (n.d.). Numerical Simulation Of A Reinforced Embankment On Soft Ground Constructed Up To Failure, 1–6.

Mainguy, M., & Longuemare, P. (2002). Coupling Fluid Flow and Rock Mechanics : Formulations of the Partial Coupling between Reservoir and Geomechnical Simulators, 57(4), 355–367.

McTigue, Thermoelastic response of fluid-saturated porous rock. Journal of Geophysical Research, 91(B9) (1986), 9533-9542.

Minkoff, S. E., Stone, C. M., Bryant, S., Peszynska, M., & Wheeler, M. F. (2003). Coupled fluid flow and geomechnical deformation modeling, 38, 37–56. doi:10.1016/S0920-4105(03)00021-4

Patzek, T., Engineering, E., & Berkeley, U. C. (2005). Biot Theory (Almost) For Dummies.

Phillips, P. J., & Arbogast, T. (2005). Finite Element Methods in Linear Poroelasticity : Theoretical and Computational Results.

Prokofiev, D., & Dunec, J. (2005). Multiphysics Model of Soil Phenomena Near a Well.

Przemieniecki, J.S., 1985.Theory of Matrix Structural Analysis. McGraw Hill Book Co., New York, USA, 480pp.

R.W. Zimmerman, Compressibility of sandstones, Elsevier Sci., Amsterdam, 1991.

Rutqvist, J.,Barr,D.,Birkholzer,J.T.,Chijimatsu,M.,Kolditz,O.,Liu,Q., Oda, Y.,Wang,W.,Zhang,C.,2008.Results from an international simulation study on coupled thermal, hydrological,and mechanical processes near geologicalnuclearwasterepositories.NuclearTechnology163(1), 101–109.

Rutqvist, J.,Barr,D.,Datta,R.,Gens,A.,Millard,A.,Olivella,S.,Tsang,C.F.,Tsang, Y.W.,2005a.Coupledthermal-hydrological-mechanicalanalysesoftheYucca Mountain drift scale test—comparison of field measurements to predictions of four different numerical models. International Journal of Rock Mechanics and Mining Sciences 42 (5–6),680–697.

Rutqvist, J.,Bo¨ rgesson,L.,Chijimatsu,M.,Kobayashi,A.,Nguyen,T.S.,Jing,L., Noorishad, J.,Tsang,C.F.,2001a.Thermohydromechanicsofpartiallysaturated geological media—governing equations and formulation off our finite element models. InternationalJournalofRockMechanicsandMiningSciences38, 105–127.

Rutqvist, J.,Chijimatsu,M.,Jing,L.,DeJonge,J.,Kohlmeier,M.,Millard,A.,Nguyen, T.S.,Rejeb,A.,Souley,M.,Sugita,Y.,Tsang,C.F.,2005b.Numerical study of the THM effects on the near-field safety of hypothetical nuclear waste repository—BMT1 oftheDECOVALEXIIIproject,Part3:effectsofTHM coupling. In fractured rock. International Journal of Rock Mechanics and Mining Sciences 42,745–755.

Sanavia, L. (2008). Numerical modelling of a slope stability test by means of porous media mechanics.

Sedano, J. A. I., Evgin, E., & Fu, Z. (2011). A Coupled Analysis of Heat and Moisture Transfer in Soils, (1).

V. Palciauskas, P.A. Domenico, Characterization of drained and undrained response of thermally loaded repository rocks. Water Resources Research, 18(1982), No. 2,281-290.

Wang, P., Yotov, I., Wheeler, M., Arbogast, T., Dawson, C., Parashar, M., Sepehrnoori, K., 1997. A new generation EOS compositional reservoir simulator: Part I. Formulation and discretization. Proceedings of the 14th Reservoir Simulation Symposium, No. 37979. SPE, Richardson, TX.

Wang, W., Kosakowski, G., & Kolditz, O. (2009). Computers & Geosciences a parallel finite element scheme for thermo-hydro-mechanical (THM) coupled problems in porous media, 35, 1631–1641. doi:10.1016/j.cageo.2008.07.007

Wellman, G.W., 1999. MAPVAR—a computer program to transfer solution data between finite elements meshes. Technical Report, SAND99-0466, Sandia National Labs, Albuquerque, NM.

Wheeler, M., Arbogast, T., Bryant, S., Eaton, J., Lu, Q., Peszynska, M., Yotov, I., 1999. A parallel multiblock/multidomain approach for reservoir simulation. Proceedings of the 15th Reservoir. Simulation Symposium, No. 51884. SPE, Richardson, TX,pp. 51– 61.

Wheeler, M., Wheeler, J., Peszynska, M., 2000. A distributed computing portal for coupling multi-physics and multiple domains in porous media.

Yale, D. P., & Upstream, E. (2002). SPE / ISRM 78202 Coupled Geomechanics-Fluid Flow Modeling : Effects of Plasticity and Permeability Alteration.

Zheng, Y., Burridge, R., & Burns, D. (1955). Reservoir Simulation with the Finite Element Method Using Biot Poroelastic Approach (pp. 1–20).

Zvanut, P. (2003). Settlements of an Embankment Founded On a Soft Soil.